

9-15-2014

A Homogenization Approach for Design and Simulation of Blast Resistant Composites

Michael Sheyka

Follow this and additional works at: https://digitalrepository.unm.edu/me_etds

Recommended Citation

Sheyka, Michael. "A Homogenization Approach for Design and Simulation of Blast Resistant Composites." (2014).
https://digitalrepository.unm.edu/me_etds/21

This Dissertation is brought to you for free and open access by the Engineering ETDs at UNM Digital Repository. It has been accepted for inclusion in Mechanical Engineering ETDs by an authorized administrator of UNM Digital Repository. For more information, please contact disc@unm.edu.

Michael Sheyka

Candidate

Mechanical Engineering

Department

This dissertation is approved, and it is acceptable in quality and form for publication:

Approved by the Dissertation Committee:

Dr. Mahmoud Reda Taha, Chairperson

Dr. Arup K. Maji

Dr. Yu-Lin Shen

Dr. Marwan Al-Haik

A Homogenization Approach for Design and Simulation of Blast Resistant Composites

by

Michael Sheyka

B.S., University of New Mexico, 2006

M.S., University of New Mexico, 2008

Dissertation

Submitted in Partial Fulfillment of the

Requirement for the degree of

Doctor of Philosophy

Engineering

The University of New Mexico

Albuquerque, New Mexico

December, 2011

Dedication

To my father, mother, grandmother, sister and nephew.

Acknowledgements

I would like to thank Dr. Mahmoud Reda Taha, my advisor and dissertation chair, for pushing me to strive for higher goals and produce quality work. He gave me opportunities that were beyond what I had imagined when I started out as a graduate student. I feel that he has prepared me for whatever I may face in my career.

I would also like to thank my committee members, Dr. Arup K. Maji, Dr. Yu-Lin Shen and Dr. Marwan Al-Haik for their recommendations pertaining to my graduate work. My understanding of what it truly means to be a successful and ethical engineer was greatly influenced by them.

Gratitude is extended to the Defense Threat Reduction Agency (DTRA) Student Research Assistant (SRA) fellowship and the Army Research Office for their financial support throughout my graduate studies. This monetary support was essential to my success in graduate school.

To Arife Burcu Altunc, Post Doc, for help with coding all of the executables. I couldn't have done it without you.

To my family, thank you for putting up with me for the last couple of years. I appreciate your encouragement and support. Thanks Dad and Cathy for always being there for me. To my mom, thanks for always keeping me positive and optimistic.

Preface

During the course of this dissertation proposal (2008-2011) the following papers have been published or submitted for publication in reviewed proceedings or scholarly journals:

1. Soliman, E. M., Sheyka, M. P. and Reda Taha, M. M. “Ballistic impact of thin woven carbon fabric composites incorporating carbon nanotubes”, *International Journal of Impact Engineering*, In Review
2. Sheyka, M., Kim, J.J., Altunc, A.B., Reda Taha, M.M., “A Reliability-based Energy Approach for Design Optimization of Blast Resistant Composites,” *Proceeding of the ASME International Mechanical Engineering Conference & Exposition, IMECE, Denver, USA, November 2011.*
3. Sheyka, M.P., Cruz, G., Altunc, A.B., Connolly, T., Reda Taha, M.M., “Multi-objective genetic topological optimization for design of blast resistant composites, *Journal of Composite Science and Technology*, in Review
4. . Sheyka, M., Colak-Altunc, B., Reda Taha, M. M., Cruz, G., Connolly, T., Tortorelli, D. “Multi-objective Blast Resistant Composite Plate Design Optimization” *51st AIAA Conference, Orlando, FL. April 2010.*
5. Reinhardt, A., Soliman, E., Sheyka, M., Al-Haik, M., Reda Taha, M.M., “Fracture Toughness of Hydrated Cement Using Nanoindentation”, *CD Proceedings of 7th*

International Conference on Fracture Mechanics of Concrete and Concrete Structures (FraMCoS-7), Jeju, South Korea, May 2010.

6. Reinhardt, A. L., Sheyka, M. P., Garner, A. P., Al-Haik, M. and Reda Taha, M. M. “Experimental and Numerical Nano-Characterization of Two Phases in Concrete”, International Journal of Material and Structural Integrity, Vol. 3, No. 2/3, 2009, pp. 134-146.
7. Reinhardt, A., Sheyka, M., Tehrani, M., Al-Haik, M. and Reda Taha, M.M., “Experimental and Numerical Investigation of Nano-Indentation of Self-Consolidating Concrete (SCC)”, CD Proceedings of Annual Conference of Society of Experimental Mechanics, Albuquerque, NM, June 2009.
8. Sheyka, M., El-Kady, I., Su, M. and Reda Taha, M.M. “Photonic sensors for micro-damage detection: A proof of concept using numerical simulation,” Journal of Smart Structures & System, Vol. 5, No. 4, 2009, pp. 483-494

Abstract

Structural composites have been used in aerospace and structural engineering due to their high strength to weight ratio. Composite laminates have been successfully and extensively used in blast mitigation. This dissertation examines the use of the homogenization approach to design and simulate blast resistant composites. Three case studies are performed to examine the usefulness of different methods that may be used in designing and optimizing composite plates for blast resistance. The first case study utilizes a single degree of freedom system to simulate the blast and a reliability based approach. The first case study examines homogeneous plates and the optimal stacking sequence and plate thicknesses are determined. The second and third case studies use the homogenization method to calculate the properties of composite unit cell made of two different materials. The methods are integrated with dynamic simulation environments and advanced optimization algorithms. The second case study is 2-D and uses an implicit blast simulation, while the third case study is 3-D and simulates blast using the explicit blast method. Both case studies 2 and 3 rely on multi-objective genetic algorithms for the optimization process. Pareto optimal solutions are determined in case studies 2 and 3. Case study 3 is an integrative method for determining optimal stacking sequence, microstructure and plate thicknesses. The validity of the different methods such as homogenization, reliability, explicit blast modeling and multi-objective genetic algorithms are discussed. Possible extension of the methods to include strain rate effects and parallel computation is also examined.

Contents

CHAPTER 1	INTRODUCTION	1
1.1	Motivation and Background	1
1.2	Dissertation Outline.....	3
CHAPTER 2	LITERATURE REVIEW.....	4
2.1	Structural Composites.....	4
2.2	Fiber Reinforced Composites.....	9
2.3	Metallic Composites.....	10
2.4	Blast.....	12
2.5	Strain rate effects upon materials	15
2.6	Failure of composites due to impact and blast	20
2.7	Optimization.....	22
2.7.1	Topology Optimization and Homogenization	22
2.7.2	Sensitivity Analysis	25
2.7.3	Multi-Objective Optimization.....	28
CHAPTER 3	METHODS FOR DESIGN OPTIMIZATION OF BLAST RESISTANT COMPOSITES 32	
3.1	Homogenization.....	32
3.2	Blast Load Simulation using Computational Fluid Dynamics	34
3.3	Finite Element Simulation of Structural Response.....	36

3.4	Explicit Finite Element Modeling Multi-physics	38
3.5	Effect of damping upon composite structures subjected to blast	46
3.6	Multi-Objective Genetic Algorithm.....	48
3.7	Reliability Analysis.....	51
CHAPTER 4 CASE STUDIES.....		55
4.1	First Case Study: Design Optimization of Stacking Sequence of metallic Composite Laminates	55
4.1.1	Introduction.....	55
4.1.2	Methods	56
4.1.3	Case Study	61
4.1.4	Results and Discussion	66
4.1.5	Conclusions.....	77
4.2	Second Case Study: Design Optimization of Two Dimensional Composite Plate 77	
4.2.1	2-D Homogenization Method Applied to the Two-Layer Composite	78
4.2.2	CFD Model	80
4.2.3	FEA Model.....	81
4.2.4	Design Optimization.....	82
4.2.5	Results and Discussion	86
4.2.6	Conclusions.....	91

4.3	Third Case Study: Design optimization of Three Dimensional Composite Plate	92
4.3.1	Three Dimensional Homogenization.....	93
4.3.2	Explicit FE Blast Modeling	102
4.3.3	Design Optimization.....	109
4.3.4	Results and Discussions.....	111
4.3.5	Conclusions.....	127
4.4	Conclusions.....	128
CHAPTER 5 CONCLUSIONS AND FUTURE WORK		130
5.1	Conclusions.....	130
5.2	Future Work.....	135
REFERENCES		138
APPENDIX		145

LIST OF FIGURES

Figure 2-1: (a) Schematic representation of loaded laminate (b) Geometry of layered composite laminate.....	6
Figure 2-2: Schematic representing the Kirchoff hypothesis assumption that normals remain normal after deformation.....	6
Figure 2-3: (a) Pressure as a function of distance from explosion (b) peak over pressure as a function of time after explosion	14

Figure 2-4 Strain rate effect upon stress-strain curve of general metallic material	15
Figure 2-5 3-D view of blast model incorporating strain rate effects	17
Figure 2-6 Comparison of Von-Mises stress as a function of time with and without strain rate effects	18
Figure 2-7 Strain rate contours in 3-D blast model	19
Figure 2-8: GLARE composite lay-up (Taken from [20])	22
Figure 2-9: Schematic illustration of topology optimization showing tractions.....	23
Figure 3-1: Periodic composite and modeling of a discretized unit cell	32
Figure 3-2 3-D finite element model used for Explicit blast modeling.....	41
Figure 3-3 Displacement vs. time curve for Tungsten plate.....	42
Figure 3-4 Pressure vs. time curves in air directly above the plate for three different materials	44
Figure 3-5 Location of element above the plate for pressure comparisons	44
Figure 3-6 Von Mises stress vs. time for three different materials	45
Figure 3-7 Location of element on plate for Von Mises stress comparisons.....	46
Figure 3-8 Joint density function of resistance and load effects	53
Figure 4-1 Lumped mass modeling of a composite plate	58
Figure 4-2 Elastoplastic model of layer “A”	58
Figure 4-3 Friedlander blast air pressure wave ($P_m = 80$ MPa and $t_d = 0.018$ sec).....	63
Figure 4-4 Transferred stress f_{tr}	63
Figure 4-5 The maximum stress in Titanium.....	64
Figure 4-6 The maximum strain in Aluminum	65
Figure 4-7 Reliability index surfaces of Titanium layer β_R	66

Figure 4-8 Reliability index surfaces of Aluminum layer β_A	67
Figure 4-9 β_R contour	68
Figure 4-10 Overlapping β_A and β_R contours to show the optimal combination of layer thicknesses (as marked in black dot) and the corresponding weight cost function for reference.....	69
Figure 4-11 Dynamic responses of Aluminum layer of the composite plate consisting of 40 mm Titanium and 130 mm Aluminum due to blast air pressure wave as shown in Figure 4-3.....	70
Figure 4-12 Dynamic responses of Titanium layer of the composite plate consisting of 40 mm Titanium and 130 mm Aluminum due to blast air pressure wave as shown in Figure 4-3.....	71
Figure 4-13 Blast modeling using finite element analysis of 40 mm Titanium and 130 mm Aluminum composite plate to 104 MPa peak blast pressure at the center of the plate	72
Figure 4-14 The applied pressure distribution along y-axis	72
Figure 4-15 Plastic strain contours at time 1.5 ms	74
Figure 4-16 Von Mises stress along the mid-axis	75
Figure 4-17 Plastic strain contours at time 1.5 ms considering strain rate effect	75
Figure 4-18 Von Mises stress along the mid-axis considering strain rate effect	76
Figure 4-19: Three load cases showing unit strain in (a) x direction, (b) y direction and (c) shear.....	78
Figure 4-20: Mesh of CFD model showing buried TNT and composite plate.	80

Figure 4-21: (a) Finite element model showing the two-layer composite plate considered in the case study with ¼ removed for clarity and (b) pressure distribution at t = 0.35 ms.	82
Figure 4-22: Flowchart of optimization method and its integration with the blast simulation.....	85
Figure 4-23: Pareto front for weight and stress-to-strength ratio as two objective functions with different material microstructures and thicknesses per layer.....	86
Figure 4-24: Comparison of gradient and genetic algorithm Pareto fronts	91
Figure 4-25 Order of operation for integrated optimization environment.....	93
Figure 4-26: 6 unit strain cases used for 3-D Homogenization	94
Figure 4-27 Boundary conditions for 3-D Homogenization.....	98
Figure 4-28 In plane deformation showing shear strain	99
Figure 4-29 Boundary conditions for unit shear strain for 3-D Homogenization.....	100
Figure 4-30 Unit shear strain applied to a finite element model.....	101
Figure 4-31 Finite Element blast model developed in LS-DYNA.....	104
Figure 4-32 Pressure wave right after detonation of explosive material (t = 0.1 ms)	107
Figure 4-33 Pressure wave right before interaction with composite plate (t = 0.16 ms).107	
Figure 4-34 Pressure wave after encountering composite plate obstruction (t = 0.19 ms)	108
Figure 4-35 Stress distribution in the composite plate after (t = 0.6 ms)	108
Figure 4-36 Flowchart of optimization method and its integration with the blast simulation for the second case study	111

Figure 4-37 Pareto front for blast resistant 3-D composite plate optimization with 2 objective functions.....	113
Figure 4-38 Unit cell and coordinate system reference	115
Figure 4-39 Iteration number vs. stress/strength ratio	118
Figure 4-40 Iteration number vs. weight	118
Figure 4-41 Cost comparison of design alternatives	119
Figure 4-42 Elemental Numbering Scheme for results table.....	124

LIST OF TABLES

Table 3.1 Material Properties.....	40
Table 4.1 Characteristics of the two layers of the composite plate.....	62
Table 4.2 Constants for JWL [73].....	71
Table 4.3 Summary of results presenting ten Pareto solutions*	87
Table 4.4 Material Properties of Tungsten and Titanium.....	106
Table 4.5 Initial start point and 4 example optimal solutions labeled on the Pareto Front (White: T, Black: W)	119
Table 4.6 Stiffness matrix (GPa) Solution 8 Layer 1 $\rho = 1.38E+04 \text{ kg/m}^3$	122
Table 4.7 Stiffness matrix (GPa) Solution 8 Layer 2 $\rho = 1.15E+04 \text{ kg/m}^3$	122
Table 4.8 Stiffness matrix (GPa) Solution 7 Layer 1 $\rho = 6.56E+03 \text{ kg/m}^3$	122
Table 4.9 Stiffness matrix (GPa) Solution 7 Layer 2 $\rho = 6.00E+03 \text{ kg/m}^3$	122
Table 4.10 Stiffness matrix (GPa) Solution 2 Layer 1 $\rho = 9.33E+03 \text{ kg/m}^3$	123
Table 4.11 Stiffness matrix (GPa) Solution 2 Layer 2 $\rho = 8.77E+03 \text{ kg/m}^3$	123
Table 4.12 Stiffness matrix (GPa) Solution 1 Layer 1 $\rho = 9.88E+03 \text{ kg/m}^3$	123

Table 4.13 Stiffness matrix (GPa) Solution 1 Layer 2 $\rho = 8.77\text{E}+03 \text{ kg/m}^3$	123
Table 4.14 Summary of all Pareto front optimal solutions	125

CHAPTER 1 INTRODUCTION

1.1 Motivation and Background

Composite materials are being used for structural applications due to their high strength-to-weight ratio and flexibility in obtaining desired material properties by intelligently combining different materials. This issue becomes critical when structural applications require mechanical properties that are not available with currently used or known materials. However, the lack of plasticity mechanisms leading to premature failure is a major downfall of structural composites [1-2]. This limitation may be overcome if the composite material is designed in such a way that the weak phases are allowed to fail first, while the strong phases take over the stress via stress redistribution so that the overall composite material does not fail. Micro and nano-synthesis may be used to reinforce the weak phases with the strong phases. The issue regarding the insufficient ductility of composites becomes significant when blast resistance is of interest. Blast resistance may also be increased in laminated composites by adjusting the composite's different layer's stiffness such that the stress evolution in the composite material does not result in failure of the weak layer. This concept may be realized via multi-objective topological optimization using the microstructural homogenization method. This dissertation examines this possibility.

This dissertation introduces the homogenization technique to the design of blast resistant composites. The methods that will be integrated into the design model will include finite element (FE), computational fluid dynamics (CFD), Multi-objective genetic algorithms

(MOGA). Reliability theory is also discussed as a viable method for design. Typically, design optimization utilizes gradient-based methods. We suggest using non-gradient based methods because the design variables of our problem are discrete rather than continuous. The integration of homogenization technique for design and simulation is shown to cause little degradation in accuracy while enhancing efficiency due to computational constraints.

Design of blast resistant composites is of great interest. Most terrorist attacks are performed using some type of explosive device. Similarly, one of the greatest threats to soldiers on the modern battlefield are improvised explosive devices (IEDs). New techniques are required to design and optimize armor for blast resistance. We suggest that through optimizing microstructures using the previously introduced methods that a new generation of blast resistant composites may be designed. The new technique could be used to design armor for a range of applications from personal body armor to structural applications such as embassies.

While the methods that are presented in this dissertation are not new, the way in which the methods are being utilized and integrated is a new approach and framework. Through combining advanced simulation programs and optimization methods a new way of designing composite plates is introduced and examined using specific case studies. The validity of integrating different methods is exemplified when comparing specific cases such as the behavior of blast loading upon pure homogeneous materials versus the optimal composite plate designs. Implicit blast methods apply the same pressure wave irrelevant of the material properties or size of the plate. However, the explicit blast method allows pressure update based on stiffness and therefore is also extremely

important when optimizing structures under blast loading. The explicit blast simulation method is described in detail and is shown to be a necessary component because the blast pressure transfer is directly tied to the material properties of the plate. Therefore, each composite plate experiences a different magnitude of pressure transfer. This is crucial in terms of optimization, as the microstructure needs to be updated each iteration.

The integration of homogenization, explicit blast modeling and optimization algorithms such as multi-objective genetic algorithms is not a trivial task. Homogenization in 3-D is much more complicated than it is in 2-D. It requires more simulations to extract the homogenized properties than is required in 2-D. Each of the methods requires different inputs and outputs as well as different formatting. Multiple executables must be created to connect all the parts of the integrated optimization environment. 3-D explicit blast simulation is extremely complex and requires knowledge on a broad range of engineering practices including fluid dynamics, structural dynamics, fluid structure interaction, structural mechanics and material science. The combination of these different methods will yield new optimal microstructures that should have a good resistance to blast loading.

1.2 Dissertation Outline

The remainder of the dissertation is structured as follows: A literature review is presented in Chapter 2. Methods used for blast resistant composite design optimization are discussed in Section 3. Chapter 4 describes the case studies and is followed by Conclusions and proposed Future Work in Chapter 5.

CHAPTER 2 LITERATURE REVIEW

2.1 Structural Composites

Composite materials are one of the most widely used materials today and are used for an array of applications ranging from aircraft, spacecraft, automobiles, trains to civil structures. Many bulk materials with metallic behavior during processing are polycrystalline and therefore have approximately isotropic behavior. Isotropy does have certain areas of application, but composites can fill the niches where common metals perform poorly at. Using composites, the material can be processed in such a way that that strength and stiffness of the material is aligned so that the structure maintains the loading along the stiff directions whereas the weak directions attain only a fraction of the loading required to result in failure.

While composites exhibit poor transverse properties, the specific strength, which is the strength normalized by the density and the specific stiffness of the composite, is greater than that of homogeneous materials [3]. Therefore, the weight of composite structures is much less than that of other homogeneous metals such as steel. Composite materials include but are not limited to large-particle (particulate) composites, dispersion-strengthened composites, polymer-matrix composites, metal-matrix composites, ceramic-matrix composites, carbon-carbon composites and hybrid composites. Two general kinds of structural composites are laminar composites and sandwich panels.

Composites may be built in layers or laminae, in which there is a specific fiber orientation in each laminae. A sequence of laminae is referred to as a laminate. The method for determining the fiber orientations, raw materials and number of laminae is determined through experimental, analytical and numerical techniques. These techniques

include but are not limited to impact testing, tensile and compressive testing, classical lamination theory, multi-continuum theory, and finite element modeling [3].

The anisotropic nature of composite laminate materials requires a methodology for understanding how laminates respond to loads, how the angle of the fibers within different layers influences the behavior, and how changing the material properties in a group of layers may influence the response. Similarly, the stress and strain distribution depends not only on the type and magnitude of loading, but also the fiber orientation, stacking sequence and material distribution. The method for simplifying the analysis of fiber-reinforced composite materials is known as classical lamination theory (CLT) [4]. CLT is also known as the Kirchhoff Hypothesis. The theory makes some basic assumptions regarding the deformation of the laminate. Firstly, CLT assumes that normals remain straight (no bending) [4]. Secondly, normals maintain their original length after deformation. Finally, normals remain normal after deformation (90 degrees with the neutral plane). These assumptions are represented schematically in Figure 2-1 a) and b) and Figure 2-2. Figure 2-1 a) shows the loaded laminate and Figure 2-1 b) shows a x-z cross section of the laminate. Figure 2-2 shows the deformed laminate and the normal lines after deformation. Another set of assumptions that are required are related to the actual bonding between laminae. Perfect bond between the layers is assumed (no gap). There is no slip between layers and shear forces will not separate the layers. The overall laminate behaves like a single laminae with averaged properties. The geometric mid-plane in Figure 2-2 is considered the reference surface.

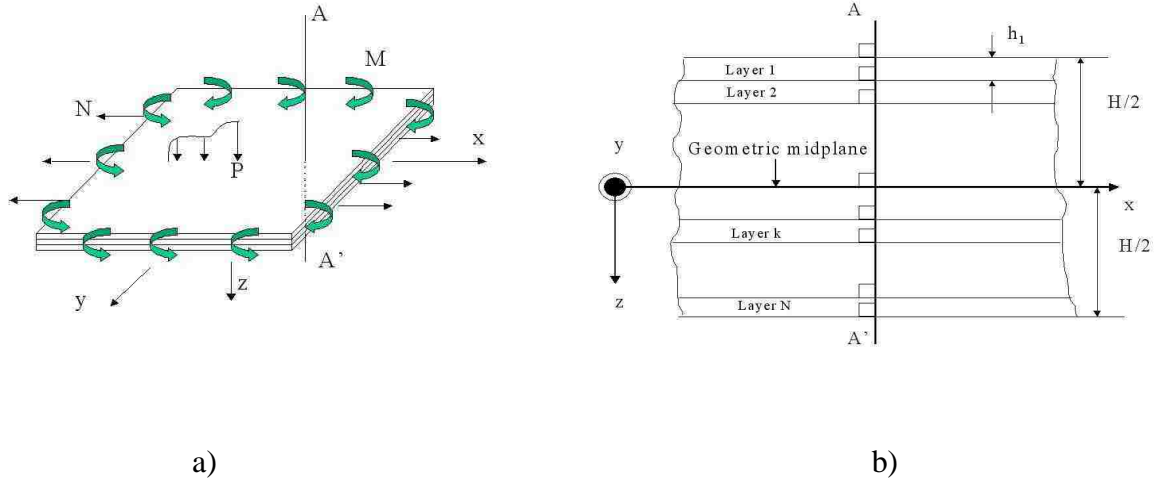


Figure 2-1: (a) Schematic representation of loaded laminate (b) Geometry of layered composite laminate

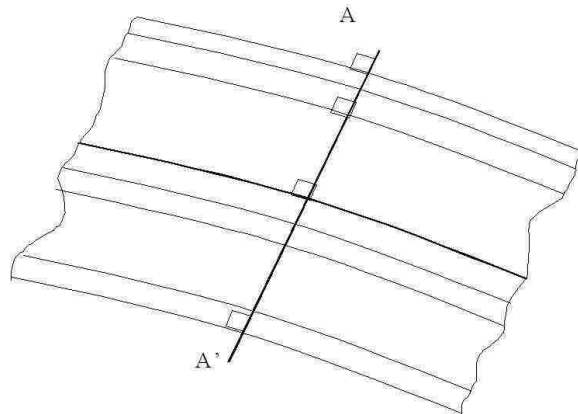


Figure 2-2: Schematic representing the Kirchhoff hypothesis assumption that normals remain normal after deformation

CLT is very similar to plate theory. The difference between the two is that plate theory assumes linear elastic isotropic properties, whereas CLT assumes that the material properties are anisotropic. This means that the stress-strain relations are more complex and the stiffness matrix of a composite laminate has many more terms than the two

independent terms of linear elastic stiffness matrices. Finally, CLT assumes the plane-stress assumption, which means that the out of plane stress, namely σ_z is set to zero. The orientation of the plate is then parallel to the x-y plane.

The displacements and non-zero strains that are a direct result of the Kirchhoff hypothesis and its assumptions are summarized below [4].

$$u(x, y, z) = u^0(x, y) - z \frac{\partial w^0(x, y)}{\partial x} \quad (1)$$

$$v(x, y, z) = v^0(x, y) - z \frac{\partial w^0(x, y)}{\partial y} \quad (2)$$

$$w(x, y, z) = w^0(x, y) \quad (3)$$

$$\varepsilon_x(x, y, z) = \varepsilon_x^0(x, y) + z\kappa_x^0(x, y) \quad (4)$$

$$\varepsilon_y(x, y, z) = \varepsilon_y^0(x, y) + z\kappa_y^0(x, y) \quad (5)$$

$$\gamma_{xy}(x, y, z) = \gamma_{xy}^0(x, y) + z\kappa_{xy}^0(x, y) \quad (6)$$

Where the strain and displacement values such as ε^0 or u^0 are the values of strain and displacement at the geometric midplane and κ is the curvature. The relationship between loading and strain for laminates using CLT theory is shown below. The matrix that relates the loading and midplane strains is known as the ABD matrix [4].

$$\begin{Bmatrix} N_x \\ N_y \\ N_{xy} \\ M_x \\ M_y \\ M_{xy} \end{Bmatrix} = \begin{bmatrix} A_{11} & A_{12} & A_{16} & B_{11} & B_{12} & B_{16} \\ A_{12} & A_{22} & A_{26} & B_{12} & B_{22} & B_{26} \\ A_{16} & A_{26} & A_{66} & B_{16} & B_{26} & B_{66} \\ B_{11} & B_{12} & B_{16} & D_{11} & D_{12} & D_{16} \\ B_{12} & B_{22} & B_{26} & D_{12} & D_{22} & D_{26} \\ B_{16} & B_{26} & B_{66} & D_{16} & D_{26} & D_{66} \end{bmatrix} \begin{Bmatrix} \varepsilon_x^0 \\ \varepsilon_y^0 \\ \gamma_{xy}^0 \\ \kappa_x^0 \\ \kappa_y^0 \\ \kappa_{xy}^0 \end{Bmatrix} \quad (7)$$

There are specific formulas for calculating the coefficients in the ABD matrix. N and M are the line loads and moments respectively. ε is the strain at the midplane and κ is the curvature at the midplane.

Multi-continuum theory (MCT) is another theory used for simplifying the analysis of composite laminates. MCT is a true mechanics based failure theory for composites. The theory is independently applied to both the fiber and matrix, without modeling individual fibers throughout the structure. It is called MCT because both the fiber and the matrix are modeled as a continuum [4]. MCT models the independent mechanics of fiber and matrix deformation and failure. It also recognizes the relationship between stresses in local fiber and matrix stresses. Typically, as in CLT theory, the average composite stresses are calculated. Given average stresses, MCT can calculate the fiber and matrix stresses. Similar to rule of mixtures (ROM) techniques, an analytical model is used to decompose the composite stress and strain fields into fiber and matrix stress and strain fields. The difference is that for MCT the analytical model is much more complex. MCT can include a non-linear finite element analysis of a unit cell that includes progressive material stiffness and strength degradation.

We can define the averaged stress over the domain as [4]:

$$\bar{\sigma} = \frac{1}{V} \int_D \tilde{\sigma}(x) dV \quad (8)$$

This is the method used by traditional failure theories which are applied at the continuum level. We can then define an average stress over the fiber (α) and an average stress over that matrix (β).

$$\sigma_{\alpha} = \frac{1}{V_{\alpha}} \int_{D_{\alpha}} \sigma_{\alpha}(x) dV_{\alpha} \quad (9)$$

$$\sigma_{\beta} = \frac{1}{V_{\beta}} \int_{D_{\beta}} \sigma_{\beta}(x) dV_{\beta} \quad (10)$$

Therefore we retain the identity of the constituents and refer to their coexistence as a multi-continuum. Then the average stress over the composite domain is:

$$\tilde{\sigma} = \phi_{\alpha} \tilde{\sigma}_{\alpha} + \phi_{\beta} \tilde{\sigma}_{\beta} \quad (11)$$

Where ϕ_{α} is the fiber volume fraction and ϕ_{β} is the matrix volume fraction. MCT may be used to extract continuum (averaged) constituent (fiber and matrix) stress and strain fields during the course of a routine finite element analysis. Failure theory is then applied at the constituent level. This provides more information regarding the failure or damage state of a material. The computational efficiency of MCT is also paramount to other methods [4].

Composites may be produced by intelligently designing the macro, meso, micro and nanostructures to combine different materials. A composite is the combination of any two or more materials in order to achieve an enhancement in properties. Composites may be, but are not limited to, the combination of fibers, metals, ceramics and polymers as well as combinations of three or more of the previously listed materials.

2.2 Fiber Reinforced Composites

Fiber-reinforced composite (FRC) materials are composite materials that are composed of fibers that are surrounded by a matrix of a different material type. The idea of utilizing the weak and strong phases of a material to orient the composite for a given loading

application is the central idea to FRC. Fibers must be aligned with the loading direction, the loading must be transferred from the fiber to the matrix, and finally the fibers must stay aligned to restrain the loading [3]. While FRCs perform well along the fiber direction, the transverse properties and shear properties are poor because of being governed by the matrix. This is not a bad thing as long as the application of the final structure has been carefully studied and all possible loads have been considered. Fibers usually have diameters on the order of 5 μm -100 μm [5]. Stiffness and strength of fibers range between 70-800 GPa and 1000-7000 MPa respectively. Failure strains as high as 5% are attainable [5].

Matrix materials are typically polymer based and are referred to as resins. Resins make up between 30-40 percent of the composite by volume. The matrix also acts as a barrier to protect the fibers from the environment. There are two types of resins, which are thermosets and thermoplastics. The main difference is their behavior under temperature. Thermosets cure when they are heated during which irreversible crosslinks are formed [3]. Subsequent heating will only degrade the resin. On the other hand thermoplastics can be continually heated and cooled. This process can be utilized to repair portions of the resin. The stiffness and strength of resins are about 2-5 GPa and 50-100 MPa respectively. Resins are also strain rate dependent because of the temperature effect.

2.3 Metallic Composites

New synthesis methods have been created to produce new generations of composites with enhanced mechanical properties. Suiyuan et al. [6] produced copper-based self lubrication composites with different amounts of graphite. The Cu based composites

were produced using powder metallurgy by atomizing Cu₁₀Ni₃Sn₃Pb (wt.%) alloy with 0.5 wt.% Y₂O₃ as the matrix [6]. Lower graphite percentages yielded better mechanical and frictional properties, while larger graphite percentages resulted in enhanced lubrication properties. Enhanced surface properties generally result in a better overall mechanical behavior to loading and crack propagation.

Metallic composites may also be in the form of nanoparticles and nanocomposites. The electrical and mechanical properties of nanocomposites created through implantation of Gold and Titanium into polydimethylsiloxane were reported by Niklaus and Shea [7]. They were able to show the electrical conductivity and Young's modulus were directly tied to the implantation parameters and the volume fractions. It was shown that percolation theory could describe the conductivity and stiffness of the composite very well. The interactions between nanoparticles have different effects upon the material properties.

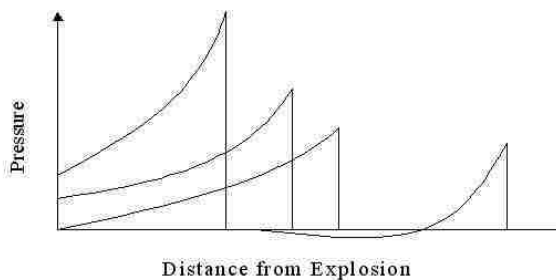
Another type of metallic based composite is the metal matrix cast composite. Tests have been performed on Mg₂Si particulate Aluminum matrix cast composites [8]. The effect of tool rotation speeds and welding upon both the microstructure and mechanical properties was examined. Optical and SEM techniques were used. The composite was tested for microhardness and tensile strength. It was shown that changes in synthesis processing and the composite microstructure have strong reflection on composite properties [8].

2.4 Blast

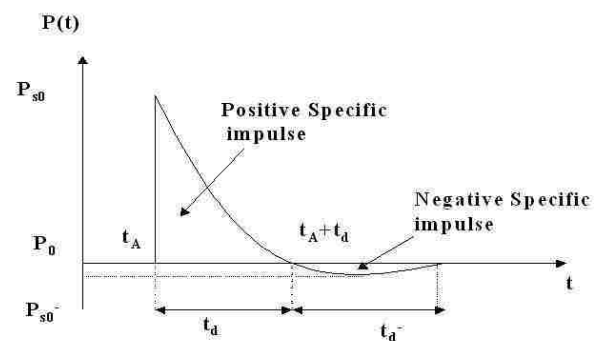
Explosives have been used to defeat both structures and people for over a thousand years. Some of the first bombs used in anger were thought to have been used by the Mongols against the Japanese during the Mongol invasion of Japan after the Yuan Dynasty [9]. During the 20th century the invention of Trinitrotoluene (TNT), smokeless powder and nuclear weapons radically expedited the effectiveness and devastating ability of explosives [10]. Through knowledge of mechanics, fluid dynamics and fluid structure interaction, the process of physical, chemical and nuclear explosions have been rigorously examined. Great improvements have been made with regard to gaining a detailed understanding of blast phenomena [10].

Explosions are classified as a sudden or instantaneous release of energy. This process proceeds rapidly with in a very short period of time [11]. Examples of physical explosions are volcanic eruptions and failure of pressurized gas containment vessels such as a diver's oxygen tank. Finally, chemical explosions are the result of combining two different materials such as oxygen with hydrocarbons which results in combustion [11]. Explosives may be created from different phases of materials including solids, liquids and gases. Generally, high explosive materials are formed from solid base materials. There are two main types of explosives: Primary and Secondary. Primary explosives may detonate easily and sometimes just on contact. Armstrong's mixture which contains Potassium Chlorate and Red Phosphorus is extremely sensitive explosive material and is usually considered a primary high explosive [12]. Primary explosives such as blasting caps are used to detonate secondary explosives. A common secondary explosive is Trinitrotoluene (TNT) [10-11].

During a detonation of a high explosive material (chemical) the pressure may rise to around 30 GPa and the temperature may get as hot as 4000° C. Since the gas is both hot and extremely pressurized, the currently occupied volume is forced outward in order to equilibrate. Consequently, this moving hot pressure wave compresses the air around it. This compressed air is what is called the blast wave. It is within this blast wave that most of the energy is released. This blast wave will rise to a maximum value of pressure greater than ambient pressure. At a given time during the explosion process, the pressure behind the blast wave can drop below the ambient pressure creating a partial vacuum. The pressure as a function of distance and the pressure as function of time are shown in Figure Figure 2-3 (a) and Figure 2-3 (b) respectively. In Figure 2-3 (b) P_{s0} is the peak over pressure, P_0 is the ambient pressure, t_A is the arrival time and t_d and t_d^- are the positive and negative impulses times respectively. As can be seen in Figure 2-3 (a) the pressure profile is a function of the distance from the point of detonation. The reason for the specific shape of the curves is due to the supersonic flow of the blast wave. The blast wave compresses the air in front of the expanding gasses which makes the air denser. This change in density increases the resistance to the blast wave itself.



(a)



(b)

Figure 2-3: (a) Pressure as a function of distance from explosion (b) peak over pressure as a function of time after explosion

The effect of blast loading upon structures has been shown to depend mostly upon the energy that is released during an explosion and the distance of the explosion from the structure. Currently, and as a matter of convenience, explosive charges are described in terms of an equivalent charge of TNT. For example, the atomic bomb Fat Man, that was dropped on Nagasaki, Japan on August 9, 1945 had a yield of about 88 Tera Joules, which equates to 21 kilo tons of TNT [13]. By always using TNT equivalents then a scaling parameter Z may be defined as

$$Z = \frac{R}{W^{\frac{1}{3}}} \quad (12)$$

Here R is the offset distance from the explosion in meters and W is the equivalent charge weight in kilograms. Approximate values of the peak overpressure P_{s0} were first performed by Brode in 1955 [14]. Here he determined two different regimes for P_{s0} .

$$P_{s0} = \frac{6.7}{Z^3} + 1(\text{bar}) \quad (P_{s0} > 10 \text{ bar}) \quad 13(\text{a})$$

$$P_{s0} = \frac{0.975}{Z} + \frac{1.455}{Z^2} + \frac{5.85}{Z^3} - 0.019(\text{bar}) \quad (0.1 \text{ bar} < P_{s0} < 10 \text{ bar}) \quad 13(\text{b})$$

A different relationship determined in 1987 by Mills [15] where P_{s0} is expressed in kPa is described as.

$$P_{s0} = \frac{1772}{Z^3} - \frac{114}{Z^2} + \frac{108}{Z} \quad (14)$$

Another important concept during blast loading is the idea of reflected pressures. When blast waves are prohibited from propagating due to an obstacle that is perpendicular to

the propagation direction then the pressure is reflected and actually increases the overpressure to maximum reflected pressure. Approximate value of the peak reflected pressure is given by Equation (15).

$$P_r = 2P_{s0} \left\{ \frac{7P_0 + 4P_{s0}}{7P_0 + P_{s0}} \right\} \quad (15)$$

Where P_{s0} is the form used in equation 13(a).

2.5 Strain rate effects upon materials

The strain rate has a significant affect when considering the response of elastic-plastic materials exposed to blast loading. If a blast, impact or other loading event causes a plastic deformation, the strain rate has a direct relation to the actual value of the yield stress. Figure 2-4 shows the effects of strain rate upon a general stress strain curve for a metallic specimen. In order to take into account the effect of strain rate upon materials many different empirical models have been proposed. The following section will introduce these models as well as examine a specific case of an Aluminum plate that is subjected to a blast loading.

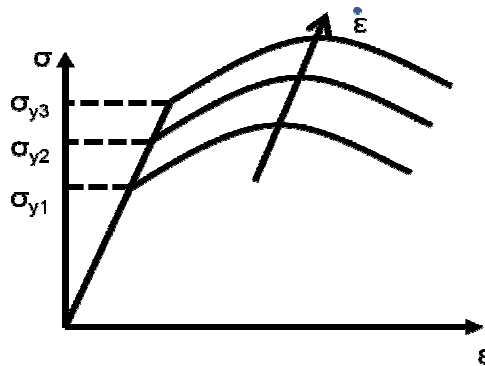


Figure 2-4 Strain rate effect upon stress-strain curve of general metallic material

The equations used to model the constitutive relationships of metallic materials that incorporate the strain rate effect are empirically based. One of the most commonly used strain rate equations is the Johnson-Cook equation [16].

$$\sigma = [A + B\varepsilon_p^n] \left[1 + C \ln \left(\frac{\dot{\varepsilon}_p}{\dot{\varepsilon}_0} \right) \right] \quad (16)$$

Here the stress is a function of the empirically determined parameters A,B and C as well as a reference strain rate $\dot{\varepsilon}_0$, and the current plastic strain ε_p and plastic strain rate $\dot{\varepsilon}_p$.

The Johnson-Cook equation may only be used for determining the stress under high strain rates. The equation was modified by Kang so that it may be used for a wide range of strain rates. This was done by making the relationship a quadratic relationship [16].

$$\sigma = [A + B\varepsilon_p^n] \left[1 + C_1 \ln \left(\frac{\dot{\varepsilon}_p}{\dot{\varepsilon}_0} \right) + C_2 \left(\ln \left(\frac{\dot{\varepsilon}_p}{\dot{\varepsilon}_0} \right) \right)^2 \right] \quad (17)$$

Finally, one of the most widely used relationships for modeling strain rate dependence upon yield stress is the Cowper-Symonds equation. The Cowper-Symonds relation is used in many commercial finite element codes and the empirical constants for a lot of different metals have been experimentally determined [17].

$$\sigma = [A + B\varepsilon_p^n] \left[1 + \left(\frac{\dot{\varepsilon}_p}{C} \right)^{1/P} \right] \quad (18)$$

The two main parameters describing effects of strain rate in this expression are P and C which are empirical parameters that are different for all metals. The Cowper-Symonds equation will be used to modify the yield stress in the first case study presented in the latter sections of this dissertation.

In order to show the significance of the Cowper-Symonds power law a finite element example will be presented. In this example a plate of Aluminum is subjected to a blast

load produced by the detonation of TNT. The model is comprised of air, TNT and Aluminum. Two separate cases are compared. The first case is without the strain rate effect and the second case includes the strain rate effect. The specifics of the finite element model are presented in chapters 3 and 4 under the explicit blast modeling. Aluminum has a young's modulus of 70 GPa, a yield stress of 55 MPa, a Poisson's ratio of 0.33 and a density of 2700 kg/m³. The Cowper-Symonds parameters C and P are 6500 and 4 respectively. An isometric view of the finite element model is shown with the pressure wave at t = 0.07 ms in Figure 2-5. The Von-Mises stress at the top of the Aluminum plate subjected to the blast load is plotted for the two cases in Figure 2-6.

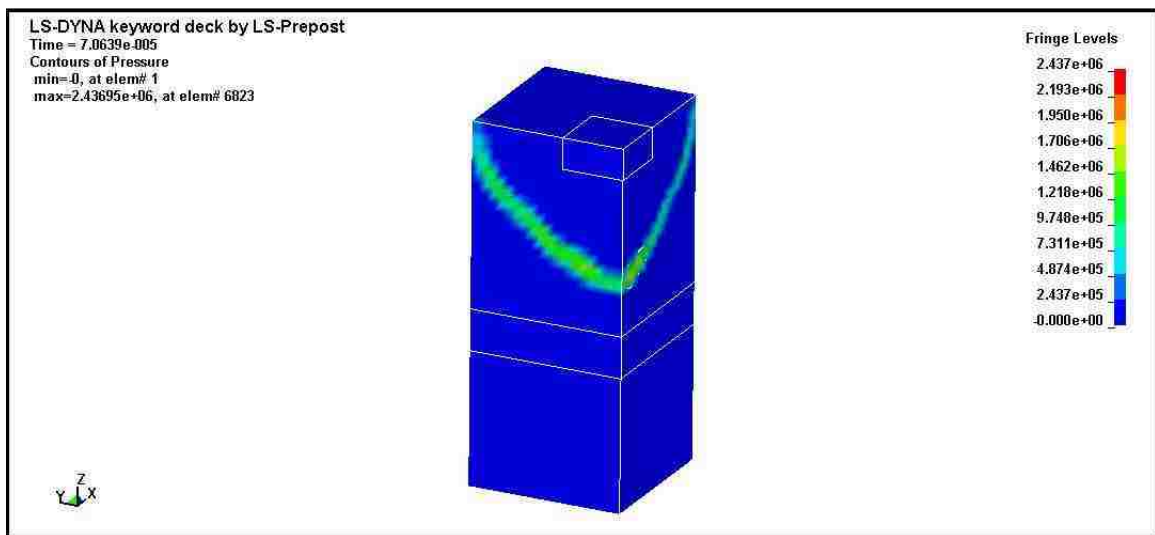


Figure 2-5 3-D view of blast model incorporating strain rate effects

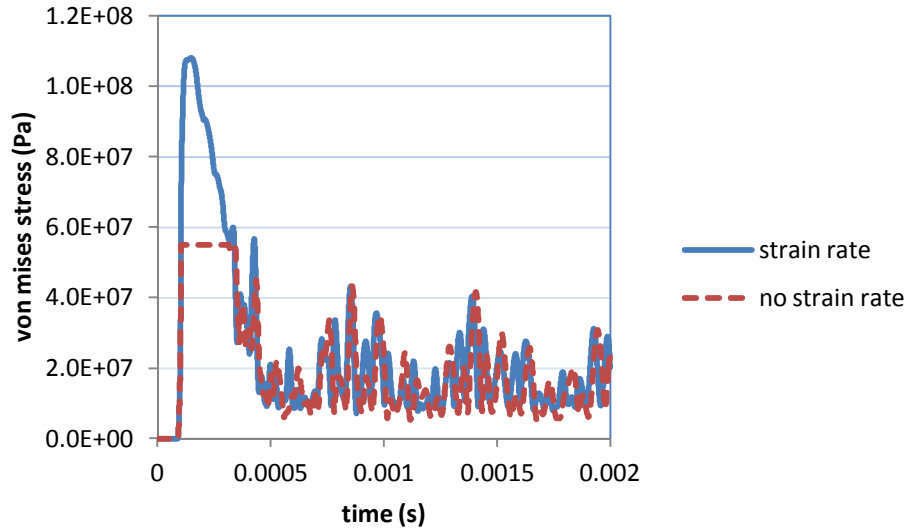


Figure 2-6 Comparison of Von-Mises stress as a function of time with and without strain rate effects

As is evident in Figure 2-6 the addition of the Cowper-Symonds strain rate effect equation to the numerical solution has a significant impact. When studying strain rate effects in solid modeling it is important to check the strain rate value and determine whether or not solid mechanics applies. The maximum strain calculated in the model is approximately 100/s. This value is much smaller than the boundary value of about $10^6/s$. If the strain rate was above $10^6/s$ then the material would act like a fluid and not a solid body. Contours of strain rate are shown in Figure 2-7.

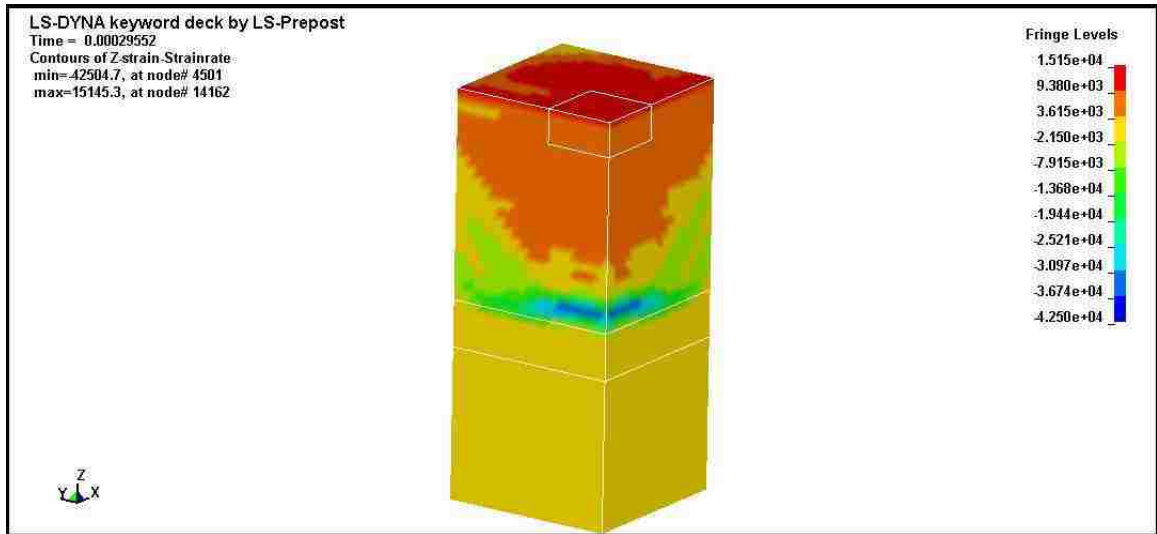


Figure 2-7 Strain rate contours in 3-D blast model

In the case in which strain rate effects are neglected, Aluminum reaches its static yield strength of 55 MPa with in a fraction of a microsecond. On the other hand when utilizing the Cowper-Symonds power law which realistically describes strain rate effect it is evident that the Aluminum plate does not yield and that the strain rate effect allows the plate to attain a stress of over 100 MPa while remaining elastic. When modeling structural materials that encounter blast waves that create stresses above the elastic limit it is necessary to include the strain rate effect. It is also important to check the wave velocity in the material to be sure that the velocity is below the speed of sound in the material. The speed of sound in Aluminum is 5090 m/s. The stress waves in the material were traveling at about 3200 m/s. Therefore, a shock wave was not created because the Mach number was below 1.

2.6 Failure of composites due to impact and blast

Composites are typically strong as long as they are loaded in the fiber direction for fiber composites or loaded in a direction that was preprocessed to have a relatively high stiffness. When a composite is subjected to a blast wave such as a CFRP laminate being subjected to a uniform pressure wave that is oriented normal to the laminate plane, the fibers do little to restrain the deformations. Similarly, the impact resistance of most composites is good as long as the developed stresses are aligned with the strong directions of the composite. In the transverse directions composites usually have a poor blast and impact resistance. Five major failure mechanisms of composite failure under impact and blast are listed in the literature [5].

These five mechanisms include fiber failure due to fiber fracture and matrix microcracks leading to macro fracture of the composite. Debonding between the fiber and the matrix may lead to failure because the stress may no longer be shared by the fiber and the matrix which can cause one phase to fail. Composites may also fail due to delamination of adjacent laminates, which results from interfacial shear stresses exceeding the shear strength. Finally, fiber pull out from the matrix and stress relaxation may lead to macro failure of the composite.

Fiber composites are easily damaged by impacts because there is little or no plastic deformation during loading [5]. They behave elastically to failure, and unlike metals that can still bear the load after deformations, composites become irreversibly damaged after large deformation. In summary, composites are impact damage prone due to low transverse and inter laminae shear strength and little or no plastic deformation. Yet, by appropriately choosing the laminar stacking sequence the anisotropy can be reduced and

blast or impact resistance might be increased [5].

Many experiments have been performed to examine the blast resistance of composite materials. Fedorenko et al. [18] utilized experimental data regarding the dynamic response and strength of simple FRP shells to propose different composite lay-ups for blast proof structures. They showed that composites out performed homogeneous metals when used as load bearing shells for blast resistant structures. A specific criterion for selecting composite fibers was described. Bambach et al. [19] tested solid Aluminum beams strengthened with CFRP sheets. Epoxy was used to bond the CFRP to the Aluminum beams. Static and impact tests were performed on the specimens. Explosives were applied to the fully clamped Aluminum beam specimens to create an impact load. Results showed that as the beams plastically deformed the CFRP sheet bonded to the beam absorbed a large amount of energy [19]. Although the tests showed an increase in blast resistance, many of the other layers debonded from one another. Another composite, with the trade name GLARE, has been suggested as a new generation of blast resistant material [20]. GLARE is a fiber metal laminate that is a new hybrid structures composite that consists of a combination of metal and FRP sheets. Langdon et al. [20] reported on blast experiments on GLARE and initial findings showed that the GLARE composite preformed similarly but with enhanced characteristics to those of monolithic Aluminum plates. The GLARE layup is shown in Figure 2-8.

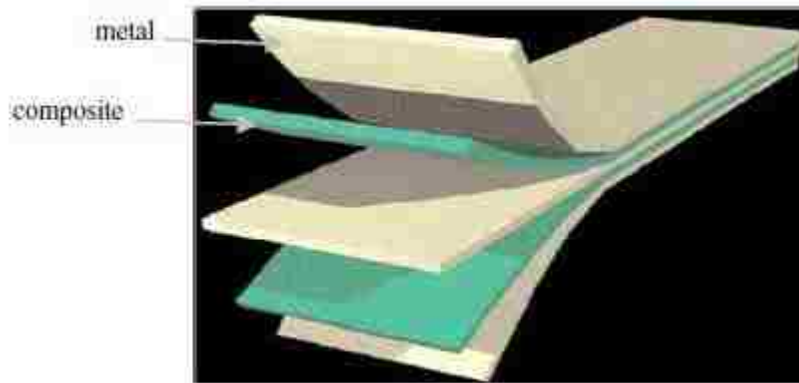


Figure 2-8: GLARE composite lay-up (Taken from [20])

2.7 Optimization

2.7.1 Topology Optimization and Homogenization

Topology optimization is of great interest to the aerospace and automobile industries. Topology optimization allows for the design of structures with holes or cavities that reduces weight while maintaining desired stiffness. The introduction of homogenization techniques by Bendsøe and Kikuchi reintroduced topology optimization to structural design [21]. Traditional topology optimization problems are defined over an elastic region V with a specific boundary A and outward normal n . Within different regions of the domain displacements, zero traction and non-zero tractions are prescribed. The goal of topology optimization is to effectively and efficiently distribute a minimal amount of strong material with an elasticity tensor C^1 and a weak material with elasticity tensor C^2 in order to minimize structural compliance. Figure 2-9 schematically represents the topology optimization problem [22].

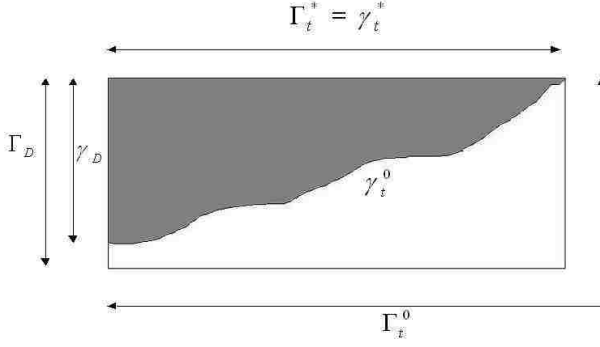


Figure 2-9: Schematic illustration of topology optimization showing tractions

The mathematical formulation of the topology problem is shown below [22]:

$$\min c(\chi) = \frac{1}{2} \int_V \varepsilon(u)(\chi C^1 + (1 - \chi)C^2)\varepsilon(u)dv \quad (19)$$

$$\chi \in \{0,1\}$$

$$\text{such that } u \in H_0^1 \text{ satisfies } \int_V \nabla v(\chi C^1 + (1 - \chi)C^2)\varepsilon(u)dv + \int_{A_t} utda \quad \text{for all } v \in H_0^1 \quad (20)$$

$$\text{and } g(\chi) = \frac{1}{vol(V)} \int_V \chi dv - v \leq 0 \quad (21)$$

Where χ is 1 for a strong material and 0 for a weak material. In the previous Equations u is the displacement field, H is the admissible displacements, v is the virtual displacements field, ε is the infinitesimal strain field, t is the tractions, and v is the maximal volume fraction of the strong material.

Topology optimization has been successfully applied to optimize structural geometry like trusses and frames [21, 23], and to optimize composite plates and membranes [24-26].

The objective functions in topology optimization are typically compliance and/or weight, but other objectives such as dynamic response and thermoelastic characteristics have also been considered [27-28]. The idea of enhancing the elastic structural response has been examined with different methods in the past. The automotive industry has examined

using shape optimization and topology optimization for mechanical design of automobile parts [29]. Size and shape optimization were demonstrated incapable of solving topology problems for either discrete or continuous structures [30]. A limitation of shape optimization is having domains with free boundaries, whereas topology optimization sets a range of possible material alternatives and chooses the optimal material alternative for given constraints and conditions. The topology optimization must be formulated correctly to ensure that the problem is not ill posed. An initial topology shall be chosen with parameterized boundaries to reduce the difficulty of dealing with the free boundary [30].

Homogenization theory achieved a breakthrough for simulation of composite structures. It enables deriving macro field Equations from micro field characteristics. Essentially, a unit cell representing the composite is simulated using known strain fields and the stress outputs are used to determine the average or homogenized properties of the unit cell. Sanchez and Palencia [30] examined wave propagation in heterogeneous media using homogenization theory. Keller [31] studied the flux through a porous media using techniques in homogenization. Bakhvalov and Panasenko introduced some of the first numerical techniques for solving the homogenization Equations [32]. De Kruijff et al. [33] presented an optimization algorithm for material design in two dimensions when considering multiple objectives. The optimization algorithm was formulated as a minimization problem that was subject to volume and symmetry constraints. A Pareto front of optimal solutions was obtained by using the multi-objective weighted sum method to address both stiffness and conductivity criteria [33]. Finally, Guedes and

Kikuchi [34] introduced an adaptive finite element technique for elasticity representation in homogenization of composites.

2.7.2 Sensitivity Analysis

Traditional optimization methods use gradient-based algorithms to determine optimal solutions. Gradient-based methods utilize objective function gradient values to update optimal designs. These derivatives (or gradients) play a fundamental and critical role with design optimization, inverse analysis and reliability. The gradients are more commonly referred to as sensitivities [22]. They are referred to as sensitivities because they represent a measure of how sensitive a response measure (objective) is to changes in the design variables. Sensitivities are also useful in trade-off studies to estimate the effects that changes in design variables will have on system performance.

Mathematically, the design variables may be expressed as: $\bar{x} = [x_1, x_2, \dots, x_i, \dots, x_n]$ (22)

x_i is the i th variable and $i = 1, 2, \dots, n$,

\bar{x} is the vector of design variables.

The objective functions are described as:

$$f_1, f_2, \dots, f_k \quad (23)$$

The inequality constraints of the optimization problem are defined as:

$$g_1, g_2, \dots, g_k \quad (24)$$

The sensitivities of the objective functions and the constraints are the gradients of the objective functions and the constraints respectively [22].

$$\nabla f(\bar{x}), \nabla g(\bar{x}) \quad (25)$$

In the case of topological optimization problems the problem is usually formulated as a non-linear programming (NLP) problem so that the design vector \bar{x} is determined in order to minimize or maximize the objective functional values while satisfying inequality constraints. Due to the nonlinearity of the problem, it must be solved in an iterative manner. At each iteration, the objective function values and constraint function values are evaluated in order to update the design. Objective function evaluations require expensive computational time, especially if the model being optimized is a finite element model. The number of design variables is directly coupled to the number of required FE or model runs that must be completed to determine sensitivities for updating model designs. Sensitivity analysis is a method for determining the sensitivities for a given problem without evaluating all the sensitivities though the typical method of changing single design variables and determining their individual changes to the objective functions and constraints. In order to simplify the manner in which we will discuss the different methods of sensitivity analysis it will be assumed that through discretizing the governing Equations of finite element a residual equation may be obtained in the form [22]:

$$R(U) = 0 \tag{26}$$

This residual Equation must be solved for the displacement vector U . This process is referred to as the primal analysis. The algorithm is initiated by assuming an initial guess U^0 . Updates are made by solving Equation 26.

$$K\Delta U = R(U^i) \tag{27}$$

K is defined as the tangent stiffness matrix where:

$$K = \frac{-dR}{dU}(U^i) \tag{28}$$

ΔU is calculated and used to update U . Iterations continue until the convergence criteria is met. The objective functions (f_i) and constraints (g_i) may be expressed in general terms as:

$$\Theta(\bar{x}) = \Pi(U(\bar{x}), \bar{x}) \quad (29)$$

Then using the chain rule, the sensitivity may be obtained as [22]:

$$\nabla\Theta = \frac{\partial\Pi}{\partial U} \frac{dU}{dx} + \frac{\partial\Pi}{\partial x} \quad (30)$$

In Equation (30) the derivatives $\frac{\partial\Pi}{\partial U}$ and $\frac{\partial\Pi}{\partial x}$ are both explicitly known whereas the

derivative $\frac{\partial U}{\partial x}$ is implicitly known. Therefore, when the number of design variables is

high then the FE simulation must be repeated numerous times. The process must be repeated for every iteration. Methods for alleviating this problem include the efficient adjoint sensitivity method and the direct differentiation method. With regard to the direct differentiation method, the derivative $\frac{\partial U}{\partial x}$ may be obtained by solving what is called the pseudo problem [22].

$$K \frac{dU}{dx} = \frac{\partial R}{\partial x} \quad (31)$$

Gradient based algorithms such as Newton, steepest decent and Fletcher-Reeves may be used for the design of composite laminate structures with increased blast resistance.

2.7.3 Multi-Objective Optimization

Classical optimization approaches have always considered a single objective function while dealing with all other objectives as constraints. The objective function is the mathematical formulation of the criteria by which all solutions must be compared [35]. These functions must be formulated and computed based on changes in the design variables. The fundamental difference between single-objective and multi-objective optimization is the ability of multi-objective optimization to avoid the artificial fixes needed for single-objective optimization methods to address tradeoffs between different objectives. For instance, to meet one desired objective one might not achieve the other optimal objective but achieve both to some extent. This is achieved by getting candidate designs to lie in the Pareto front, typically known as Pareto-optimal solutions [36]. Two categories of multi-objective optimization methods are identified in the literature [37]. The first category utilized classical single objective optimization methods while reformulating the problem to address multi-objectives considering preferences [35]. Methods in the first category include techniques such as the weighted sum method, the ε -constraint method and the hierarchical optimization method [35]. The weighted sum method has been widely used. The basic idea of weighted sum method is that all objective functions are combined to form a single function in which each individual objective is weighted differently.

$$f(\bar{x}) = \sum_{i=1}^k w_i f_i(\bar{x}) \quad (32)$$

where

$$\sum_{i=1}^k w_i = 1 \quad (33)$$

The hierarchical method finds optimal solutions by ordering criterion based on relative importance. If we consider the iterator i to range from 1- k , then the k^{th} criterion would be considered to be the least important. The objectives are then minimized separately and constraints are added after each successive objective function is minimized to reflect the previous functions. The method is described after [35].

1) find the minimum value for the 1st and most important criterion (objective).

$$\bar{x}^{(1)} = [x_1^{(1)}, x_2^{(1)}, \dots, x_n^{(1)}]^T \quad (34)$$

where

$$f_1(\bar{x}^{(1)}) = \min f_1(\bar{x}), \bar{x} \in X \quad (35)$$

2) Find the minimum of the i^{th} objective where this process is repeated for $i = 2, 3, \dots, k$.

$$\bar{x}^{(i)} = [x_1^{(i)}, x_2^{(i)}, \dots, x_n^{(i)}]^T \quad (36)$$

where

$$f_i(\bar{x}^{(i)}) = \min f_i(\bar{x}), \bar{x} \in X \quad (37)$$

At each iteration, constraints are added to the optimization problem.

$$f_{j-1}(\bar{x}) \leq \left(1 \pm \frac{\epsilon_j - 1}{100}\right) f_{j-1}(\bar{x}^{j-1}) \quad \text{for } j=2, 3, \dots, k \quad (38)$$

The second category of multi-objective optimization methods establishes an optimization method that is multi-objective in nature. Rosenberg [38] suggested using genetic search to simulate the behavior of single celled organisms with multiple objectives. Multi-

objective optimization techniques may utilize either gradient or non-gradient based algorithms.

In recent years multi-objective optimization has been utilized in optimizing composite materials and structures for enhanced behavior and properties. The new method combines the best features from local search algorithms like simulated annealing and tabu search [39]. Multiple start points are used to reduce the possibility of determining local optimal structures as opposed to global optimums. The method is tested through optimizing the stacking sequence of composite plates, shells and pressure vessels. To quantify the effectiveness of the hybrid method, it is compared with other methods such as Non sorted genetic algorithm (NSGA-II) and Pareto Achieved Evolutionary Strategy (PAES) and Multi-Objective Particle Swarm Optimization (MOPSO) [40]. Rao and Shyju [40] introduced an experienced based algorithm for multi-objective design of hybrid laminate composite structures. Abouhamze and Shakeri introduced a multi-objective optimization algorithm for determining the optimal stacking sequences of laminated cylindrical panels using genetic algorithms and neural networks [41]. An FE code capable of determining the first natural frequency as well as buckling loads of the composite laminate is integrated with the optimization algorithm. Outputs are used to train neural networks and Genetic Algorithms (GA) is used to find the optimal solution. Gillet et al. [42] studied the influence of design variables in both single and multi-objective optimization of elementary plates and structures. Component materials and all possible orientations were modeled using finite element analysis (FEA). The results of the FEA code were used to access the sensitivities of the design variables. Based on the most important parameters a design rule was formulated for optimizing high performance

composites. GA was shown to be successful when applied to both single and multi-objective optimization [42].

CHAPTER 3 METHODS FOR DESIGN OPTIMIZATION OF BLAST

RESISTANT COMPOSITES

3.1 Homogenization

The homogenization method is used to calculate the average constitutive parameters of a composite material. This is necessary for analysis of inhomogeneous material because the elasticity tensor E_{ijkl} varies at the microscopic scale. The homogenization method may be applied to periodic composites in which the composite consists of a periodic unit cell that is repeated as shown in Figure 3-1. An assumption must be made in which the microstructure is much smaller than the part or structure that will be used in a particular application. The selected unit cell shall respect the scale separation concept $L_{\text{micro}} < L_{\text{cell}} < L_{\text{macro}}$. We consider a periodic composite body as shown in Figure 3-1.

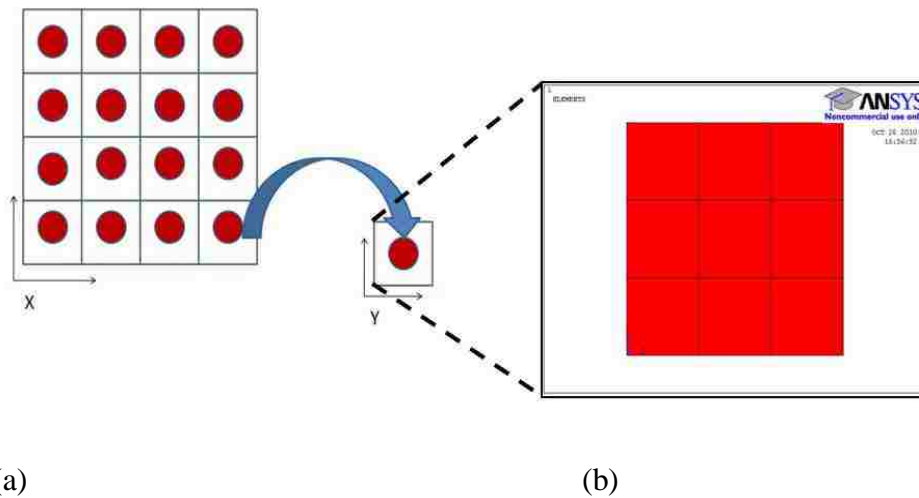


Figure 3-1: Periodic composite and modeling of a discretized unit cell

The material behavior at the macroscopic scale is described by coordinate system X while the microscopic scale is defined by coordinate system Y. Using the homogenization method for elasticity one can consider:

$$Y = [0, Y1], [0, Y2], [0, Y3] \quad (3-D) \quad (39)$$

$$Y = [0, Y1], [0, Y2] \quad (2-D) \quad (40)$$

Y1 is the horizontal length, Y2 is the vertical length, and Y3 is the depth of the unit cell.

For an inhomogeneous material the microscopic displacement u may asymptotically expanded with relation to the base cell size η [43].

$$u = u^0(x, y) + \eta u^1(x, y) + \eta^2 u^2(x, y) + \dots \quad (41)$$

$$y = x / \eta \quad (42)$$

Considering Equation (41), only the first order terms of the asymptotic expansion are used to calculate the strain fields. The strain field can be broken down into two different components when using only first order terms from Equation (41) as follows:

$$\varepsilon_{ij}^0 = 1/2 \left(\delta u_i^0 / \delta x_j + \delta u_j^0 / \delta x_i \right) \varepsilon_{ij}^0 = 1/2 \left(\delta u_i^0 / \delta x_j + \delta u_j^0 / \delta x_i \right)$$

(43)

$$\varepsilon_{ij}^* = 1/2 \left(\delta u_i^1 / \delta y_j + \delta u_j^1 / \delta y_i \right) \quad (44)$$

The overall microscopic strain field ε_{ij} is therefore a combination of the of the strain field due to the average displacement over the unit cell ε_{ij}^0 and the fluctuation strain ε_{ij}^* , which is due to the first order inhomogeneous nature of the composite unit cell [43]. The size of the unit cell η is allowed to go to zero. Then four linearly independent strain fields are applied to the unit cell in order to calculate the stiffness matrix of the composite. Four unit tensors are applied in 2-D and nine unit tensors are applied in 3-D. In 2-D the four

unit tensors are $\varepsilon^{0(11)}_{ij}=[1,0,0,0]$, $\varepsilon^{0(22)}_{ij}=[0,1,0,0]$, $\varepsilon^{0(12)}_{ij}=[0,0,1,0]$ and $\varepsilon^{0(21)}_{ij}=[0,0,0,1]$.

The homogenized stiffness tensor may be written as:

$$E^H_{ijkl} = \frac{1}{Y} \int_Y E_{ijpq} (\varepsilon^{0(kl)}_{pq} - \varepsilon^{*(kl)}_{pq}) dY \quad (45)$$

By applying these test strains along with the change in η to 0, the fluctuation strain is the solution to the following variation type problem.

$$\int_Y E_{ijpq} \varepsilon_{ij}(\mathbf{v}) \varepsilon^{*(kl)}_{pq} dY = \int_Y E_{ijpq} \varepsilon_{ij}(\mathbf{v}) \varepsilon^{0(kl)}_{pq} dY \quad \forall \mathbf{v} \in V \quad (46)$$

The four independent strain fields must be applied to Equation (46) to calculate ε^*_{ij} . All ε^*_{ij} are then substituted into Equation (45) to find all of the stiffness coefficients in the homogenized stiffness tensor E^H_{ijkl} . The stiffness matrix is symmetric such that $E_{ijkl} = E_{jikl} = E_{ijlk} = E_{klij}$. This symmetry reduces the number of required test strain fields to 3 for 2-D simulation and 6 for 3-D simulation [43].

3.2 Blast Load Simulation using Computational Fluid Dynamics

Fluid flows are governed by three basic principles: The conservation of mass, Newton's second law $F = ma$, where F is the externally applied force, m is the fluid mass and a is the fluid acceleration and the conservation of energy [44]. These three fundamental principles may be represented as differential Equations. Computational Fluid Dynamics (CFD) is the method in which the governing partial differential Equations (PDE) are solved numerically. Occasionally CFD incorporates the solutions to integral Equations rather than PDEs depending on the physical nature of the problem [44]. The first use of CFD is attributed to Kopal who numerically solved the PDEs by compiling tabular data for supersonic flow around sharp cones in 1947 [45]. Yet, the first actual CFD codes

were developed by Fay and Riddel for boundary layer solutions and Hall et al. [46-47] for inviscid flow analysis.

CFD modeling may be used to realistically model the pressure wave generated due to a point explosion of conventional high explosive material. The model allows for considering parameters such as burial of explosive material (if modeling underground generated blasts), height from surface of explosive material, radial distance from explosive charge as well as the TNT equivalent or weight in kilograms. CFD allows for the simulation and examination of many different boundary conditions. CFD modeling typically integrates finite elements, finite difference and finite volume methods to model fluid dynamics. A Lagrangian frame of reference is used for solid modeling while an Eulerian frame of reference is used for modeling fluid dynamics.

The fluid interaction is calculated by numerically approximating the governing partial differential Equations for Newtonian fluids. The Equations that govern the motion of a Newtonian fluid are the continuity Equation, the Navier-Stokes Equations, the energy Equation and the Equations of state for all modeled fluids [48]. These Equations can be summarized as:

$$\frac{\partial}{\partial t} + \frac{\partial}{\partial x_k} (\rho u_k) = 0 \quad (47)$$

$$\rho \frac{\partial u_j}{\partial t} + \rho u_k \frac{\partial u_j}{\partial x_k} = -\frac{\partial p}{\partial x_j} + \frac{\partial}{\partial x_j} \left(\lambda \frac{\partial u_k}{\partial x_k} \right) + \frac{\partial}{\partial x_i} \left[\mu \left(\frac{\partial u_i}{\partial x_j} + \frac{\partial u_j}{\partial x_i} \right) \right] + \rho f_i \quad (48)$$

$$\rho \frac{\partial e}{\partial t} + \rho u_k \frac{\partial e}{\partial x_k} = -p \frac{\partial u_k}{\partial x_k} + \frac{\partial}{\partial x_j} \left(k \frac{\partial T}{\partial x_j} \right) + \lambda \left(\frac{\partial u_k}{\partial x_k} \right)^2 + \mu \left(\frac{\partial u_i}{\partial x_j} + \frac{\partial u_j}{\partial x_i} \right) \frac{\partial u_j}{\partial x_i} \quad (49)$$

$$p = p(\rho, T) \quad (50a)$$

$$p = \rho RT \quad (50b)$$

$$e = e(\rho, T) \quad (51a)$$

$$e = c_v T \quad (51b)$$

A gas law such as the ideal gas law usually represents Equation 50(a). The ideal gas law is given in Equation 50(b). Similarly, a thermodynamic relationship shown in Equations 51(a) and 51(b) is required to close the system of Equations. Equation 51(b) is the form of the thermodynamic relationship for a calorically perfect gas (constant specific heat).

3.3 Finite Element Simulation of Structural Response

The blast loading upon the composite plate is simulated using the finite element (FE) method. The FE method is used to discretize the plate into finite elements that are based upon the material properties of the given layers, the mechanics that govern the constitutive relationships, and the type of element (e.g. shell, 2-D, 3-D). The finite elements are solved at the nodal locations, which are the vertices as well as other locations along the border of the element. The intermittent values are interpolated using shape functions that are coupled to the element. The standard FE Equation that governs the relationship between force and displacement for static analysis is called the global stiffness Equation which represents a set of simultaneous solutions and is shown below [49].

$$\bar{F} = \bar{K}(U(r))(U(r)) \quad (52)$$

F is the global force vector, K is the global stiffness matrix, which is a function of the displacement vector U. U is a function of the radius vector r. The previous Equation

may be modified to account for dynamic behavior. The problem of interest requires a dynamic model to simulate the effects of a nonlinear blast wave due to high explosives upon the 2-layer plate. A transient analysis is used to calculate the stresses and strains as a function of both position and time. This makes it possible to monitor the evolution of the stress to identify locations and times of maximum stress in order to intelligently make changes to the material and the geometry to increase blast resistance of the composite plate. The standard Equation used to describe transient dynamic motion is given in Equation 53 [49].

$$[M]\{\ddot{U}(r)\} + [C]\{\dot{U}(r)\} + [K(U(r))]\{U(r)\} = \{F(t)\}$$

$$[M]\{\ddot{U}(r)\} + [C]\{\dot{U}(r)\} + [K(U(r))]\{U(r)\} = \{F(t)\} \quad (53)$$

Where \ddot{U} is the time history of the nodal accelerations, \dot{U} is the time history of the nodal velocities and U is the time history of the nodal displacements. \ddot{U} , \dot{U} and U are all function of their location r along the plate as well as functions of time. The nonlinear response of the model is taken into account making the stiffness matrix a function of the displacement. M is the mass matrix of the composite and C is the damping matrix for the composite. The Newton-Raphson method is used to solve the nonlinear problem of the iterative transient analysis. The direct integration method is used to solve the Equation of motion. At each step or sub step the Equation of motion is integrated. Then the groups of static equilibrium Equations are solved simultaneously. The Newmark method, which is an implicit integration method is used for the integration. While there are many different direct integration schemes to use, the Newmark method is utilized extensively by commercial FEA software codes [49].

3.4 Explicit Finite Element Modeling Multi-physics

Previously, simulations that dealt with fluid structure interactions were handled by solving the problem using a two step process. The fluid problem is typically solved first in order to determine the pressure distributions in the fluid medium and on the object of interest that is being affected by the moving fluid. In terms of blast optimization for composite plate design, the fluid flow equations would be solved first to determine the pressure distribution upon a plate using a numerical simulation method such as CFD. Then the pressure distribution as a function of time and position would be solved and forwarded to another numerical simulation such as FEA. This approach leads to two different issues. The pressure distribution is either over or underestimated and is not updated as the geometry of the composite plate change as a result of deformation due to blast pressure. This approach of implicit blast simulation is the one that will be used in case study 2. While computationally effective, it is not the most accurate approach. For more accurate and efficient solutions, it is suggested that the use of an explicit blast model is necessary. Explicit blast modeling may be performed using coupled transient dynamic softwares such as LS-DYNA. LS-DYNA couples CFD and FEA in order to create a more realistic simulation environment. This means that modeling blast for use in optimization routines may be done in one step rather than two steps. The optimally obtained solutions will also be better optimal solutions because they were obtained for specific blast waves which are appropriately transferred to the composite plate while taking into account the stiffness of the plate. It has been shown that the pressure transfer shape and magnitude are directly related to the plate properties.

To exemplify this relationship a comparison between three different metallic homogeneous and isotropic plates will be conducted. The three materials used are Aluminum, Titanium and Tungsten. The plates are modeled in LS-DYNA and have dimensions of 300 x 300 x 170 mm. Two hundred grams of high explosive TNT are detonated 150 mm away from the homogeneous plate. The three dimensional stiffness matrices and densities are included for each material. The stiffness matrices are shown below and the material properties are listed in

Table 3.1. Everything else in the blast model is identical.

$$\begin{bmatrix} 103.7 & 51.1 & 51.1 & 0 & 0 & 0 \\ 51.1 & 103.7 & 51.1 & 0 & 0 & 0 \\ 51.1 & 51.1 & 103.7 & 0 & 0 & 0 \\ 0 & 0 & 0 & 26.3 & 0 & 0 \\ 0 & 0 & 0 & 0 & 26.3 & 0 \\ 0 & 0 & 0 & 0 & 0 & 26.3 \end{bmatrix}$$

Aluminum (GPa)

$$\begin{bmatrix} 158.5 & 81.6 & 81.6 & 0 & 0 & 0 \\ 81.6 & 158.5 & 81.6 & 0 & 0 & 0 \\ 81.6 & 81.6 & 158.5 & 0 & 0 & 0 \\ 0 & 0 & 0 & 38.4 & 0 & 0 \\ 0 & 0 & 0 & 0 & 38.4 & 0 \\ 0 & 0 & 0 & 0 & 0 & 38.4 \end{bmatrix}$$

Titanium (GPa)

$$\begin{bmatrix} 511.3 & 198.8 & 198.8 & 0 & 0 & 0 \\ 198.8 & 511.3 & 198.8 & 0 & 0 & 0 \\ 198.8 & 198.8 & 511.3 & 0 & 0 & 0 \\ 0 & 0 & 0 & 156.2 & 0 & 0 \\ 0 & 0 & 0 & 0 & 156.2 & 0 \\ 0 & 0 & 0 & 0 & 0 & 156.2 \end{bmatrix}$$

Tungsten (GPa)

Table 3.1 Material Properties

Material	Density (kg/m ³)
Aluminum	2700
Titanium	4340
Tungsten	19300

The 3-D Finite element model is shown below in Figure 3-2. The model represents a ¼ portion of the full system. This allows for the use of symmetrical boundary conditions on the interior portion of the model. The model consists of three different materials. TNT is used as the explosive material and is shown in yellow. The air is shown in green between the explosive material and the isotropic plate. The plate is shown in blue and red, yet the material properties are identical for both the red and the blue so that the plates may be considered 1 plate. This was done so that in later tests the effect of stacking plates with different material properties may be examined.

Specific boundary conditions were used to simulate the realistic behavior of the system. These boundary conditions include the symmetric boundary conditions, represented by a zero y displacement is placed on the inner x-z face of all materials and a zero x displacement is forced upon the y-z face of the model. The bottom outside edge of the plate is restricted from moving in the y direction.

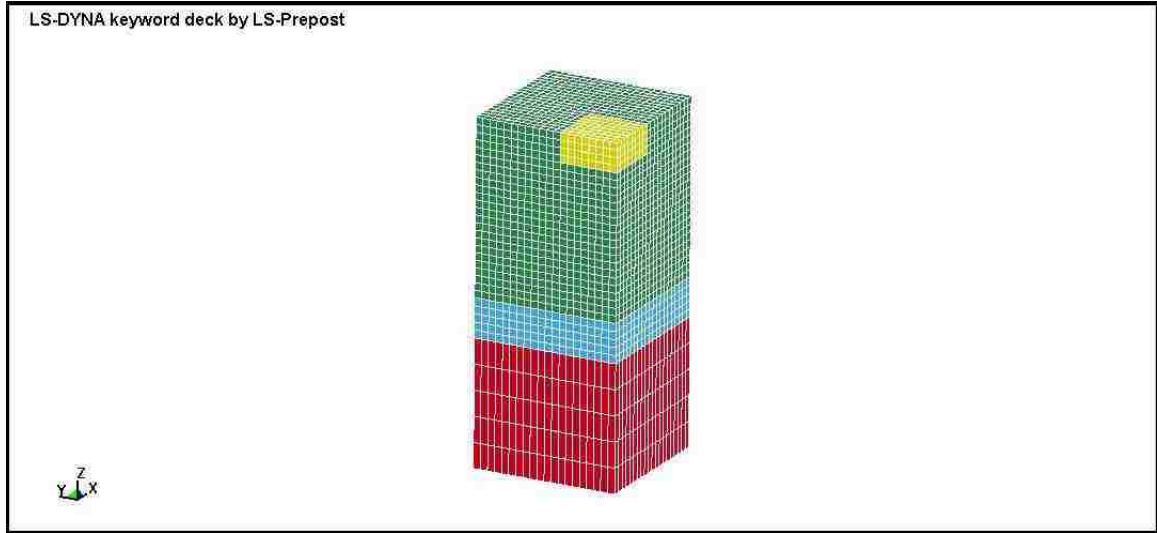


Figure 3-2 3-D finite element model used for Explicit blast modeling

An arbitrary Lagrangian Eulerian multi-material group is used for simulating the fluid dynamics. Damping is applied to the model because all real world structures experience some form of damping. The damping is applied to all parts with a value of 10% of the critical damping. Frequency range damping is applied for frequencies between 100 Hz and 100 kHz. Solid elements are used for all material types. The Jones-Wilkins-LEE (JWL) equation of state (eos) is utilized for the determination of detonation products and pressures. The JWL eos defines the pressure as a function of relative volume and internal energy per unit volume [50]. The JWL eos is described by Equation 54.

$$p = A \left(1 - \frac{\omega}{R_1 v} \right) e^{-R_1 v} + B \left(1 - \frac{\omega}{R_2 v} \right) e^{-R_2 v} + \frac{\omega E}{v} \quad (54)$$

Where ω , A , B , R_1 and R_2 are user defined inputs. The gamma equation expressed in terms of an ideal gas is the equation of state used to simulate the air. An anisotropic-elastic material model is used for the isotropic plate. The high explosive burn material is assumed to be TNT with a density of 1600 kg/m^3 . A detonation velocity of 2000 m/s and

a PCJ pressure of $2.0 \times 10^6 \text{ N/m}^2$ is typically used in numerical analysis of TNT detonations. The density of air was assumed to be 1.29 kg/m^3 . Fragmentation was neglected in the explicit blast model. The deformation of the model is monitored to make sure that the behavior of the model is realistic. A graph of deformation vs. time for a homogeneous Tungsten plate under blast load is shown in Figure 3-3.

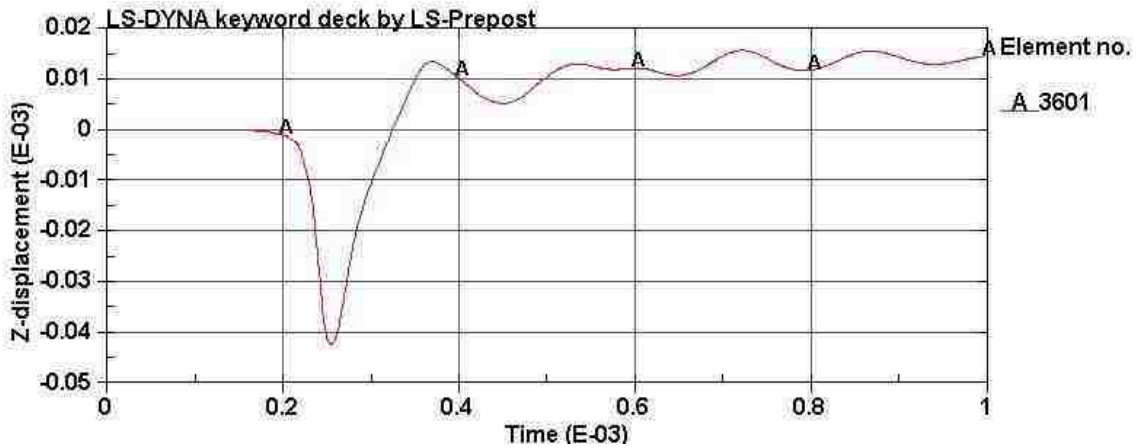


Figure 3-3 Displacement vs. time curve for Tungsten plate

The results for the examination of explicit blast modeling upon the pressure distribution around different materials using the same input files are shown below. Figure 3-4 shows the pressure vs. time curves for Aluminum, Titanium and Tungsten. While the pressure varies as both a function of position and time along the top of the plate, a specific element located at the global origin of the model was used in all cases for comparison. This element is highlighted and shown in Figure 3-5. As can be seen in Figure 3-4, the maximum pressure distribution at the global origin is not linearly related to the material properties of the system.

The Titanium model attained the highest pressure profile with a maximum above 500 MPa. The Aluminum model came in second with a value of 250 MPa and finally, the

Tungsten model achieved a pressure slightly below 100 MPa. The relative pressure differences between each case are not intuitive. The parameters that were changed between each model included the stiffness, Poisson's ratio and density. Tungsten has the highest uniaxial stiffness with a modulus of 400 GPa. While, Titanium and Aluminum are much closer to one another with moduli of 103 GPa and 70 GPa respectively. The pressure distribution does not seem to follow the stiffness trend. The densities are arranged in identical order to that of the stiffnesses, with Tungsten being the densest and Aluminum being the least dense. Finally, if the Poisson's ratios are examined there is evidence of a greater Poisson's effect upon the behavior of the system. The values of the Poisson's ratios for the three materials are as follows: Tungsten $\nu = 0.28$, Aluminum $\nu = 0.33$ and Titanium $\nu = 0.34$. The Poisson's ratio trend seems to follow the air pressure distribution trend. In fact blast modeling is not expected to follow linear relationships. Many of the governing equations are complex partial differential equations and the equations of state contain quadratic or higher terms. These complexities can lead to interesting and counterintuitive results.

While it is not definitive which parameter has the greatest effect upon the data, it has been shown that the pressure distribution is directly tied to the mechanical properties of the materials. If the geometry of any of the three plates is changed further, evidence on the significance of explicit blast modeling can be further shown. This means that explicit blast modeling is required when modeling systems that involve explosive detonations. To fully understand the parameter's effects on the system a full scale parametric analysis should be performed. This evaluation is outside the scope of this work and may be proposed as recommendations for future work.

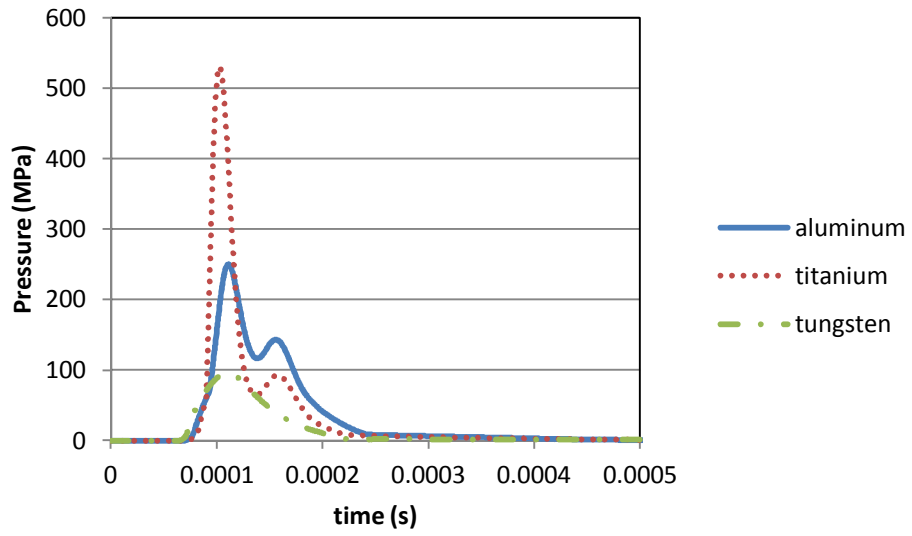


Figure 3-4 Pressure vs. time curves in air directly above the plate for three different materials

LS-DYNA keyword deck by LS-Prepost
Time = 0

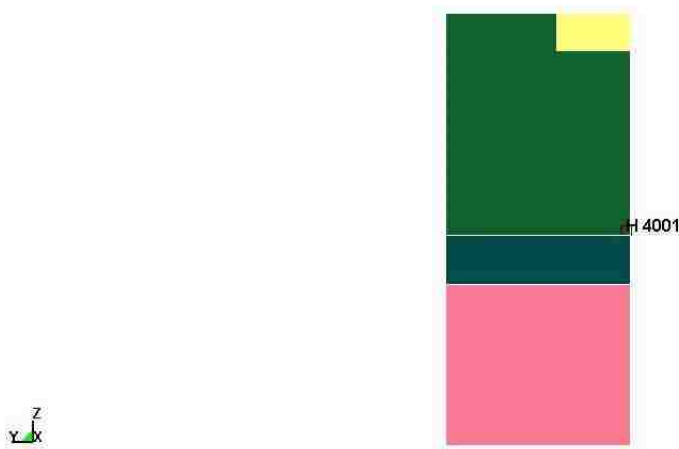


Figure 3-5 Location of element above the plate for pressure comparisons

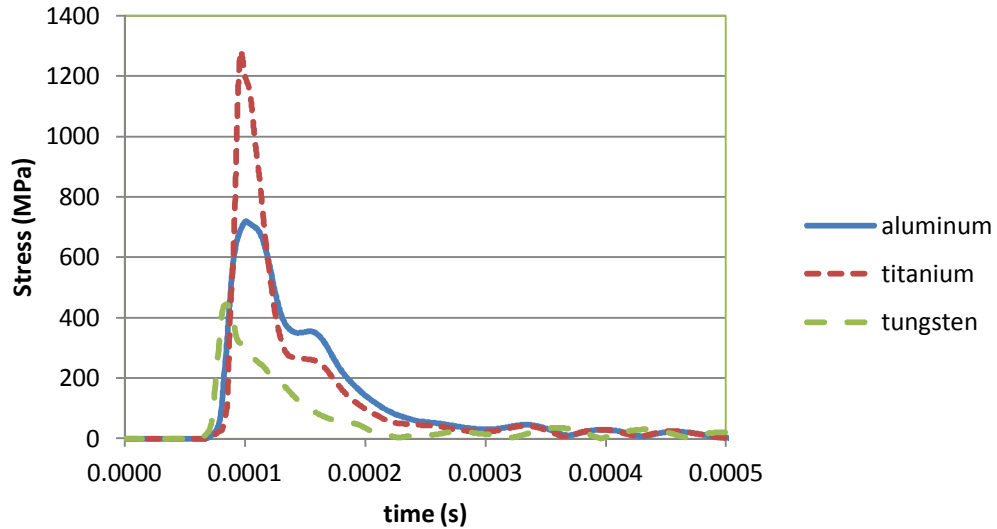


Figure 3-6 Von Mises stress vs. time for three different materials

The maximum Von Mises stress in the top layer was monitored to determine which material experienced the greatest stress. The materials experienced Von Mises stresses in that trended in the same manner as the pressure profiles. This concept is verified by the fact that the stress should follow the applied load. The Titanium experienced the greatest pressure and therefore exhibited the largest Von Mises stress. Similarly, the Tungsten had the smallest pressure transfer and in turn revealed the least amount of Von Mises stress.

In light of the previous analysis the explicit blast model is much more informative than previously used methods of blast analysis. It is necessary to update the pressure profile as the material resisting the blast is changed. This concept becomes even more important when the blast model is tied into an optimization environment. As the material properties become further apart, the effect of using the same pressure profile greatly increases the error in the calculated stress distribution.

LS-DYNA keyword deck by LS-Prepost
Time = 0

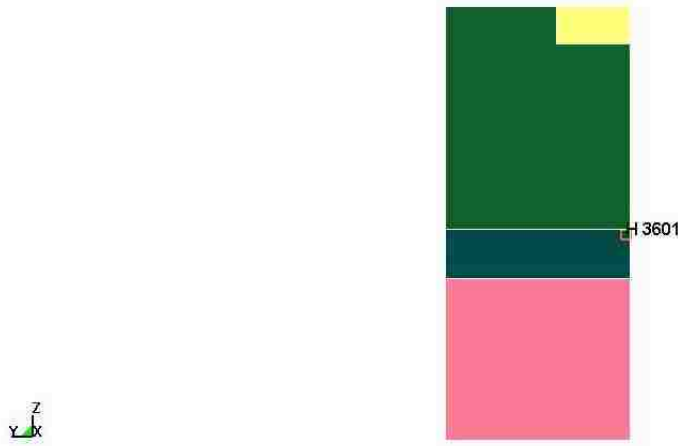


Figure 3-7 Location of element on plate for Von Mises stress comparisons

3.5 Effect of damping upon composite structures subjected to blast

In the previous section it was stated that damping is applied to the model to simulate real world behavior. After the application of the pressure wave the structure is in a state of free vibration. This means that it has been disturbed from its equilibrium position and then allowed to vibrate without any external forces. In reality all real structures exhibit damping, otherwise once excited by an external load they would oscillate or vibrate indefinitely. To incorporate damping into the simulation typically viscous damping mechanisms are used. The following equation is similar to equation 50 but rewritten for purposes of discussing damping in the explicit blast model [51].

$$[M]\{\ddot{U}\} + [C]\{\dot{U}\} + [K]\{U\} = \{F(t)\} \quad (55)$$

Equation (55) is a matrix equation that describes the dynamic motion of the finite element model. Once the pressure is no longer applied to the finite element model from the blast load the $F(t)$ term goes to zero. The structure is then in free vibration and only if

damping is applied will the structure come to rest. Equation (55) may be rewritten with no external force to represent free vibration.

$$[M]\{\ddot{U}\} + [C]\{\dot{U}\} + [K]\{U\} = 0 \quad (56)$$

This equation may be divided through by m to yield:

$$\{\ddot{U}\} + \frac{[C]}{[M]}\{\dot{U}\} + \frac{[K]}{[M]}\{U\} = 0 \quad (57)$$

Finally, the equation may be rewritten in terms of the natural frequencies of the system [51].

$$\ddot{u} + 2\zeta\omega_n\dot{u} + \omega_n^2u = 0 \quad (58)$$

$$\text{Where } \omega_n = \sqrt{k/m} \quad (59)$$

$$\text{And } \zeta = \frac{c}{2m\omega_n} = \frac{c}{c_{cr}} \quad (60)$$

Here c_{cr} is the critical damping coefficient and ζ is the damping ratio which is also known as the fraction of critical damping.

While these equations are written with regard to a single degree of freedom system, the method still applies to a 3-D dynamic system. Changing either the mass or the stiffness, results in a change of the natural frequency, the critical damping coefficient and the damping ratio.

This concept becomes extremely important with regard to the optimization problem.

When optimizing structures for blast resistance, both the stiffness and the mass of each design will be different. This means that the natural frequencies will be different for all design iterations. If one design iteration exhibits oscillatory motion at its natural frequency then resonance will occur. Therefore, damping must be added to the finite

element simulation to damp the motion of the structures that are subjected to the blast loading.

LS-DYNA has many different methods for simulating damping of dynamic motion. These methods include: damping frequency range, damping stiffness, damping mass, damping global and damping relative. The damping frequency range will be used to model damping in all explicit blast simulations. This method requires a fraction of critical damping term and the frequency range of interest. This method is advantageous to the optimization environment because before each iteration the natural frequency of a particular design is unknown. This method will allow for the greatest number of design to include damping with little loss of accuracy. A value of 10% fraction of critical damping will be used for all cases. Any vibratory motion in the frequency range between 1 and 100,000 Hz will be damped according to the fraction of critical damping. Damping is only applied to the composite plate and not to the air in the finite element model.

3.6 Multi-Objective Genetic Algorithm

The multi-objective genetic algorithm (MOGA) allows for the formulation of multi-objective optimization problems without the need to specify weights on the various objective function values. This is achieved by considering the concept of non-dominant solutions (analogous to Pareto optimal solution) suggested by Deb [52]. MOGA directly identifies non-dominated design points that lie on the Pareto front. The advantage of the MOGA method over conventional weighted-sum methods, is that MOGA finds multiple points along the entire Pareto front whereas the weighted-sum method produces only a single point on the Pareto front. Moreover, MOGA is more capable of finding points on

the Pareto front when the Pareto front is non-convex. However, the use of a genetic algorithm (GA) search method in MOGA causes the MOGA method to be much more computationally expensive than conventional derivative based multi-objective optimization algorithms.

The concept of genetic algorithms comes from the biological concept of “survival of the fittest” [53]. Through examining the process of evolution, algorithms may be formed that represent this process of natural selection. The algorithm works by first selecting possible solutions and then testing these solutions for their performance. Out of the tested solutions a portion of the good solutions are selected and the remaining solutions are discarded or eliminated. The solutions that are kept are then forced to undergo reproduction, crossover and mutation. This leads to a new generation of potentially better solutions. This overall process is repeated until the convergence criteria is satisfied. This method is advantageous because it searches through a broad solution space and does not restrict the solution to a smaller domain [53].

Schaffer proposed a vector evaluated genetic algorithm [54]. Goldberg suggested using nondomination rank order to avoid GA convergence to a single point [55]. Horn *et al.* [56] proposed a niched multi-objective genetic algorithm where comparison sets are used. In their method, Srinivas and Deb [57], individuals are selected by looking at their relative dominance. A niche count is considered to calculate the shared fitness. The niche count is the number of neighboring solutions to a solution. One solution is considered to share its fitness with its neighbors and shared fitness is calculated by dividing its fitness by its niche count. Srinivas and Deb [57] proposed nondominated sorting genetic algorithms (NSGA). NSGA basically finds the nondominated set of

points and gives them a large fitness value. Then from the remaining points it finds the nondominated ones and assigns them a smaller fitness value. This process continues until all the entire population is classified into several of dominated and nondominated sets. Sharing is applied to preserve diversity. Knowles and Corne [58] kept an archive of the nondominated points so that when a new member is generated it is not only compared to the members of the current population but to all the members in the archive. Rammohan et al. [59] showed such a technique to result in a considerable computational savings in complex optimization environments. Deb *et al.*[60] proposed NSGA-II, a fast and elitist multi-objective evolutionary algorithm based on nondominated sorting approach. Konak *et al.*[61] provided a broad survey about MOGA from literature. MOGA is successfully applied to different problems including but not limited to topology optimization, system reliability and crashworthiness [62-65]. It is important to note the uniqueness of the concept of domination used by NSGA. By performing pair-wise comparison of each possible design through the entire space of the objective functions, NSGA proved capable of identifying Pareto optimal solutions through the nondominance search approach. One of the most powerful aspects of MOGA is its ability to handle optimization problems in which the design variables are discrete and not continuous. Typically, optimization is done using gradient based methods. While sometimes the gradient methods are inefficient and require multiple start point, they can yield reasonably good results. Where gradient methods are lacking include problem statements with discrete design variables. There is no gradient to follow when the variables can be labeled for example as either 0 or 1. MOGA handles discrete problems very well because MOGA uses binary encoding. Many gradient based methods would require artificial filters to handle the discrete design

space. Additionally, MOGA can also handle continuous design variables. Therefore, when the problem involves both discrete and continuous design variables, then MOGA is the proper method for analysis.

3.7 Reliability Analysis

The response of the structure or the composite laminate to a certain type of loading depends upon the manner in which the load is applied, the magnitude of the load, as well as the stiffness and strength characteristics of the structure. The manner in which we determine if the design is acceptable or not under a given loading depends on whether certain criteria or requirements are attained or not. Examples of these requirements are limiting the amount of allowable damage, deflection, stress or combination of any of these values. Another important method is to limit the probability of failure. The probability of failure can be defined by defining limit states. We will define each of these requirements as a limit state [66]. If a limit state is violated, then the structure reached a condition that is detrimental or undesirable.

While all violations of limit states do not end in catastrophe, there are some that do. One example of catastrophic failure is the I-35W Mississippi River bridge (officially known as Bridge 9340). The bridge catastrophically collapsed without warning on August 1, 2007 killing 13 people and injuring 145. These types of events are one reason that reliability analysis is necessary when designing and monitoring structures subjected to complex loading conditions. Reliability analysis is used to calculate the probability that a limit state function is violated.

Reliability analysis takes into account the fact that loading is uncertain and not deterministic at a certain instant in time [66]. Moreover, reliability analysis also realizes

that material strength or strain limits are also uncertain and can be described using probability distribution functions.

In simple terms, the structural reliability problem can be explained by considering a load Q that is resisted by a resistance R . We can then transform the load Q to a load effect S using structural analysis. We can then describe both S and R with a probability distribution function $F_S()$ and $F_R()$. S may either be deterministic or random in nature, but both S and R must have the same units. Considering a structural element, failure will occur if the value of S is greater than R . The mathematical description of probability of failure is shown below [66].

$$p_f = P(R \leq S) \tag{61}$$

or in terms of the limit state function $G(R,S)$.

$$p_f = P[G(R,S) \leq 0] \tag{62}$$

We can define the vector of all the variables that influence the probability of failure as:

$$X = [x_1, x_2, \dots, x_i] \tag{63}$$

where the violation of the limit state can be rewritten as:

$$G(x) \leq 0 \tag{64}$$

The integration of the joint probability density function of variables (x_1, x_2, \dots, x_i) at the region of $G(X) \leq 0$ is defined as the probability of failure. A top down view of a two random variable joint density function is shown in Figure 3-8.

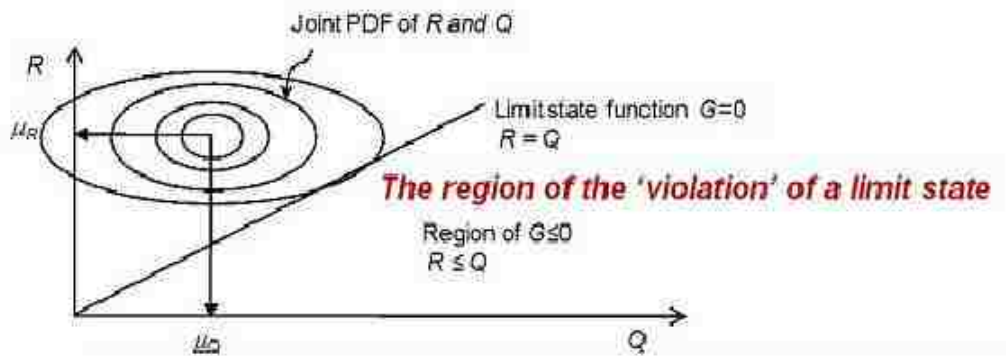


Figure 3-8 Joint density function of resistance and load effects

Equations 51 and 52 are represented by the area where $G = 0$. Therefore, the probability of failure may be written as:

$$p_f = P(R - S \leq 0) = \int_{-\infty}^{\infty} \int_{-\infty}^{\infty} f_R(r) f_S(s) dr ds \quad (65)$$

If R and S are independent and considering the random variable X described above then probability of failure can be written in a single integral form known as convolution integral.

$$p_f = P(R - S \leq 0) = \int_{-\infty}^{\infty} F_R(x) f_S(x) dx \quad (66)$$

Where $F_R(x)$ is the cumulative density function (CDF), while $f_S(x)$ is the probability density function (PDF) of loads S . There are a few distributions for R and S that can be used to analytically integrate the previous Equation. One example is the normal distribution function. For those cases where the distribution is not normal or where the violation of the limit state is non-linear, numerical techniques must be used to perform the convolution integral shown in Equation 66. When direct integration is not possible then one proposed method is to use Monte Carlo techniques. Monte Carlo methods use

random sampling to simulate a large number of tests and then are used to predict the results [66]. In simplistic terms, a random sampling of the random variable X_i will be performed to yield a sample value x_i . The value of the limit state function with respect to x is then evaluated. If the limit state is violated then the element has failed or has attained an undesirable condition. This process is repeated multiple times with a randomly chosen vector x that contains the x_i values. If this process is repeated N number of times then the probability of failure will be approximately [66]:

$$P_f \approx \frac{n(G(\bar{x}_i) \leq 0)}{N}$$

(67)he numerator in the previous equation represents the number of tests n , which the limit state was violated. Due to the uncertainty during blast and the number of variables that influence both blast and its effect upon fluid structure interaction, a Monte Carlo simulation is suggested for the method of applying reliability analysis to the multi-objective optimization of blast resistant composites. Techniques to reduce the computational expenses of Monte Carlo simulation will be examined.

CHAPTER 4 CASE STUDIES

The following chapter describes three different case studies used to portray the different methods that may be utilized to optimize composite structures to resist blast loading. The first case study uses reliability based methods and single objective optimization to optimize stacking sequence and thickness for a homogeneous layered single degree of freedom problem. The second case study uses an integrated simulation environment to optimize 2-D axisymmetric plates subjected to blast loading using homogenization, multi-objective optimization, computational fluid dynamics and finite element analysis. Finally, the 3rd case study uses similar methods to the 2nd case study that are updated for 3-D analysis.

4.1 First Case Study: Design Optimization of Stacking Sequence of metallic

Composite Laminates

4.1.1 Introduction

An explosion is an event where a significantly large amount of energy is released over a short time period. A blast wave is the volume of compressed air that expands outward from the detonation source and is located in front of the hot gas that generated due to the detonation of an explosive. Most of the energy released is contained in the blast wave. Positive and negative specific impulses as well as the value of over pressure above ambient pressure are used to describe and characterize the blast wave time history. As the blast wave moves farther from the detonation source, the over pressure decays [10]. It has been shown that fluid structure interaction has a significant effect upon the pressure distribution and transfer [11]. The material behavior under high strain rate loading must also be considered for realistic modeling [67]. While acknowledging the importance of

the above issues in rational simulation of blast events, detailed blast simulation might be useful to verify design efficiency. However, we emphasize that the complexity of blast events necessitates considering uncertainty in blast-resistant design. Deterministic blast simulations cannot provide a robust design given the significant sensitivity of blast simulation to many uncertain parameters that govern any blast [68]. Therefore, a reliability-based approach is suggested for the design of blast-resistant composites.

Armor is usually used to protect military vehicles from a blast or impact loading. Historically, steel is the most commonly used material for armor. In recent years uranium has also been used for its ability to transmit low loads due to its high density. There are also demands for lighter materials for armor to increase vehicle mobility and reduce energy consumption. In this study, a simplified dynamic model is developed to simulate dynamic behavior of a composite plate under blast air pressure. For an uncertain blast event, the probability of failure of each layer is evaluated using Monte Carlo method. By assigning a high probability of failure (*low target reliability index*) to the energy absorbing layer and a relatively low probability of failure (*high target reliability index*) to the strong layer, the thickness of the composite layers is optimized. A case study for the design of a two layer composite plate made of Aluminum and Titanium subjected to an uncertain blast event is presented and the results of a finite element (FE) simulation of the composite plate are discussed.

4.1.2 Methods

(1) Composite system

Elastoplastic dynamic responses of mass-spring-damper system [69] are used to model a composite plate subject to air pressures due to blast. The composite plate, consisting of

two layers: layer “R” and layer “A”, as shown in Figure 4-1, is modeled as two lumped mass system. Layer “R”, which is subjected to the blast pressure, is considered as reflecting layer and layer “A” is considered as absorbing layer. Therefore, constitutive response of layer “R” is modeled as elastic and that of layer “A” is modeled as idealized elastoplastic. The equation of motion of this system is then formulated as

$$M\ddot{u} + C\dot{u} + F_s(\dot{u}, u) = P(t) \quad (68)$$

where \ddot{u} , \dot{u} and u are acceleration, velocity and displacement vectors of two degree of freedom (DOF) respectively as shown in Figure 4-1. and the different components can be expressed as

$$M = \begin{bmatrix} m_A & 0 \\ 0 & m_R \end{bmatrix}, C = \begin{bmatrix} c_A + c_R & -c_R \\ -c_R & c_R \end{bmatrix}, \quad (69)$$

$$F_s(\dot{u}, u) = \begin{bmatrix} f_{s,A}(\dot{u}_A, u_A) + k_R(u_A - u_R) \\ k_R(u_R - u_A) \end{bmatrix}, P(t) = \begin{bmatrix} 0 \\ P \end{bmatrix}$$

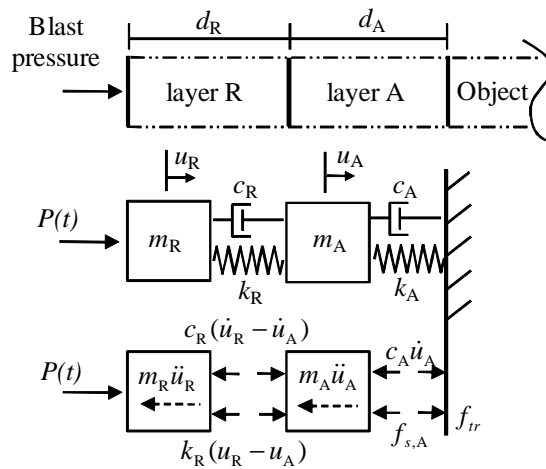


Figure 4-1 Lumped mass modeling of a composite plate

where m and c are mass and damping constant per unit area respectively. $f_{s,A}(\dot{u}_A, u_A)$ is resisting stress as shown in Figure 4-2 from elastoplastic constitutive of layer “A”. k_R is the stiffness per unit area of layer “R” computed as the modulus of elasticity E_R over the layer thickness d_R . P is the applied blast pressure with respect to time to layer “R”.

Subscript “A” and “R” represent layer “A” and “R” respectively. For our interest, the maximum stress f_R in layer “R” and the maximum demanding strain ϵ_A in layer “A” during the response time are computed as

$$f_R = \max\{k_R[u_R(t) - u_A(t)]\} \tag{70}$$

$$\epsilon_A = \max\{u_A(t)/d_A\} \tag{71}$$

where, d_A is the thickness of layer “A”. It is noticeable that the stress f_{tr} transferred to object as shown in Figure 4-2 will be constrained to the yield strength of layer “A”, $f_{sy,A}$.

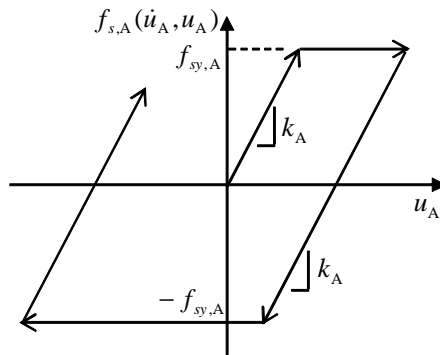


Figure 4-2 Elastoplastic model of layer “A”

(2) Reliability computation

Reliability analysis has been used to incorporate uncertainties in applied load to a structure and mechanical material properties of the structure to structural design [66],[70]. A limit state of each layer is defined to establish undesirable conditions for the composite plate. For the limit state of layer “R”, the maximum stress f_R in the layer during dynamic response to a blast wave should be less than yield strength $f_{sy,R}$ of material for layer R to reflect all energy applied to the layer. Therefore, the limit state G_R of layer “R” is defined as

$$G_R = f_{sy,R} - f_R \quad (72)$$

In this case, layer “R” is considered to fail for design purpose when G_R is less than or equal to zero. Considering that the use of layer “A” is for absorbing applied blast energy in the layer as strain energy, this layer needs to yield. If the strain energy capacity of layer “A” is incapable of absorbing the demanding strain energy for layer “A”, the layer response is undesirable. Therefore, the limit state G_A of layer “A” is defined as

$$G_A = \varepsilon_f - \varepsilon_A \quad (73)$$

where, ε_f is failure strain of material for layer “A”. The failure of layer “A” will take place when G_A is less than or equal to zero. The integration of joint probability density functions (PDF) of ε_f and ε_A for the violation region of limit state $G_A \leq 0$ will give the probability of failure $p_{f,A}$ of layer “A”. The probability of failure $p_{f,R}$ of layer “R” is also computed by integrating joint PDF of $f_{sy,R}$ and f_R in the region of $G_R \leq 0$. These integrations are numerically evaluated using Monte Carlo (MC) simulation. MC

simulation has been proven efficient for modeling uncertainty in complex systems [71],[72]. To simplify the design problem, the probability of failure is converted to reliability index β using the relationship as:

$$\beta = -\Phi(p_f) \quad (73)$$

where Φ is the standard normal cumulative density function (CDF). It is important to note that although a series system is used to model the mechanical response of the composite plate, system reliability is not applied to compute the probability of failure of the plate as the combined reliability of a series system is governed by one layer.

(3) Optimization

The objective of the optimization process is to identify the optimal thickness of each layer to have a certain level of reliability of the composite plate subjected to an uncertain blast event. To find the optimal thickness combination of the composite plate layers α_2 , that gives the desired reliability index, denoted β_{target} , the optimization problem can be posed as:

$$\begin{aligned} & \min (\beta - \beta_{\text{target}})^2 \quad \text{s.t.} \quad d_{\min} \leq d \leq d_{\max}, \forall d \\ & \text{where } \beta = \begin{bmatrix} \beta_A \\ \beta_R \end{bmatrix}, \beta_{\text{target}} = \begin{bmatrix} \beta_{\text{target},A} \\ \beta_{\text{target},R} \end{bmatrix}, \\ & d = \begin{bmatrix} d_A \\ d_R \end{bmatrix}, d_{\min} = \begin{bmatrix} d_{\min,A} \\ d_{\min,R} \end{bmatrix}, d_{\max} = \begin{bmatrix} d_{\max,A} \\ d_{\max,R} \end{bmatrix} \end{aligned} \quad (74)$$

where d_{\min} and d_{\max} are α_{\min} vectors containing the lower and upper bounds of the layer thickness respectively.

(4) Explosion model for finite element analysis

For the analysis of the structural response of the composite plate subjected to a high explosive (HE) detonation, the Jones Wilkins Lee (JWL) equation of state was used to calculate the products of detonation for the FE analysis. The model assumes that the energy released during detonation is contained in the compressed wave that travels in front of the hot gases. All of the high explosive material was transformed into products of detonation as described by Equation (75)

$$p = A \left(1 - \frac{\omega}{R_1 V} \right) \exp(-R_1 V) + B \left(1 - \frac{\omega}{R_2 V} \right) \exp(-R_2 V) + \frac{\omega E}{V} \quad (75)$$

where p , V and E represent the pressure, the volume and the internal energy of the detonation products respectively. A , B , R_1 , R_2 and ω are the JWL empirical constants for a certain HE. For modeling air, a linear polynomial equation of state is used to initialize the initial thermodynamic state of the material. The linear polynomial may be used to simulate gas with the gamma law [73]. Pressure for ideal gas is given as:

$$p = (\gamma - 1) \left\{ \frac{\rho}{\rho_0} E \right\} \quad (76)$$

where p represents the pressure of the gas and γ equals the ratio of the specific heat of the gas at constant pressure c_p over that at constant volume c_v . ρ and ρ_0 are current density and reference density respectively. E represents the internal energy.

4.1.3 Case Study

A case study of a two layer composite plate made of Titanium and Aluminum is considered. Titanium is considered as a material of the outer side layer “R” reflecting blast energy while Aluminum is considered as a material of the inner side layer “A”

absorbing the blast energy. Material properties of Titanium (ASTM Grade 1) and Aluminum are presented in Table 4.1 Aluminum Type 6061-O is used for its relatively high failure strain.

Table 4.1 Characteristics of the two layers of the composite plate

Material	Density (kg/m ³)	Modulus (GPa)	Tensile and compressive strength (MPa)	Failure strain
Titanium	4500	105	240	-
Aluminum	2700	70	55	25%

It is important to note that strain rate-independent constitutive material properties are used in this case study. For accurate modeling, it might be necessary to consider strain rate-dependent dynamic constitutive material properties. Therefore, accurate simulation would require modifying the proposed analytical model to account for the significance of the high strain rate of blast loading on the material constitutive model used during analysis. This can be done by using different dynamic elastoplastic models that vary according to the corresponding strain rate for each time step. This modification is beyond the scope of this article but its significance is examined below using the finite element method.

To simulate blast pressure, Friedlander decay function [10],[74],[75] is used here such as

$$P = P_m \left(1 - \frac{t}{t_d} \right) e^{-\alpha \frac{t}{t_d}} \quad (77)$$

where P_m is the maximum magnitude of the positive pressure due to blast. t_d is the time duration of the positive pressure and α is the shape factor for the blast model.

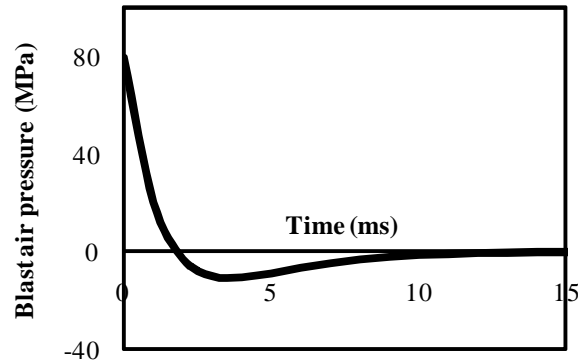


Figure 4-3 Friedlander blast air pressure wave ($P_m = 80$ MPa and $t_d = 0.018$ sec)

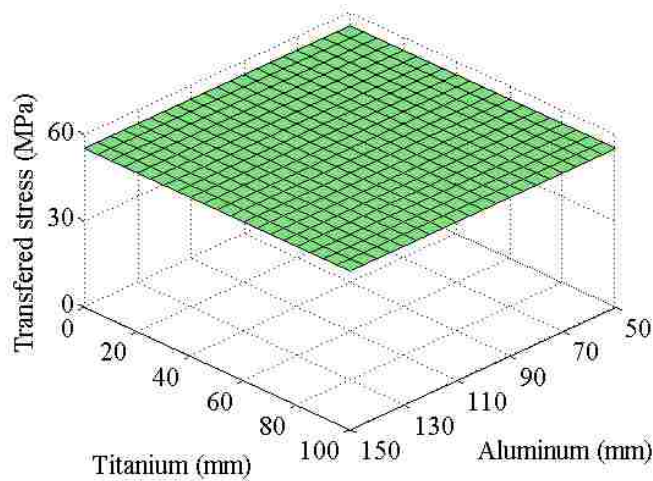


Figure 4-4 Transferred stress f_{tr}

The selected blast produced an incident pressure of 80 MPa on the outer composite surface plate [76]. Selection of the blast incident was performed with the intention to produce significantly high stress in the composite laminate. In this model t_d and α are

selected as 0.0018 sec and 1.0 respectively. The blast model is formulated in Figure 4-3. Dynamic responses of the composite plate due to the blast load were analyzed according to the layer thicknesses of Titanium and Aluminum varying from 5 mm to 100 mm and from 50 mm to 150 mm respectively. The damping coefficients for both layers are assumed as viscous damping $c = 2\zeta\sqrt{km}$ [51]. Here, the damping ratio ζ of 1% is used for both layers. It is also assumed that bonding between two layers holds perfectly during the blast loading.

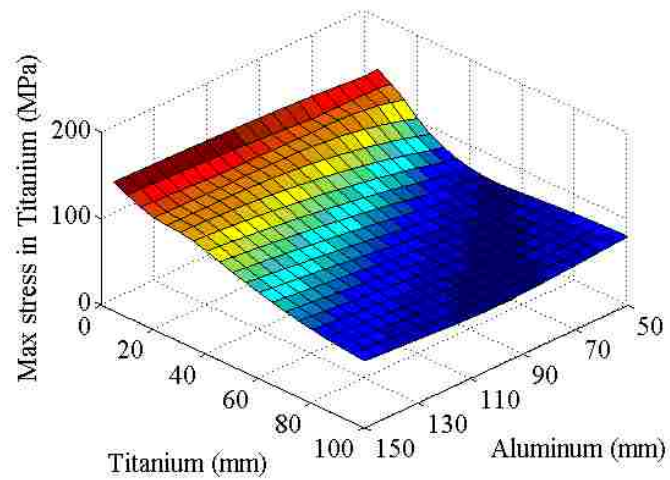


Figure 4-5 The maximum stress in Titanium

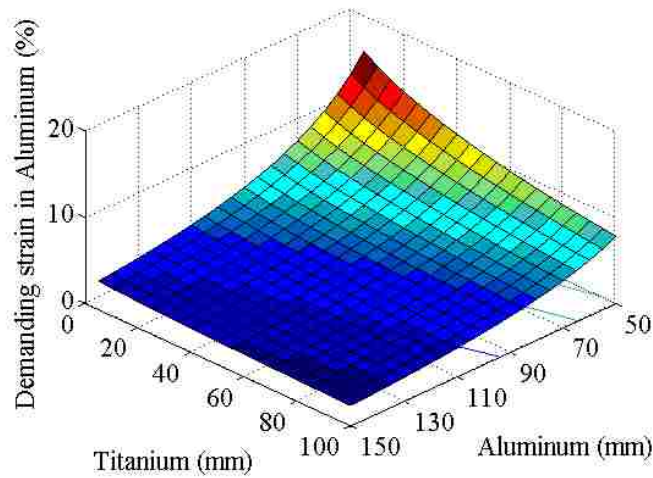


Figure 4-6 The maximum strain in Aluminum

The ratio of transferred stress f_{tr} to the maximum blast stress 80 MPa is formulated with respect to the mechanical response of the combinations of Titanium and Aluminum thicknesses using the mechanical model described above (Equation (68) to (71)). The ratio transferred of stress f_{tr} is shown in Figure 4-4. As expected, the yield strength 55 MPa of Aluminum governed the ratio of the transferred stress for all the selected thickness ranges. The maximum stress f_R in Titanium and the maximum demanding strain ϵ_A in Aluminum with respect to the combinations of Titanium and Aluminum thicknesses are computed in Figure 4-5 and Figure 4-6 respectively.

As shown in Figure 4-5, the maximum stress in Titanium decreases when Titanium layer (layer R) thickness increases. The maximum demanding strain of Aluminum for layer A is computed under its failure strain 25% for all selected analysis region as shown in Figure 4-6.

4.1.4 Results and Discussion

Considering uncertain blast event, the magnitude of blast pressure P_m was assumed normally distributed to have a coefficient of variation (COV) of 30% [76]. In the mean time, the yield strengths of Titanium and the failure strain of Aluminum were assumed to be normally distributed with COVs of 10% for both properties. By assigning these uncertainties to the limit state functions in Equations (72) and (73), probability of failure for layer R and A with respect to layer thicknesses are computed and formulated as reliability index in Figure 4-7 and Figure 4-8 respectively. One thousand random variants for the magnitude of blast pressure are generated to evaluate the probability of failure. The same set of the magnitude of blast pressure variants are used for each combination of layer thicknesses to get consistent response surface. Reliability for both layer “R” and “A” increases with increase of layer thicknesses.

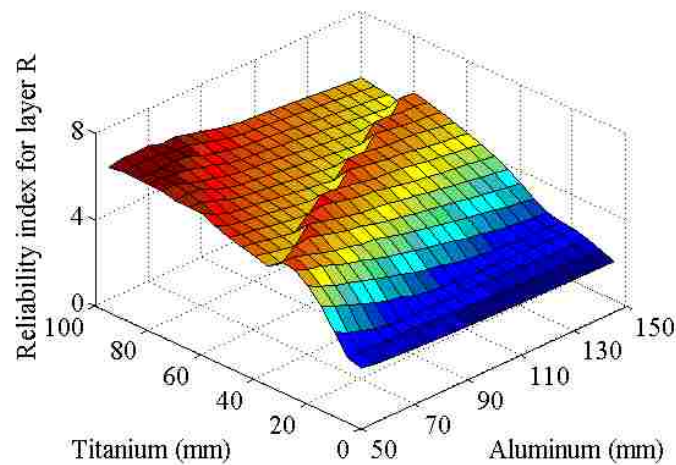


Figure 4-7 Reliability index surfaces of Titanium layer β_R

To determine optimum thicknesses of Titanium and Aluminum for an uncertain blast event, we considered the following parameters: $\beta_{\text{target, R}} = 4$ for Titanium layer

(corresponding to probability of failure of 0.003%) and $\beta_{\text{target, A}} = 3.5$ for Aluminum layer (probability of failure of 0.023%). $\beta_{\text{target}} = 4$

Reliability index for conventional strength design is assigned to Titanium layer while a relatively low reliability index is assigned to Aluminum layer by considering layer A as a consumable and replaceable layer. Based on these target reliability indices, the optimal combination of Titanium layer 40 mm and Aluminum layer 130 mm for the composite plate can be obtained as shown in Figure 4-9 by overlapping β_A contour to β_R contour in Figure 4-10.

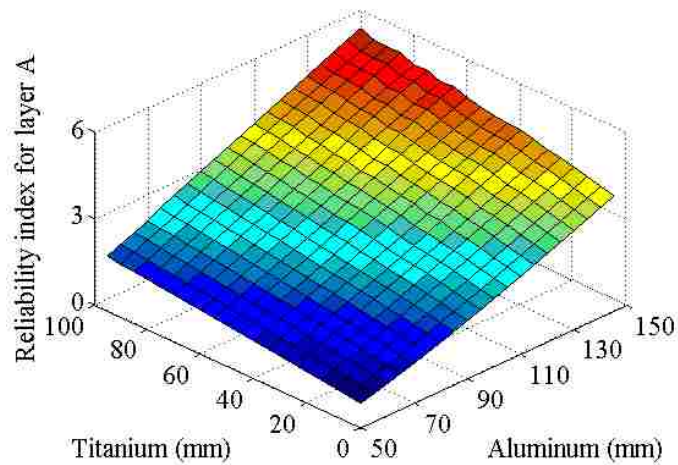


Figure 4-8 Reliability index surfaces of Aluminum layer β_A

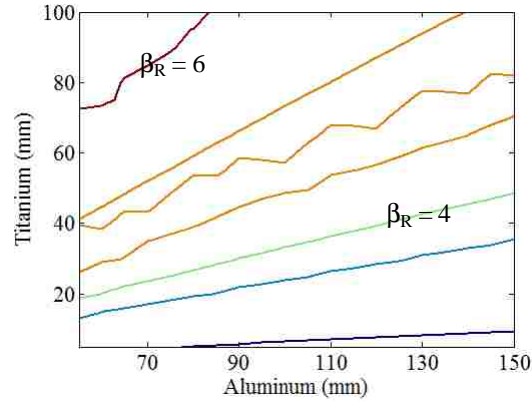


Figure 4-9 β_R contour

If more than two optimal solutions exist, due to significant non-linearity of the beta surfaces, the optimal solution can be determined by minimizing the use of materials, that gives the minimum overall cost and weight of the composite plate. In this case, a cost function can be utilized as a secondary objective. As the cost of the composite plate is a function of Titanium and Aluminum layer thicknesses, a linear cost model was used here:

$$Cost = w_R d_R + w_A d_A \quad (78)$$

where w_R and w_A are the unit cost or weight of Titanium and Aluminum respectively.

Hence the optimal design is the one that minimizes the cost and achieves $\beta = \beta_{target}$. For the optimal thickness of Titanium layer 40 mm and Aluminum layer 130 mm, the corresponding cost function shown in Figure 4-10 can be formulated for example using density of the two materials in Table 4.1.

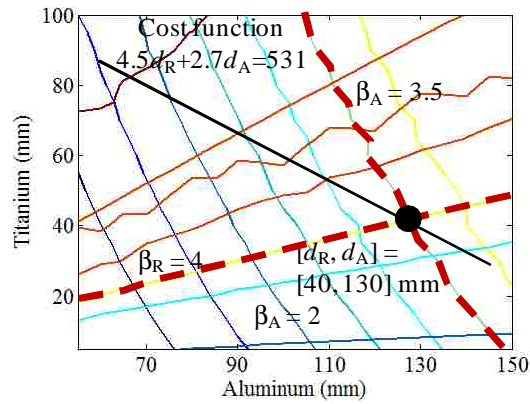


Figure 4-10 Overlapping β_A and β_R contours to show the optimal combination of layer thicknesses (as marked in black dot) and the corresponding weight cost function for reference

The optimal composite plate to resist this uncertain blast event having a mean maximum pressure 80 MPa with 30% COV is then determined to have a total thickness of 170 mm (40 mm Titanium and 130 mm Aluminum). While the optimal composite plate thickness seems to be relatively thick, it is worth noting that the weight of this composite plate per unit area is equivalent to 68 mm steel plate. The dynamic responses for this composite plate is computed using the above mechanical model and is presented in Figure 4-11 for Aluminum layer and Figure 4-12 for Titanium layer.

The residual strain of Aluminum approaches 3.3% as shown in Figure 4-11, while Titanium layer stress reaches 115 MPa right after blast as shown in Figure 4-12. By comparing stress evolutions in Titanium and Aluminum layers, Titanium is restrained during Aluminum yield. Although Aluminum layer thickness is determined by assuming that the layer is consumable, the maximum strain 3.3% seems relatively high for practical

use. It is important to note that a realistic blast event will not generate uniform pressure on the surface of the composite plate and materials yield typically happens locally. Therefore, while the above method provides a simplified approach for design of the composite plate, FE analysis of the composite plate (300 mm × 300 mm) is necessary to examine the effect of the blast event.

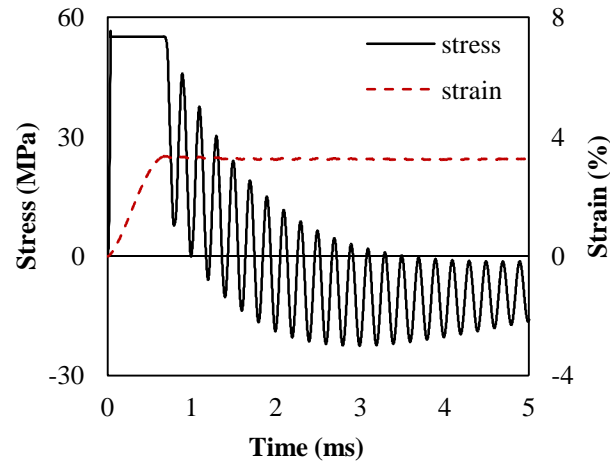


Figure 4-11 Dynamic responses of Aluminum layer of the composite plate consisting of 40 mm Titanium and 130 mm Aluminum due to blast air pressure wave as shown in Figure 4-3

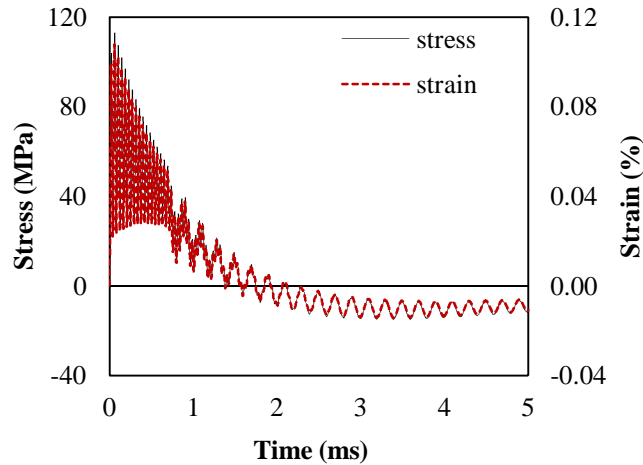


Figure 4-12 Dynamic responses of Titanium layer of the composite plate consisting of 40 mm Titanium and 130 mm Aluminum due to blast air pressure wave as shown in Figure 4-3

The FE analysis examined the structural response of the composite plate subjected to a high explosive (HE) detonation. Using values from literature for the blast parameters an explosive charge of 0.2 kg of C4 detonated in air at an offset distance of 160 mm from the composite plate. C4 is a particular type of high explosive that contains three major ingredients: explosive, plasticizer and marker. The explosive most commonly used in C4 is research development explosive (RDX) also known as cyclonite ($C_3H_6N_6O_6$) [10].

Table 4.2 Constants for JWL [73]

HE	ρ (kg/m ³)	A (GPa)	B (GPa)	R_1	R_2	ω
C4	1600	609.77	12.95	4.5	1.4	0.25

The plasticizer is a plastic binder and the marker is used to trace the origin of the HE. The C4 was considered to have dimensions of 30 mm x 60 mm x 60 mm to produce a

maximum pressure 104 MPa, which is determined as the average 80 MPa plus the standard deviation 24 MPa of the maximum blast pressure for design, at the center of the composite plate.

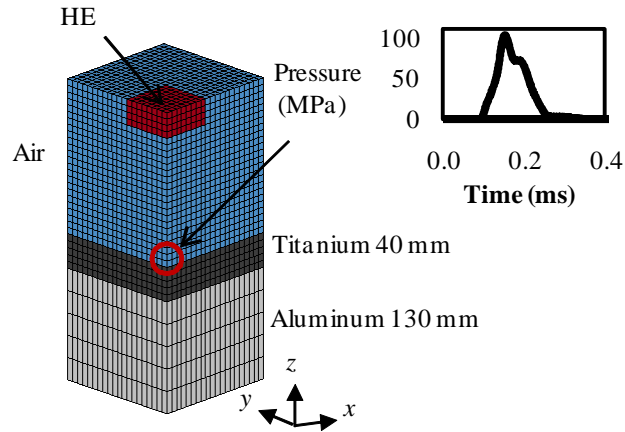


Figure 4-13 Blast modeling using finite element analysis of 40 mm Titanium and 130 mm Aluminum composite plate to 104 MPa peak blast pressure at the center of the plate

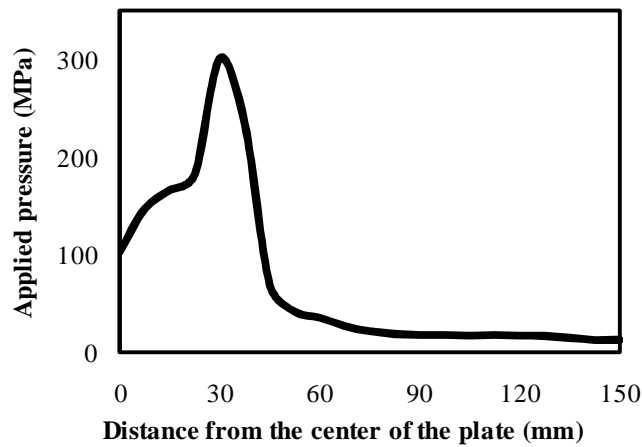


Figure 4-14 The applied pressure distribution along y-axis

The simulation was performed using LS-DYNA®. LS-DYNA® is transient dynamic finite element software that has been proven effective at modeling blast events [50]. The finite element mesh was performed using the Euler formulation. The Arbitrary Lagrangian Eulerian [30] formulation was used to augment the Euler formulation. Solid elements of the 8-noded hexahedrons in LS-DYNA® were used to mesh both the air and the composite plate. The FE model consists of 14,240 elements, which equates to 29,888 nodes. The detonation was performed using material model 8 after Hallquist [50]. This model represents a high explosive burn material. The constants for the JWL model corresponding to Equation (75) are presented in Table 4.2 [73]. A quarter of the composite plate subject to HE is modeled as shown in Figure 4-13. The maximum applied air pressure distribution at the top of the plate is computed from the center of the plate to the end as shown in Figure 4-14. Although the maximum pressure at the center of the plate was constrained to 104 MPa, a pressure of 300 MPa occurred at 30 mm from the center of the plate.

Due to the excessively high pressure of 300 MPa, the plastic strain up to 3.3% is developed locally at 1.5 ms after blast in Titanium layer as shown in Figure 4-15. A higher volume fraction of the Aluminum layer also yields at plastic strain of 0.58% as shown in Figure 4-15. Von Mises stress evolutions at the center of the composite plate are presented in Figure 4-16. Stress at the top of the Aluminum layer reaches yield while that stresses at the bottom do not reach the yield strength of 55 MPa. It is noticeable that while Titanium layer stresses both at the top and the bottom are under the elastic limit of Titanium, the stress level at the top of Aluminum layer approaches its yield strength.

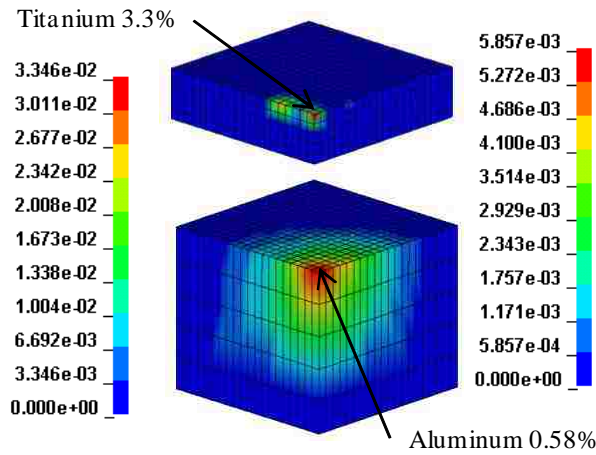


Figure 4-15 Plastic strain contours at time 1.5 ms

The FE analysis proved that both Titanium and Aluminum yielded locally due to the blast event. Therefore, it might be necessary to increase the target reliability index for layer “R” to prevent unexpected localized yield of the layer due to blast load effect as shown in Figure 4-14. However, the target reliability index for the design of absorbing layer “A” thickness might be decreased to consider the high variation of the applied air pressure distribution on the plate surface as shown in Figure 4-14. The FE analysis results can thus be used to enhance the proposed design method and might allow examining several combinations of materials which are relatively strong and ductile such as ceramics or mild steel for high blast resistance.

Cowper and Symonds model [17] is used to scale the yield strength of the materials according to the strain rate $\dot{\epsilon}$ as:

$$f_{sy,d}(\dot{\epsilon}) = f_{sy} \left[1 + \left(\frac{\dot{\epsilon}}{H} \right)^{1/p} \right] \quad (79)$$

where $f_{sy,d}$ and f_{sy} are dynamic and static yield strengths respectively. p and H are material constants taken as 4 and 6500 /s for Aluminum [77] and 9 and 120 /s for Titanium [78] respectively. The plastic strain contours and the Von Mises stresses in the composite plate considering strain rate-dependent yield strengths of the two materials are presented in Figure 4-17 and Figure 4-18 respectively.

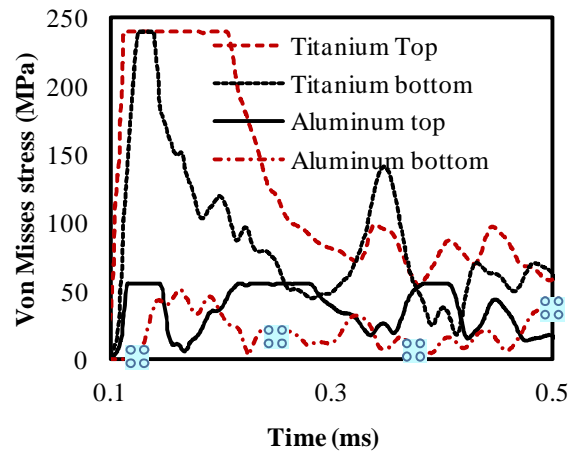


Figure 4-16 Von Mises stress along the mid-axis

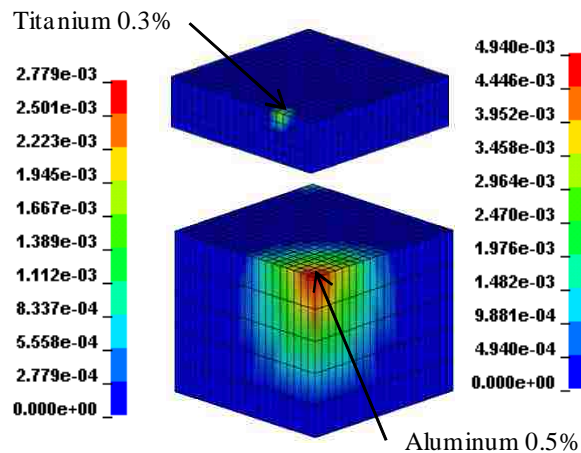


Figure 4-17 Plastic strain contours at time 1.5 ms considering strain rate effect

Comparing the plastic strain predictions in Figure 4-15 and Figure 4-17, it is apparent that the Titanium layer almost does not yield when the strain rate-dependent material properties are considered for the FE analysis. Moreover, as shown in Figure 4-18, the stress at the top of Titanium layer reaches 440 MPa below Titanium strain-dependent yield strength and the stress at the bottom of Aluminum layer also does not reach to the static yield strength of Aluminum of 55 MPa. The comparison between the two finite element models with and without strain rate-dependent properties indicates that it is important to consider strain rate-dependent properties of the materials. It is therefore noted that the simplified analytical method described early underestimates the mechanical properties of materials and can be considered as conservative method. It is expected that altering the proposed analytical and optimization methods to consider strain rate-dependent material properties might result in thinner optimal plates than those suggested early.

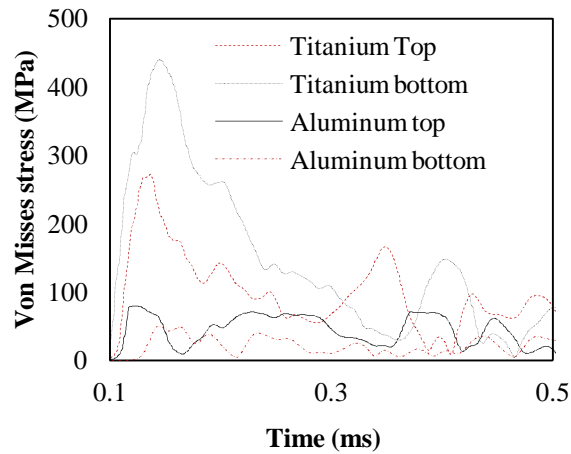


Figure 4-18 Von Mises stress along the mid-axis considering strain rate effect

4.1.5 Conclusions

In this study, a simplified reliability-based design method of blast-resistant composite plate is presented along with a case study. The composite plate consists of resisting and absorbing layers to reflect and absorb the blast energy. Different levels of target reliability indices are assigned to each layer to consider the different purposes of each layer. A design example of a two layer composite plate made of Aluminum and Titanium subjected to an uncertain blast event is presented. A finite element analysis of the optimized Titanium and Aluminum composite plate proved that the ability of the plate to resist blast events. However, the FE model showed the necessity to alter the target reliability values in design to account for possible local yielding. The FE analysis also showed the importance of considering strain rate-dependent material properties in the analysis. The proposed design method can be used for conservative design of composite plates for enhanced blast resistance.

4.2 Second Case Study: Design Optimization of Two Dimensional Composite Plate

The second case study considers the design of blast resistant two-layer metallic composite plate in which two materials, Aluminum and Titanium, are distributed in each layer. The mechanical properties of Aluminum include yield strength (55 MPa), ultimate tensile strength (115 MPa), density (2700 kg/m^3), Young's modulus of Elasticity (70 GPa) and Poisson's ratio (0.33) while for Titanium yield strength (170 MPa), ultimate tensile strength (234 MPa), density (4500 kg/m^3), Young's modulus of Elasticity (116 GPa) and Poisson's ratio (0.34) [79]. The composite plate is a two-layer cylindrical plate

with a 250 mm radius and a thickness that can range between 10 – 30 mm per layer. The plate is subjected to an under soil buried explosive.

4.2.1 2-D Homogenization Method Applied to the Two-Layer Composite

The process of determining the properties for a given layer of the composite for a single iteration is discussed here. This process is repeated for all iterations during the optimization processes. A two dimensional (2-D) unit cell of the composite material is considered here for determining the properties of each layer. The unit cell is discretized into 3x3 sub cells as shown in Figure 4-19. The unit cell consists of 9 total elements. Each of the elements is then assigned either the material properties of Aluminum or Titanium. Since this is a 2-D problem, only three independent unit strain fields need to be applied to the model in order to extract the material properties. The three strain fields are shown in Figure 4-19.

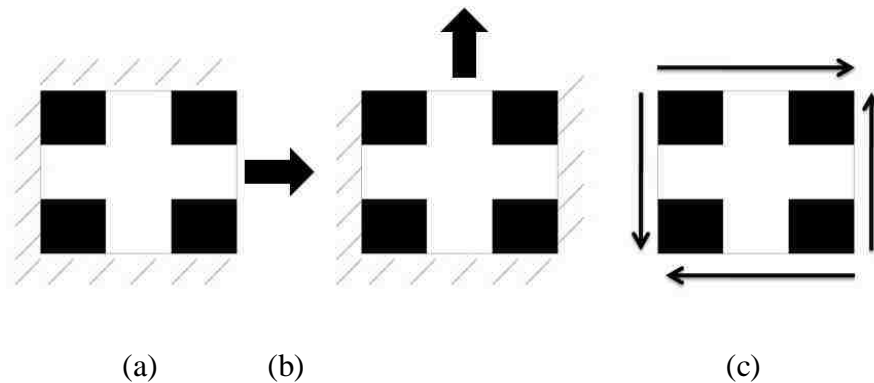


Figure 4-19: Three load cases showing unit strain in (a) x direction, (b) y direction and (c) shear.

There are a total of 16 nodes in each unit cell model. After the displacements are applied, the FEA model is solved for the unknown stresses at all nodal locations. The homogenization method allows for the calculation of the averaged properties of the unit cell. The four independent components of the stiffness matrix can be calculated as:

$$S_{11} = \frac{1}{E_1}, S_{12} = \frac{-\nu_{12}}{E_1}, S_{22} = \frac{1}{E_2} \text{ and } S_{66} = \frac{1}{G_{12}}, \begin{Bmatrix} \varepsilon_1 \\ \varepsilon_2 \\ \gamma_{12} \end{Bmatrix} = \begin{bmatrix} S_{11} & S_{12} & 0 \\ S_{12} & S_{22} & 0 \\ 0 & 0 & S_{66} \end{bmatrix} \begin{Bmatrix} \sigma_1 \\ \sigma_2 \\ \tau_{12} \end{Bmatrix} \quad (80)$$

Then the stresses are summed for each direction and divided by the number of total nodes. This new stress value represents the average stress for the homogenized unit cell.

The homogenized properties of the unit cell are then calculated as:

$$\nu = \frac{\sigma_{11}\sigma_{12}}{(\sigma_{11}\sigma_{22} + \sigma_{12}(\sigma_{12} - \sigma_{21}))} \quad (81)$$

$$E_1 = \frac{\sigma_{11}(\sigma_{11}\sigma_{22} - \sigma_{12}\sigma_{21})}{(\sigma_{11}\sigma_{22} + \sigma_{12}(\sigma_{12} - \sigma_{21}))} \quad (82)$$

$$E_2 = \frac{(\sigma_{11}\sigma_{22} - \sigma_{12}\sigma_{21})}{\sigma_{11}} \quad (83)$$

$$G_{12} = \tau_{123} \quad (84)$$

Where the subscript numbers on the left hand side of Equations (81-84) represent the modulus direction, the subscript numbers on the average stress values (σ_{ij}) represent the

load case number and the stress direction respectively and τ_{123} is the average shear stress from load case 3.

4.2.2 CFD Model

CFD allows for modeling of the transient solid and fluid interactions. The model consists of 2 kg of TNT that is detonated at a location 150 mm below the soil surface. The explosion is simulated and the pressure transfer to the composite plate is monitored for 1 ms. The composite plate is centered above the explosive material at a height of 260 mm above the soil surface as shown in Figure 4-20. The model is simulated in a 2-D plane in which quadrilateral elements are used for discretizing the simulation space. ANSYS-AUTODYN was used to simulate the pressure wave generated by the high explosive material [80].

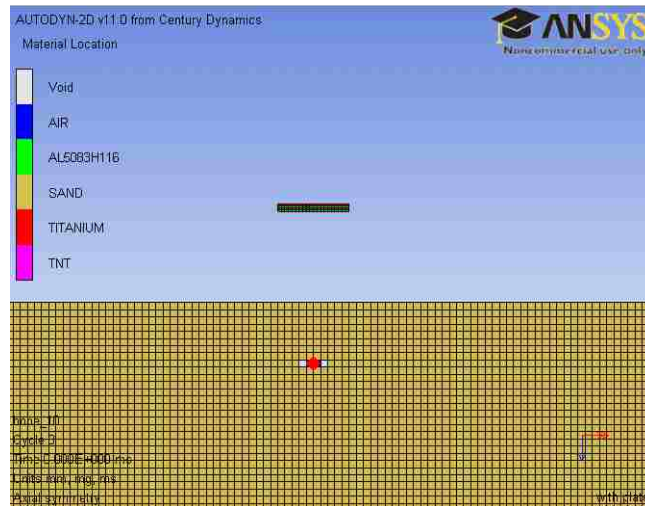


Figure 4-20: Mesh of CFD model showing buried TNT and composite plate.

Five materials were used in the simulation process: air, sand, TNT, Aluminum and Titanium. The gas dynamics are calculated using the Euler algorithm, while the solid dynamics are simulated with the Lagrangian algorithm [80]. The air was simulated as an

ideal gas. The Jones-Wilkins-Lee Equation of state is used to simulate the explosion of the TNT [80]. The time history of the pressure wave was recorded by placing gauges along the lower surface of the composite plate where the blast will first impact the composite plate. The pressure of the blast wave was then used in modeling the transient structural behavior of the plate in finite element analysis. The gauges were placed every 25 mm along the surface of the plate.

4.2.3 FEA Model

The FE model is simulated using ANSYS. The composite plate was modeled as a 2-D axisymmetric model using transient analysis. As discussed above, the homogenization method was used to determine the properties of the composite plate. The properties used by the FE model are the modulus of elasticity in the radial direction, the modulus of elasticity in the y direction, Poisson's ratio and the shear modulus. The density of the layers is calculated using the rule of mixtures method. The thickness of each layer of the composite plate is a design variable. This necessitates the use of an automatic meshing routine in the FE model. Eight node Plane 82 elements are used for meshing the two-layer composite plate. Plane 82 elements have two degrees of freedom per node and have the capability to simulate plasticity, creep, stress stiffening, large displacement and large strain [81]. A zero $|y|$ displacement boundary condition is forced upon the lower right node to restrain the model. This is the equivalent boundary condition to constraining a 3-D cylinder from moving in the y direction along its circumference. A 3-D expansion of the 2-D mesh is shown in Figure 4-21 (a).

At each load step in the FE analysis, a specific load profile output from the CFD simulation is applied to the bottom layer of the composite plate. The load profile shown

in Figure 4-21 (b) is an example of a specific profile used at a given time for analysis. It may also be observed that location of maximum pressure does not occur at the center of the plate, nor is the blast wave uniform. The FE analysis solution is obtained using the Newton-Raphson method. For each time step, the stress distribution in both layers of the composite plate is saved for post processing.

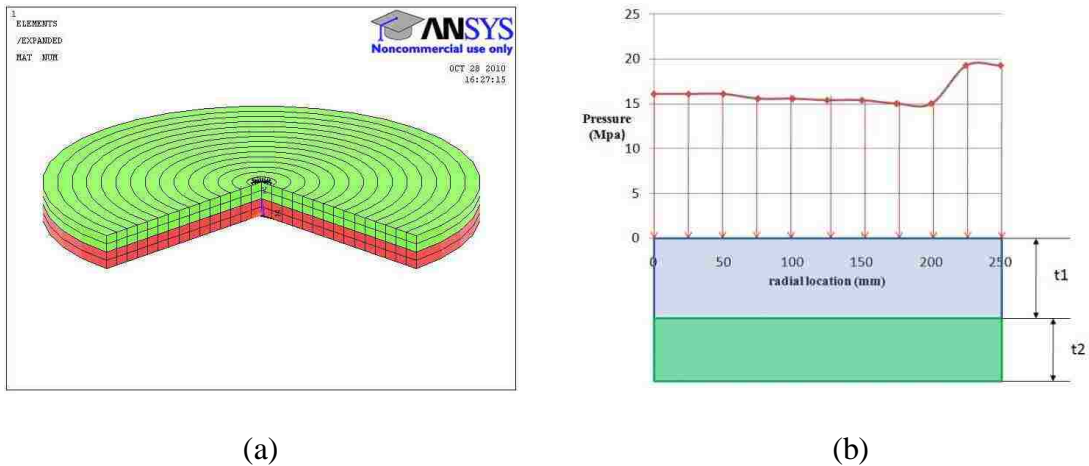


Figure 4-21: (a) Finite element model showing the two-layer composite plate considered in the case study with $\frac{1}{4}$ removed for clarity and (b) pressure distribution at $t = 0.35$ ms.

4.2.4 Design Optimization

The optimization for the case study was performed using algorithms that were coded into an optimization software called DAKOTA (Design Analysis Kit for Optimization and Terascale Applications) toolkit[82]. DAKOTA implements algorithms for both gradient and nongradient-based methods; uncertainty quantification with sampling, reliability, and stochastic finite element methods; parameter estimation with nonlinear least squares

methods; and sensitivity analysis with design of experiments and parametric study methods. These methods may be used individually and on their own or as a specific component integrated within advanced strategies like surrogate based optimization, mixed integer NLP, or uncertainty optimization [82]. DAKOTA is a flexible and extensible problem solving software for the design and analysis of complex computational models and may be integrated with high performance computers. Two objective functions representing the maximum stress-to-strength ratio and the weight of the composite denoted as f_1 and f_2 are defined as:

$$f_1 = \max_{1 \leq m \leq n} \left\{ \frac{\max(\sigma_m^T)}{\sigma_m^{UT}}, \frac{\max(\sigma_m^C)}{\sigma_m^{UC}} \right\} \quad \& \quad f_2 = \sum_{m=1}^N \pi r^2 T_m \rho_m \quad (85)$$

In this formulation, f_1 is the maximum stress-to-strength ratio in all individual layers and f_2 is the weight of the composite. N is the total number of layers in the composite; $\max(\sigma_m^T)$ is the maximum tensile stress observed in the m^{th} layer due to the applied stress wave; σ_m^{UT} is the ultimate tensile strength of the m^{th} layer; $\max(\sigma_m^C)$ is the maximum compressive stress observed in the m^{th} layer due to the applied stress wave; σ_m^{UC} is the ultimate compressive strength of the m^{th} layer. r is the radius of the composite plate, T_m is the thickness of the m^{th} layer and ρ_m is the density of the m^{th} layer calculated using the rule of mixtures based on the unit cell of that layer. The optimization problem is formulated as a multi-objective nonlinear optimization that targets to minimize the maximum stress-to-strength ratio and to minimize weight of the composite while meeting the bounds for layer thicknesses as follows:

$$\text{Minimize} \quad f_1, f_2 \quad \text{Subject to} \quad T_m^{\min} \leq T_m \leq T_m^{\max} \quad 1 \leq m \leq N \quad (86)$$

For our case study, we have a two-layer ($N = 2N = 2$) axisymmetric composite plate with $r = 250 \text{ mm}$. The thicknesses of each layer in the model may vary between $T_m^{\min} = 10 \text{ mm}$ and $T_m^{\max} = 30 \text{ mm}$. The layers are given elastic properties that vary between 116 GPa for Titanium and 70 GPa for Aluminum. These bounds are the extreme limits of the design space for a given layer.

There are a total of 20 design variables, 18 of which are the elastic properties and 2 of the design variables are the thickness of each layer. In the optimization process the vector of design variables (DV) is passed by the optimization environment to the simulation algorithm to compute the objective function values: maximum stress-to-strength ratio overall layers and the weight of the composite plate. The design variables are updated using GA method. The optimization finishes when the stopping criteria is met and the final design variables are then saved.

NSGA was used with the steps shown schematically in Figure 4-22 using DAKOTA as the optimization toolbox. A population size of 50 is selected and generated randomly without duplicates. Binary representation is used. For crossover and mutation, design variables are selected randomly from two parents to produce two children.

Crossover rate is selected as 0.8, while mutation rate is selected as 0.1. Domination-based fitness assessment is used to force the algorithm to move towards the non-dominated frontier. All non-dominated designs are assigned a layer of 0, then from what remains, all the non-dominated ones are assigned a layer of 1, and so on until all designs have been assigned a layer. Then, these values are negated for the higher-is-better fitness

convention. For replacement elitist strategy is used where most fit members are selected and the rest are discarded.

Niche pressure is applied to prevent the algorithm from converging to a single solution.

The solutions that are too close to the current design are removed except the ones that are defined as the maximal or minimal in all but one objective dimension. A distance of 0.01 and 0.1 for stress-to-strength ratio and weight, respectively, are selected. Test for convergence includes the tests for how the expanse of the front is changing, density of the non-dominated front and goodness of the non-dominated front. The maximum number of function evaluations is set to 100.

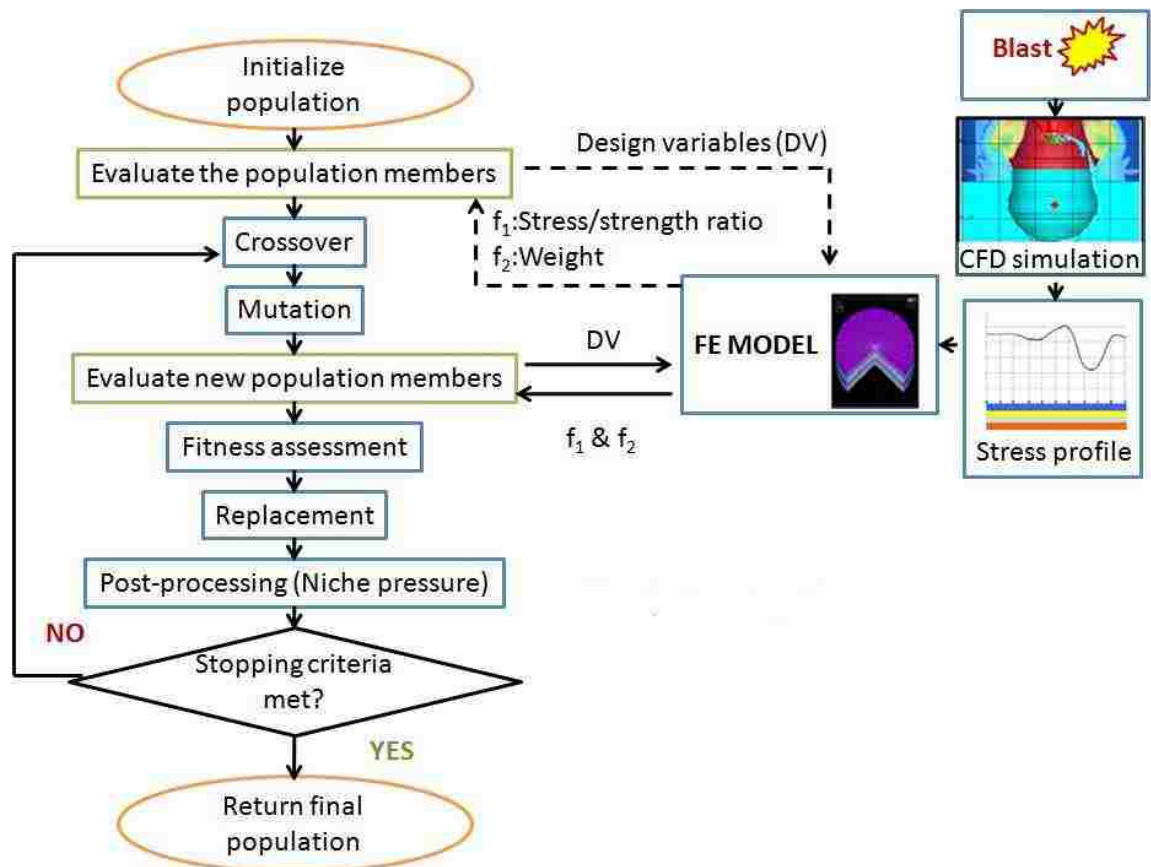


Figure 4-22: Flowchart of optimization method and its integration with the blast simulation.

4.2.5 Results and Discussion

The optimization process allowed identifying Pareto-optimal solutions for the material microstructures across the two layers to minimize the stress-to-strength ratio and weight. The MOGA method produced a Pareto front in which each Pareto point represents a microstructure for layer 1 with thickness 1 and a microstructure for layer 2 with thickness 2. The results of the MOGA optimization are presented in Figure 4-23 and in Table 4.3. Figure 4-23 shows microstructure and thickness of each layer for four example solutions along the Pareto front. The black represents the Titanium phase and the white represents the Aluminum phase. Each of the points shown in Figure 4-23 represents an optimal solution. Table 4.3 presents ten solutions some of which are labeled along the Pareto front.

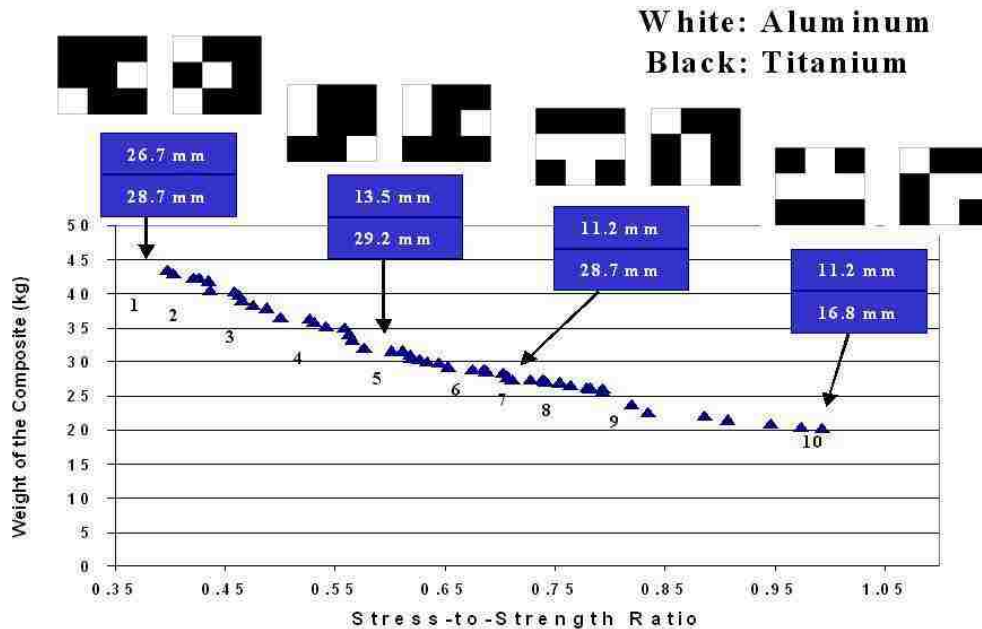

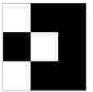
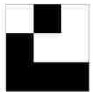
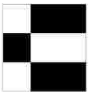
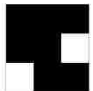
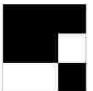
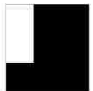
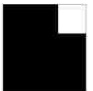
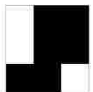
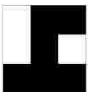

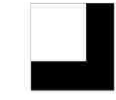
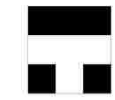

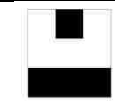


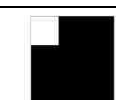
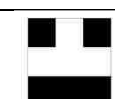
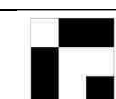


Figure 4-23: Pareto front for weight and stress-to-strength ratio as two objective functions with different material microstructures and thicknesses per layer.

As it can be observed from Figure 4-23, the solutions with lower stress-to-strength ratios such as point 1 have the highest overall composite weight. On the other hand, solutions like point 9 have a low composite weight but a relatively high stress-to-strength ratio. Any composite structures that exhibited stress-to-strength ratios above 1.0 are excluded. Those solutions with stress-to-strength ratios below 1.0 are all viable solutions and should have a good blast resistance. It may also be observed from Figure 4-23 that the amount of Titanium used in the composite is greatly reduced when moving from low

Table 4.3 Summary of results presenting ten Pareto solutions*

Solution #	T1 (mm)	T2 (mm)	Stress/Strength	Weight	Micro 1	Micro 2
1	26.7	28.7	.396	43.4		
2	29.9	25.9	.436	40.6		
3	26.1	28.7	.500	36.5		
4	17.7	28.4	.561	34.1		
5	13.5	29.2	.618	31.0		

6	11.2	28.7	.675	28.9		
7	11.2	28.7	.711	27.4		
8	11.2	28.7	.754	26.9		
9	17.7	21.8	.790	25.5		
10	11.2	16.8	.945	21.0		

* Micro: microstructure white areas represent Aluminum while black represents Titanium

stress-to-strength ratios to high ones approaching 1.0 with a relatively low weight. This is important because Titanium is a much heavier metal and more expensive to process than Aluminum. By considering other constraints such as cost, a solution may be chosen from any of those solutions on the Pareto front. It is obvious from Figure 4-23 and Table 4.3 that changes in the material's microstructure as well as the two layers' thicknesses allow for changing the stiffness distribution across the composite plate and therefore producing stresses in the composite lower than the material strength of each layer. Some of the non-dominated solutions produced stress-to-strength ratios around 0.6 while reducing the overall weight to close to 60% of the maximum possible weight using only Titanium in each layer. Allowing the thickness to change between 10 – 30 mm per layer reduced the overall stress even further.

A unit cell of 3x3 for each layer was chosen for the simulation environment because discretizing the solution space increases the number of required calculations exponentially. Using MOGA, 1000 evaluations resulted in 67 solutions. 16 of these solutions were infeasible because they yielded a stress-to-strength ratio greater than 1.0. For the 3x3 case 1000 evaluations is only about 0.38% of the total solution space. In order to cover 0.38% of the 4x4 case would require 16,384,000 evaluations. Currently, the run time is 43.7 hours, while increasing the unit cell to 4x4 would require 7.16×10^5 hours. The exponential growth of the solution space and run time is the reason why the 3x3 arrangement is the smallest microstructure that will yield useful information regarding the composite lay-up, while being able to solve in a reasonable amount of time. Unless a parallel computing approach is considered, which can significantly reduce the computational time, a 3x3 microstructure is the most suitable formulation of the problem. Further work is underway to re-formulate the optimization algorithm considering parallel computing capabilities.

Although gradient-based methods would require less computational time, a decision was made to use MOGA based on our preliminary investigation. Gradient-based methods worked well when using a rule of mixtures method to determine elastic properties. This is because the design variables were continuous. In the homogenization method the design variables are discrete and filters must be used for gradient-based methods. This adds extra computation time and introduces artificial filters. Genetic algorithms may be used with both continuous and discrete design variables. Figure 4-24 shows a schematic representation of the Pareto fronts for both gradient and non-gradient based methods for the optimization of blast resistant composites. By using MOGA for the multi-objective

optimization, artificial fixes were avoided. Moreover, using the binary encoding, artificial filters were avoided, which would normally be required if gradient based optimization was used. Based on the weights chosen and the seeding point the gradient-based optimization methods might converge to a very good solution. However, given the ability of MOGA to converge independent of the types of weights chosen and the seeding point, it clearly surpasses gradient-based methods for the problem considered in this paper. Also, another advantage of the MOGA method is that it finds multiple points along the entire Pareto front whereas the weighted-sum method or other conventional methods would produce only a single point on the Pareto front. This is demonstrated in Figure 4-24. Figure 4-24 shows the results of 2 different optimization runs using the same simulation loop shown in Figure 4-22 but with the optimization component run with both MOGA and gradient based methods. The two integrated optimizations were allowed to run for same total number of functional evaluations. It can be observed from the figure, that MOGA was able to identify a Pareto Front in which the optimal solutions were much better alternatives than the solutions of the gradient based methods. Gradient based methods are highly dependent upon starting point, which is not an issue with genetic algorithm methods. Gradient based methods should be able to eventually identify equivalent optimal solutions, but the required computational time would be much greater. A major limitation of the above work is its use of implicit method to model the transfer of the blast wave to the composite plate. The use of explicit simulation has been shown in case study 1 for validating the results of the optimization of plate sequence and will be shown later in case study 3 for 3-D homogenization and blast simulation. Furthermore, the second case study neglected the significance of strain rate on the behavior of

materials. Which was shown to significantly affect the results in the FE simulation of case study one.

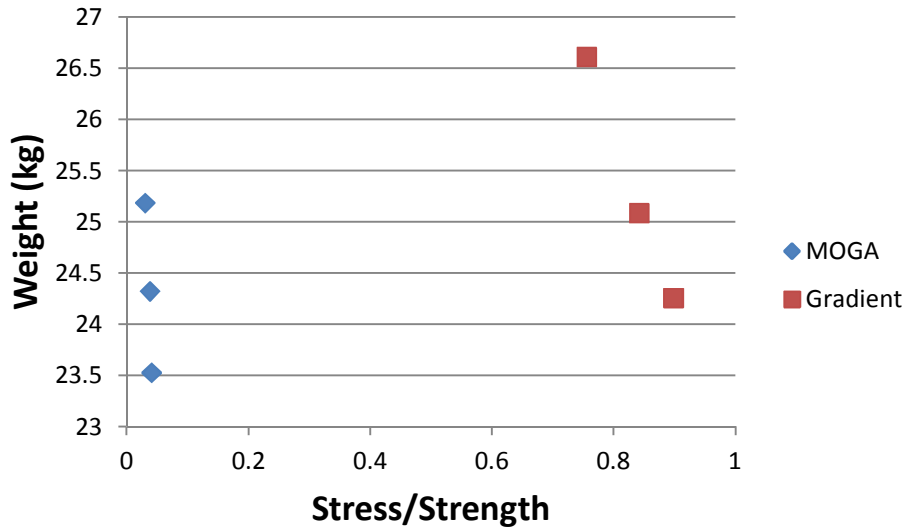


Figure 4-24: Comparison of gradient and genetic algorithm Pareto fronts

4.2.6 Conclusions

The fundamental problem of design optimization of a two-layer blast resistant composite plate is examined. A composite plate subjected to a non-uniform blast load is considered. CFD is used to obtain spatial and temporal distributions of the blast load. FEA is used to calculate the stress evolution in the plate due to the blast load. The design optimization process was performed where both material micro-structure and thickness were concurrently optimized. A multi-objective genetic algorithm optimization method is developed and used. A case study of a two-layer axisymmetric Aluminum and Titanium composite plate subjected to blast is discussed. The results show that several microstructures and thickness alternatives can be used. It is demonstrated that the use of

the homogenization method can provide design alternatives for blast resistant composites that are not available using classical design methods.

4.3 Third Case Study: Design optimization of Three Dimensional Composite Plate

The third case study considers the design of blast resistant two-layer composite plate in which two materials, Tungsten and Titanium, are distributed in each layer. The composite plate is a two-layer rectangular plate. The rectangular composite plate is modeled in 3-D. The model is a simulation of the structural dynamic response of a composite plate to an above ground high explosive detonation.

The third case study will be similar to the second case study, but it is modeled using 3-D homogenization. The two dimensional FEA code for the homogenization is replaced by 3-D homogenization and the implicit blast simulation is replaced by an explicit blast simulation where a new combined multi-physics method is used. The explicit model is simulated in LS-DYNA and is used to calculate the stress-evolution in the plate, which is then used to update the objective functions. The optimization algorithm is performed under DAKOTA computational environment. The 3-D homogenization code developed in ANSYS environment includes 56 design variables (27 design variables per layer and the thickness of each layer). Design parameters include the material properties of Tungsten and Titanium. The stiffness tensors determined in the homogenization step are transferred to the transient dynamic analysis simulating blast. Tensor values are still appropriate for being extracted from static homogenization. A more accurate

homogenization approach to perform homogenization under transient analysis is currently being developed by other researchers at the University of Illinois at Urbana Champagne. The general flowchart for the order of operations of the integrated simulation and optimization environment is shown in Figure 4-25.

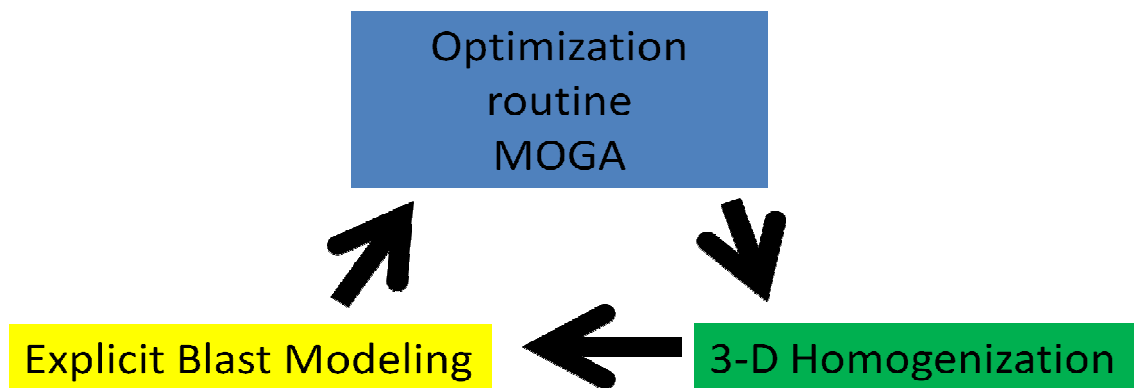


Figure 4-25 Order of operation for integrated optimization environment

4.3.1 Three Dimensional Homogenization

The 2-D homogenization method used in section 4.1 is insufficient for use with an explicit blast model. The reason for this is that when using the explicit blast model a 3-D FE simulation is necessary to capture the multi-physics environment. If a 3-D blast model is necessary, or more accurate, then a 3-D homogenization technique must be implemented such that all material properties are known and used in the blast simulation. The technique in 3-D homogenization is similar to the technique in 2-D homogenization. A unit cell is created and certain strain cases are applied to the model in order to solve backwards for the homogenized properties of the unit cell. While three unit strains were applied to the unit cell in 2-D homogenization, 6 unit strains need to be applied in 3-D homogenization. Assumptions were also made about the transversely isotropic nature of

the composite plate in 2-D. The new homogenization technique shall make no assumptions about isotropy. Therefore, the new 3-D technique will extract all of the stiffness values for the 6x6 stiffness tensor. This will allow the FE model to simulate the anisotropic behavior of the composite as well as aid in determining the true microstructure that can result in the minimal objective function values when integrated with the optimization routine. This way we will have a realistic and accurate representation of the composite plate given a certain microstructure. The 6 unit strain cases are shown in Figure 4-26.

The first three images in the first row of Figure 4-26 represent uniaxial unit strains. Moving in a clockwise direction, the first image is a unit strain in the x direction, the second image is a unit strain in the z direction and finally, the last image is a unit strain in the y direction.

The second row of images are unit shear strains. The first image is a unit x-z shear strain, the second image is unit y-z shear strain and the final image is a unit x-y shear strain.

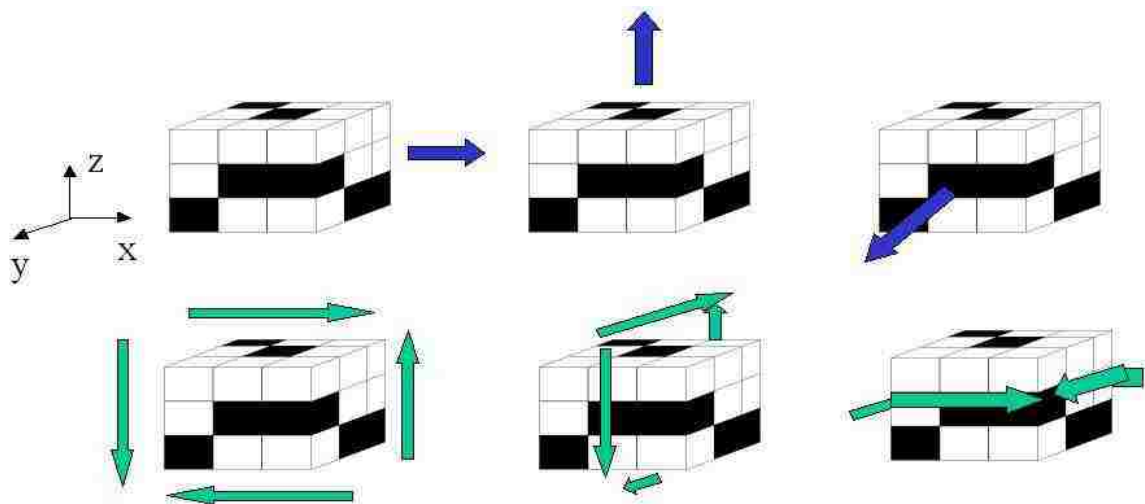


Figure 4-26: 6 unit strain cases used for 3-D Homogenization

The appropriate boundary conditions are necessary when calculating the homogenized unit cells of the model. This becomes even more important in 3-D. Each of the 6 faces of the unit cell must have the correct displacement conditions imposed upon them to accurately determine the 6x6 stiffness matrix. While imposing one type of condition will yield the modulus of elasticity of the material, imposing another type will yield the terms in the stiffness matrix. These terms are related to the modulus of elasticity, but are not exactly the same.

The above idea may be shown through examining the stiffness matrix of an isotropic unit cell. The unit cell of an isotropic material only has three constants and is shown below.

$$\begin{bmatrix} C_{11} & C_{12} & C_{12} & 0 & 0 & 0 \\ C_{12} & C_{11} & C_{12} & 0 & 0 & 0 \\ C_{12} & C_{12} & C_{11} & 0 & 0 & 0 \\ 0 & 0 & 0 & C_{44} & 0 & 0 \\ 0 & 0 & 0 & 0 & C_{44} & 0 \\ 0 & 0 & 0 & 0 & 0 & C_{44} \end{bmatrix} \quad (87)$$

Where

$$C_{11} = \frac{(1-\nu)E}{(1+\nu)(1-2\nu)} \quad (88)$$

$$C_{12} = \frac{\nu E}{(1+\nu)(1-2\nu)} \quad (89)$$

$$C_{44} = G = \frac{E}{2(1+\nu)} \quad (90)$$

C_{44} is usually referred to as the isotropic shear modulus of the material. If we assume that the isotropic material for the test case is Aluminum, then the modulus of elasticity of Aluminum is 70 GPa. The Poisson's ratio of Aluminum is 0.33, therefore the first coefficient in the matrix C_{11} would be 103.71 GPa. If the unit cell is isotropic Aluminum

and a unit x strain is imposed upon the right hand side of the unit cell as shown in Figure 4-26 and the left x face is restrained with a 0 displacement condition, then following Hooke's law $\sigma = E\varepsilon$. The calculated E would be 70 GPa. Yet, this is not the value that we want to calculate numerically. The value that needs to be calculated is C_{11} .

The boundary conditions control which terms you can calculate when placing strains on the unit cell. The boundary conditions come from the definition of Hooke's law in 3-D.

The equations of generalized Hooke's law are repeated here for examination [79].

$$\sigma_x = \frac{E}{1+\nu} \left[\varepsilon_x + \frac{\nu}{1-2\nu} (\varepsilon_x + \varepsilon_y + \varepsilon_z) \right] \quad (91)$$

$$\sigma_y = \frac{E}{1+\nu} \left[\varepsilon_y + \frac{\nu}{1-2\nu} (\varepsilon_x + \varepsilon_y + \varepsilon_z) \right] \quad (92)$$

$$\sigma_z = \frac{E}{1+\nu} \left[\varepsilon_z + \frac{\nu}{1-2\nu} (\varepsilon_x + \varepsilon_y + \varepsilon_z) \right] \quad (93)$$

If we use the strain values that are depicted in Figure 4-26 then we should obtain the coefficients of the stiffness matrix. Setting $\varepsilon_x = 1$, $\varepsilon_y = 0$ and $\varepsilon_z = 0$ Equations 91 to 93 become:

$$\sigma_x = \frac{(1-\nu)E}{(1+\nu)(1-2\nu)} = C_{11} \quad (94)$$

$$\sigma_y = \frac{\nu E}{(1+\nu)(1-2\nu)} = C_{12} \quad (95)$$

$$\sigma_z = \frac{\nu E}{(1+\nu)(1-2\nu)} = C_{12} \quad (96)$$

This exercise validates the values of the applied strains in Figure 4-26 and relates the coefficients of the stiffness matrix to Hooke's generalized law.

In order to calculate the stiffness matrix terms C_{nn} the following assumptions must be made. The unit cell has unit dimensions and is $1 \times 1 \times 1$. Then when a unit displacement of

1 is applied on any of the faces, then the strain becomes a unit strain. This is shown below.

$$\varepsilon = \frac{\Delta L}{L} = \frac{1}{1} = 1 \quad (97)$$

Therefore, when a unit strain is applied on 1 face the other 5 faces must be held to zero displacement. For example, if the first load case shown in Figure 4-26 is applied then a unit strain is placed on the right y-z face and a 0 displacement in the x direction is imposed on the left y-z face. A zero displacement boundary condition in the y and z directions are placed on both x-z and x-y faces respectively. This methodology will yield the first row and first column of the stiffness matrix. Following this method but applying a unit strain in the y and z directions will yield the stiffness terms in the 2 and 3 rows and columns respectively. The appropriate boundary conditions for the x unit strain case are shown below in Figure 4-27 for clarity. The directions the triangles are pointing with are each labeled next to the triangles in the figure with their appropriate displacement condition.

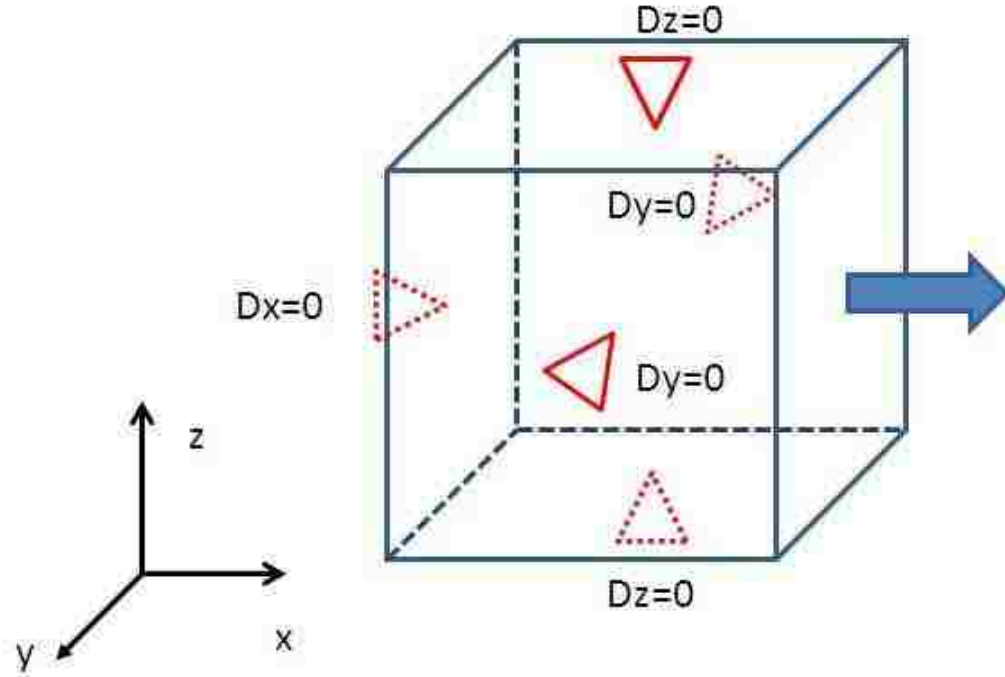


Figure 4-27 Boundary conditions for 3-D Homogenization

The next set of boundary conditions that must be appropriately formulated are the boundary conditions for the shear strain cases. These boundary conditions are much different than the unit strain cases. The shear strain is defined for the unit cell as the change in angle between the two axes of the unit cell after deformation. This is depicted in 2-D for a deformed rectangular object in Figure 4-28. From Figure 4-28 it can be shown that the shear strain in the x-y plane is defined as:

$$\gamma_{xy} = \pi/2 - \beta = \theta_1 + \theta_2 \sim \tan(\theta_1) + \tan(\theta_2) = \Delta u/\Delta y + \Delta v/\Delta x. \quad (98)$$

These assumptions are typically used during small deformation analysis. With regard to the homogenization method the last definition of γ will be used so that for the numerical analysis:

$$\gamma = \Delta u/\Delta y + \Delta v/\Delta x. \quad (99)$$

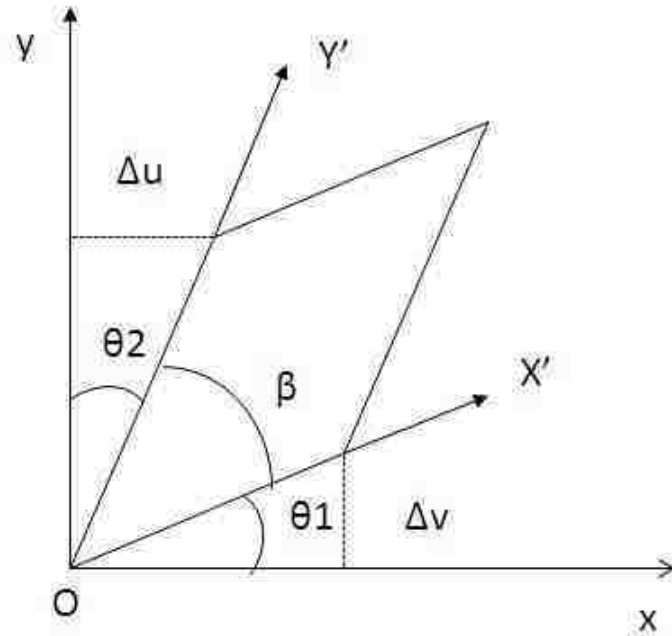


Figure 4-28 In plane deformation showing shear strain

The correct boundary conditions necessary to numerically calculate the shear modulus in the three planes is described below. Figure 4-29 shows the boundary conditions on a unit cell for a unit shear strain in the x-z plane. These boundary conditions are used to determine the shear modulus G_{xz} . The two grayed out faces in the figure are the front and back x-z faces. These two faces are constrained to a zero displacement in the y direction. The arrows in the figure specify the direction of the applied displacement. The arrow on the front y-z face has a positive displacement of 0.25, while the back y-z face has a displacement of -0.25. Similarly, the top x-y face has a displacement of 0.25 and the bottom x-y face has a displacement of -0.25. The unit displacement is obviously divided to the four faces for symmetry.

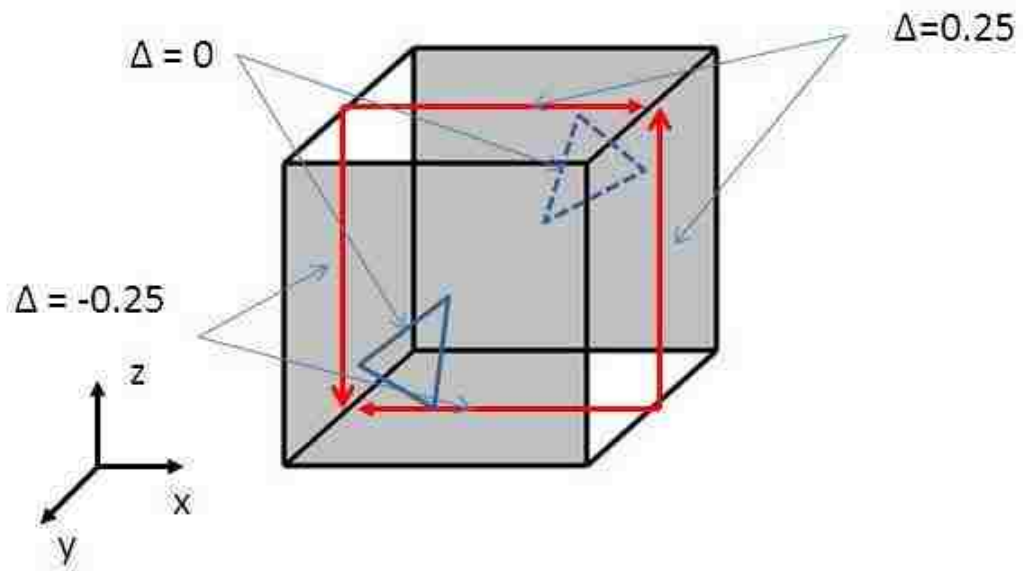


Figure 4-29 Boundary conditions for unit shear strain for 3-D Homogenization

The deformed and un-deformed shapes of the unit cell under a unit shear strain is shown using a finite element model in Figure 4-30. The previously stated boundary conditions may be used to calculate the shear modulus in the other two planes, namely G_{xy} and G_{yz} .

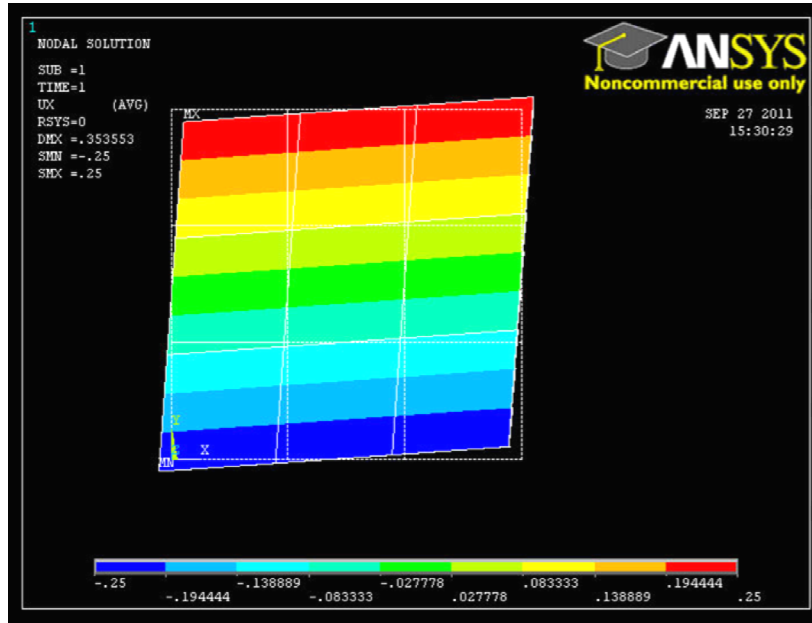


Figure 4-30 Unit shear strain applied to a finite element model

Mathematically the relationship between stress, strain and the compliance matrices in all directions is described by Equation 100 after [4].

$$\begin{Bmatrix} \varepsilon_{1i} \\ \varepsilon_{2i} \\ \varepsilon_{3i} \\ \gamma_{23i} \\ \gamma_{13i} \\ \gamma_{12i} \end{Bmatrix} = \begin{bmatrix} S_{11} & S_{12} & S_{13} & S_{14} & S_{15} & S_{16} \\ S_{21} & S_{22} & S_{23} & S_{24} & S_{25} & S_{26} \\ S_{31} & S_{32} & S_{33} & S_{34} & S_{35} & S_{36} \\ S_{41} & S_{42} & S_{43} & S_{44} & S_{45} & S_{46} \\ S_{51} & S_{52} & S_{53} & S_{54} & S_{55} & S_{56} \\ S_{61} & S_{62} & S_{63} & S_{64} & S_{65} & S_{66} \end{bmatrix} \begin{Bmatrix} \sigma_{1i} \\ \sigma_{2i} \\ \sigma_{3i} \\ \tau_{23i} \\ \tau_{13i} \\ \tau_{12i} \end{Bmatrix} \quad (100)$$

The numerical subscripts in Equation 100 represent the loading directions shown in Figure 4-26, where 1 refers to x, 2 refers to y and 3 refers to z. The subscript i refers to the actual load case. For example the first unit cell shown in Figure 4-26 is being loaded in the 1 or x direction and refers to the $i = 1$ load case. σ_{1i} is the average stress in the 1

direction for the i th load case. Equation 100 has 36 terms in the compliance matrix. The compliance matrix is symmetric so there are actually 21 independent variables only. If there are no shear-extensional coupling terms or shear-shear coupling terms in the matrix then the number of independent variables may be reduced. In terms of actual material property values, the relationship may be rewritten as Equation 101. In order to evaluate which compliance matrix type should be used a parametric analysis of different 3-D microstructures must be performed to determine whether the shear-extensional and shear-shear coupling are negligible or not. Once the compliance matrix is identified, it is forwarded to the explicit FE blast model.

$$\begin{Bmatrix} \varepsilon_{1i} \\ \varepsilon_{2i} \\ \varepsilon_{3i} \\ \gamma_{23i} \\ \gamma_{13i} \\ \gamma_{12i} \end{Bmatrix} = \begin{bmatrix} \frac{1}{E_1} & -\nu_{21} & -\nu_{31} & 0 & 0 & 0 \\ \frac{-\nu_{12}}{E_1} & \frac{1}{E_2} & \frac{-\nu_{32}}{E_3} & 0 & 0 & 0 \\ \frac{-\nu_{13}}{E_1} & \frac{-\nu_{23}}{E_2} & \frac{1}{E_3} & 0 & 0 & 0 \\ 0 & 0 & 0 & \frac{1}{G_{23}} & 0 & 0 \\ 0 & 0 & 0 & 0 & \frac{1}{G_{13}} & 0 \\ 0 & 0 & 0 & 0 & 0 & \frac{1}{G_{12}} \end{bmatrix} \begin{Bmatrix} \sigma_{1i} \\ \sigma_{2i} \\ \sigma_{3i} \\ \tau_{23i} \\ \tau_{13i} \\ \tau_{12i} \end{Bmatrix} \quad (101)$$

4.3.2 Explicit FE Blast Modeling

In order to realistically simulate the pressure wave due to a high explosive detonation near the composite plate surface a new explicit FE blast model is required. The difference between the implicit blast model and the explicit blast model is that the explicit blast model considers the plate deformation during analysis. Previously, in the

second case study, the blast model was performed in two independent steps. The CFD model was used to determine the pressure on the plate as a function of time and location. The pressure data was then transferred to the FE model. A transient analysis was performed using the pressure data from the CFD model. The issue is that the CFD model assumed a particular composite plate stiffness based on a specific microstructure and material properties. In the mean time, the integrated optimization environment continuously updates the microstructure based on the stresses generated due to the original pressure wave that encountered a different plate with different stiffness. This process is obviously flawed and an update of the composite plate stiffness is necessary. This update is known as explicit blast modeling. To accurately represent the true transfer of the pressure wave to the composite plate, the computational fluid dynamics and the structural analysis must be coupled (integrated) and performed in one step for each iteration.

The explicit blast model is simulated in LS-DYNA. LS-DYNA is a general purpose transient and dynamic finite element software that can solve complex multi-physics problems [50]. LS-DYNA couples the CFD analysis with the structural analysis. Once the two analyses are coupled into one step, then the material properties that were determined using the homogenization technique will be used to update the pressure wave in each optimization step. The process will continue until the convergence criteria are met and an optimal set of microstructures is found.

(1) Three Dimensional Explicit Blast Model

The model and parameters used in the optimization loop were modified to represent a robust repeatable model that could be used to compare cases between two different

materials and utilize materials with very different properties to portray the usefulness of the integrated optimization environment.

The new blast model was created using LS-DYNA's finite element software. The finite element model is shown below in Figure 4-31. The model is a $\frac{1}{4}$ symmetric simulation of an air burst explosion on a composite plate. The three materials in the model are TNT, air and the composite plate as shown in Figure 4-31. The model is used to solve both the flow field due to the explosion as well as the structural response of the composite plate under blast loading.

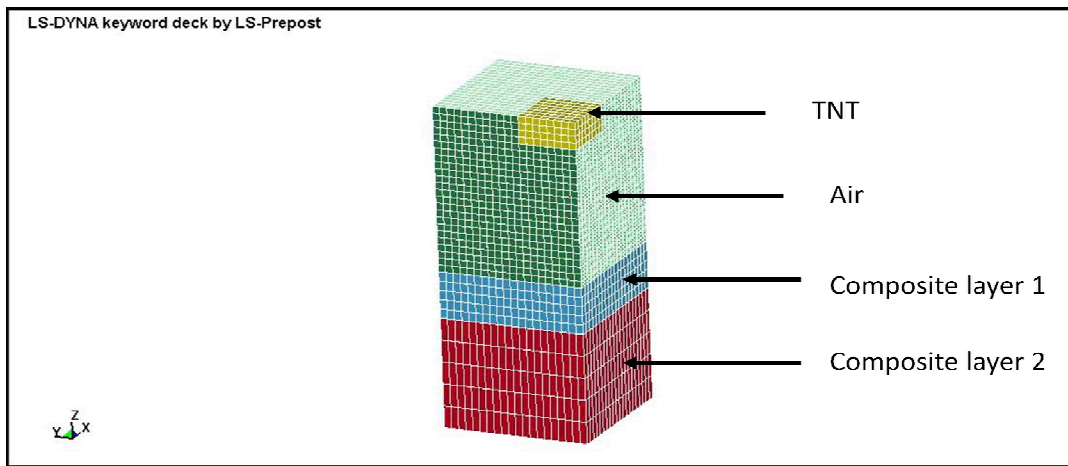


Figure 4-31 Finite Element blast model developed in LS-DYNA

The model uses an Arbitrary Lagrangian-Eulerian formulation to perform automatic rezoning of the mesh. Rezoning changes the nodal locations of the FE model to capture simulation zones where load effects are changing rapidly. This process works by performing a Lagrangian time step first. Then, an advection step is performed that includes multiple parts. Advection is the process of rezoning the mesh by making incremental changes to the nodal locations of the mesh. The advection step works by first determining which nodes should be moved. The boundary nodes are then moved to

their updated positions. Moving the interior nodes follows this step. Finally, the transport of element centered variables and momentum are calculated. These values are used to update the nodal velocities.

The model is simulated for $t = 2$ ms in which the time step size is taken as 0.001 ms. The analysis includes contact behavior as well as stonewall energy assumptions.

The Equation of state used for the TNT is the same as the verification model used in case study 1 the Jones-Wilkins-LEE (JWL) eos. The parameters of the JWL equation were listed previously in Table 4.2. The JWL eos is used in conjunction with material model 8 in LS-DYNA, which determines the lighting time of the high explosive material. The third case study also uses the gamma law as in case study 1 to simulate an ideal gas.

The three different material types all used different constitutive relationships. The TNT was modeled using a high explosive burn material. The properties used in the high explosive burn model include density, detonation velocity and Chapman-Jouget pressure. The air was modeled using a Null material type, which relies mainly on the density for calculations. Finally, the composite plate was modeled using an anisotropic elastic model for metals. Two element section types were used in the model, a solid section is used for the plates and a solid ALE section was used for the air. Specific boundary conditions were imposed on all nodes located along all of the 6 boundary faces of the model to simulate $\frac{1}{4}$ of the total blast-plate model. Frequency range damping was used for frequencies between 1 and 100,000 Hz. All the parameters used for calculating the properties of the composite plates in this model are listed in Table 4.4. The TNT has a density of 1600 kg/m^3 , a Chapman-Jouget pressure of 2 MPa and a detonation velocity of 2000 m/s. Strain rate effects were neglected because the properties are extracted from the

homogenization step and there has been no methodology for homogenizing strain rate parameters such as Cowper-Symonds power law parameters. Also, strain rate only becomes critical under loadings that exceed the elastic limit. The blast loading was designed to produce stresses beneath the yield point for a large portion of material models.

Table 4.4 Material Properties of Tungsten and Titanium

Titanium	Titanium	Tungsten
E	103 GPa	400 GPa
ρ	4340 kg/m ³	19300 kg/m ³
ν	0.34	0.28
σ_y	170 MPa	760 MPa

The results of a specific set of microstructures and thicknesses are shown below for three different time steps in the simulation process. Figure 4-32 shows the pressure wave at t = 0.1 ms right after detonation of the high explosive material. The dark color (blue) represents the ambient pressure and the pressure wave is shown with the lighter colors according to the scale bar shown at the right hand side of the figure. Figure 4-33 shows the pressure wave at t = 0.16 ms.

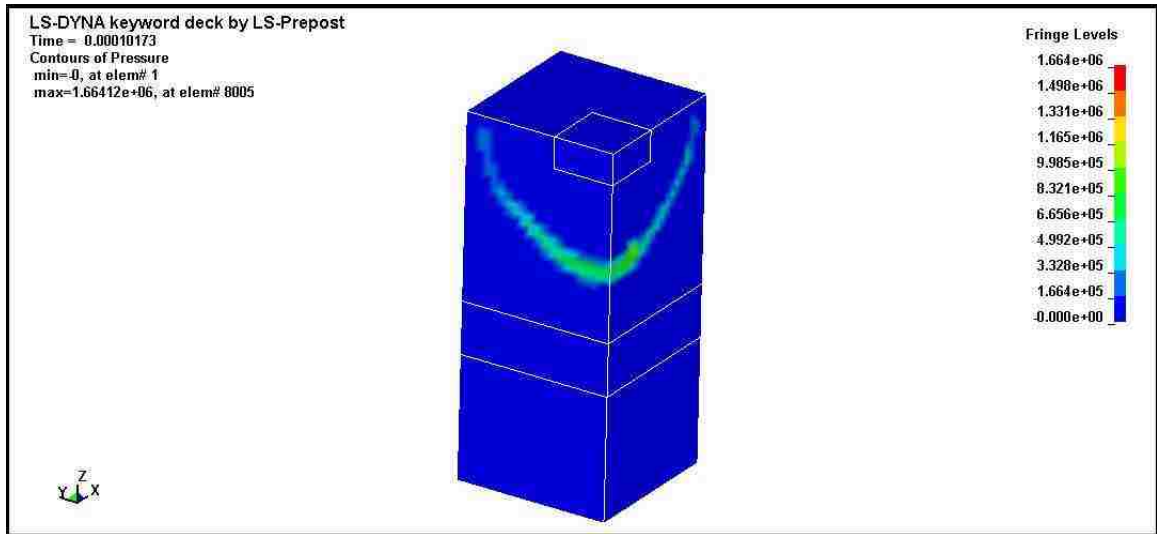


Figure 4-32 Pressure wave right after detonation of explosive material (t = 0.1 ms)

The pressure wave is fully developed in Figure 4-33 and is shown at the moment right before the pressure wave encounters the composite plate. The dark (red) color shown in the Figure 4-32 represents the highest compressive pressure in the blast wave.

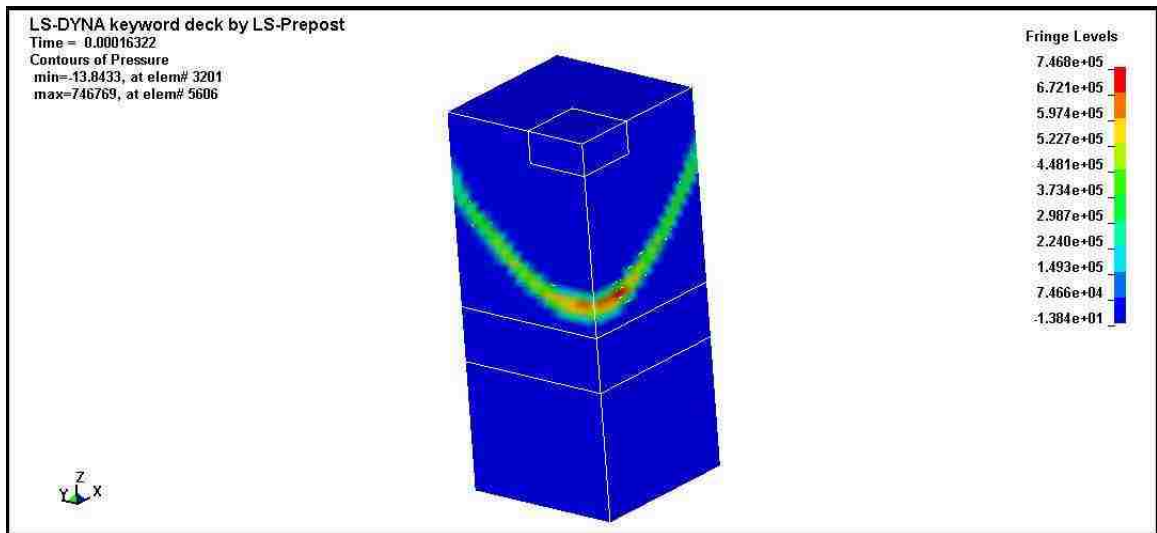


Figure 4-33 Pressure wave right before interaction with composite plate (t = 0.16 ms)

This portion of the blast wave is the part of the wave that contains the greatest amount of energy release. Figure 4-34 is taken at $t = 0.19$ ms and is the moment in time in which the blast wave is being transferred to and reflected from the composite plate. The magnitude of the stress accumulates very rapidly in the composite plate layers.

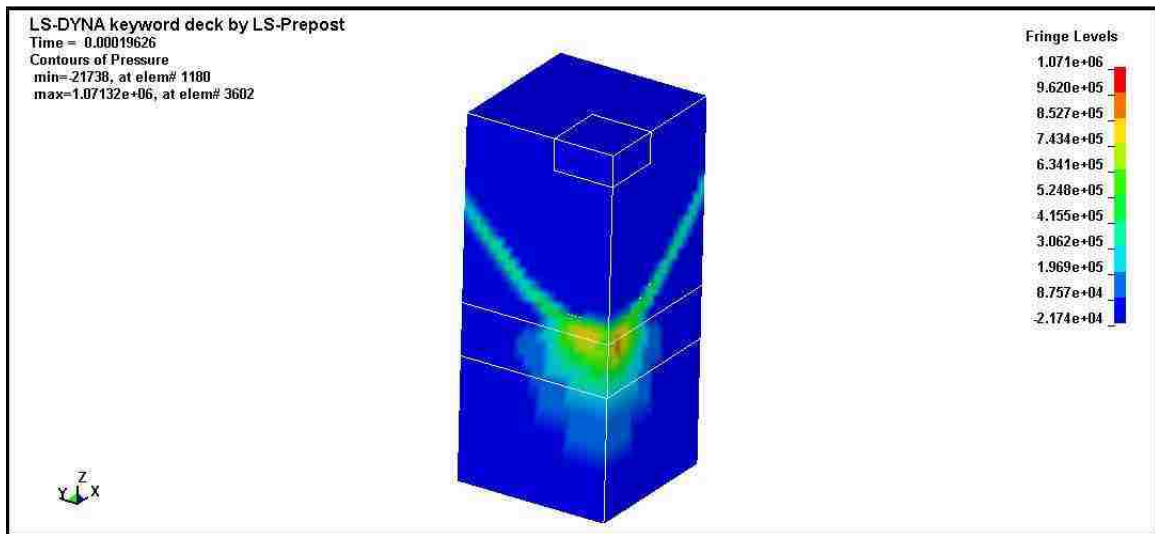


Figure 4-34 Pressure wave after encountering composite plate obstruction ($t = 0.19$ ms)

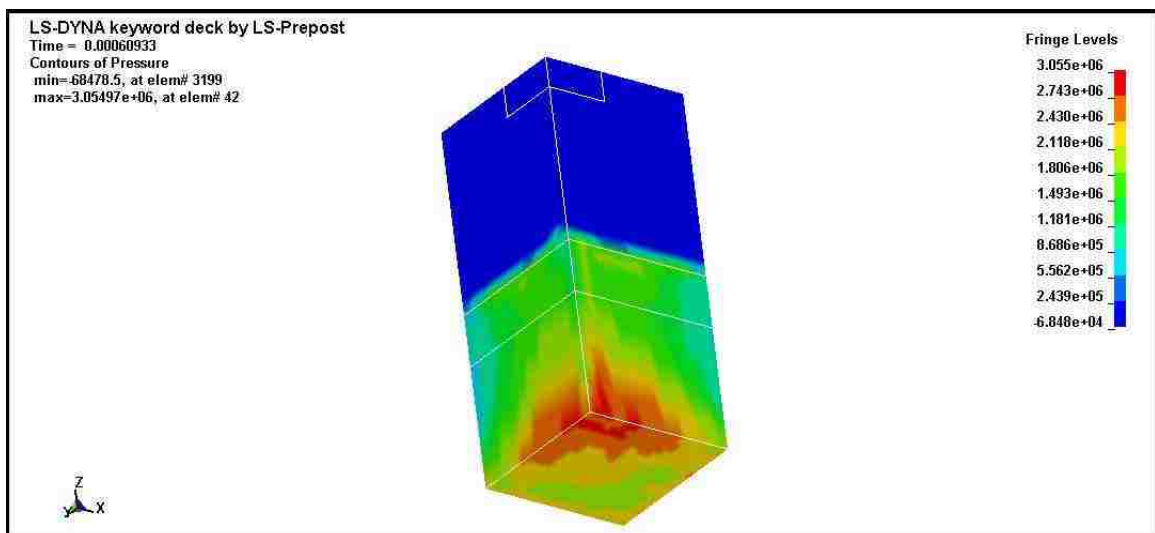


Figure 4-35 Stress distribution in the composite plate after ($t = 0.6$ ms)

The final results shown are a rotated view of the composite plate, seen from the negative x direction. Figure 4-35 shows this relative view at $t = 0.6$ ms. The maximum bending stresses in the model fluctuate between the z and y bending stresses. While the pressure wave transfers all of the energy with in 1 ms, the model is simulated for 2 ms to capture all of the dynamic behavior and interaction. The output of the model is the overall composite weight and a time history of the stress evolution in all of the composite plate nodes.

4.3.3 Design Optimization

The design optimization process is similar to that used in case study 2. Two objective functions representing the maximum stress-to-strength ratio and the weight of the composite denoted as f_1 and f_2 are defined as:

$$f_1 = \max_{1 \leq m \leq n} \left\{ \frac{\max(\sigma_m^T)}{\sigma_m^{UT}}, \frac{\max(\sigma_m^C)}{\sigma_m^{UC}} \right\} \quad \& \quad f_2 = \sum_{m=1}^N 0.09 T_m \rho_m \quad (100)$$

In this formulation, f_1 is the maximum stress-to-strength ratio in all individual layers in Pa and f_2 is the weight of the composite in kg. N is the total number of layers in the composite; $\max(\sigma_m^T)$ is the maximum tensile stress observed in the m^{th} layer due to the applied stress wave; σ_m^{UT} is the ultimate tensile strength of the m^{th} layer; $\max(\sigma_m^C)$ is the maximum compressive stress observed in the m^{th} layer due to the applied stress wave; σ_m^{UC} is the ultimate compressive strength of the m^{th} layer, 0.09 is 0.09 m^2 which is the top area of the composite plate, T_m is the thickness of the m^{th} layer and ρ_m is the density of the m^{th} layer calculated using the rule of mixtures based on the unit cell of that layer. The optimization problem is formulated as a multi-objective nonlinear

optimization that targets to minimize the maximum stress-to-strength ratio and to minimize weight of the composite while meeting the bounds for layer thicknesses as follows:

$$\text{Minimize } f_1, f_2 \quad \text{Subject to } T_m^{\min} \leq T_m \leq T_m^{\max} \quad 1 \leq m \leq N \quad (101)$$

For our case study, we have a two-layer ($N = 2N = 2$) 3-D composite plate with base and height of 300 mm . The thicknesses of each layer in the model may vary between

$T_m^{\min} = 50 \text{ mm}$ and $T_m^{\max} = 120 \text{ mm}$. There is a linear constraint between T_1 and T_2 such that $T_1 + T_2 = 170 \text{ mm}$. The layers are given elastic stiffness matrices that vary between 103 GPa for Titanium and 400 GPa for Tungsten. These bounds are the extreme limits of the design space for a given layer.

There are a total of 56 design variables, 54 of which are the elastic properties and 2 of the design variables are the thickness of each layer. In the optimization process the vector of design variables (DV) is passed by the optimization environment to the simulation algorithm to compute the objective function values: maximum stress-to-strength ratio overall layers and the weight of the composite plate. The design variables are updated using GA method. The optimization finishes when the stopping criteria is met and the final design variables are then saved.

NSGA was used with the steps shown schematically in Figure 4-36 using DAKOTA as the optimization code. A population size of 50 is selected and generated randomly without duplicates. Binary representation is used. For crossover and mutation, design variables are selected randomly from two parents to produce two children. Crossover rate is selected as 0.8, while mutation rate is selected as 0.1. The associated crossover

type is shuffle random and the mutation type is replace uniform. The fitness type is domination count with a replacement type with a limit below 6. The algorithm uses a shrinkage percentage of 0.9 and a metric tracker for convergence. The allowable percent change is 0.05 and the numbers of generations are 40. The maximum number of function evaluations is set to 1000. The integrated optimization algorithm for explicit blast modeling and 3-D homogenization is shown schematically in Figure 4-36.

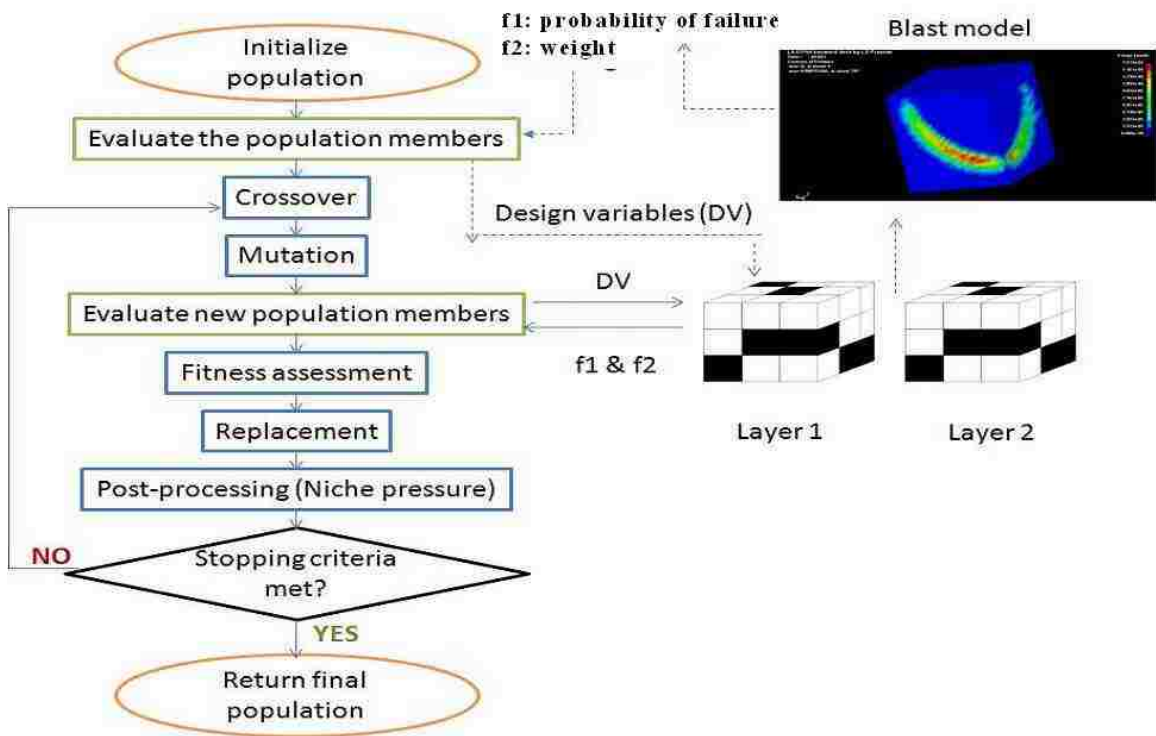


Figure 4-36 Flowchart of optimization method and its integration with the blast simulation for the second case study

4.3.4 Results and Discussions

The integrated 3-D simulation and optimization environment allowed for the identification of Pareto-optimal solutions for the composite microstructures and

thicknesses of layers 1 and 2 when minimizing two objective functions with the purpose of increasing blast resistance. The two objective functions are stress/strength ratio as well as overall composite structure weight. The MOGA optimization method identified points on the frontier of the solution space in which each point represents 2 microstructures and 2 respective thicknesses. The associated microstructures are directly related to 2 different densities and 2 different stiffness matrices. The results of the microstructural topology optimization are presented in Figure 4-37, Table 4.5 and Table 4.14. Figure 4-37 shows 8 optimal solutions along the Pareto front. The initial starting point for the optimization gave a stress/strength ratio of 21.5 and an overall composite weight of 187 kg. The original starting point is not shown in Figure 4-37 because both the stress/strength ratio and weight are significantly far from the optimal solution space. The optimal solutions shown in Figure 4-37 are obviously much better solutions than the starting point values and both stress/strength ratio and weight have been significantly reduced compared to the starting point. The 8 optimal solutions are the best solutions found using the MOGA method. These solutions are non dominant solutions that attempt to simultaneously satisfy minimizing objective one and objective two. The solutions range from number 1 being the lightest with the largest stress/strength ratio to number 8 being the heaviest with the smallest stress/strength ratio. The solutions make sense and are logically ordered. Along with each point in Figure 4-37 the percentage of Tungsten and Titanium in each layer is indicated. When moving from points 1- 8 the percentage of Tungsten in each layer increases drastically. Table 4.5 shows microstructure and thickness of each layer for four example solutions along the Pareto front and the initial starting point. Additionally, three different cross sections are shown so that all elemental

locations and material type can be presented. The cross sections represent the different layers of the microstructure. With reference to Figure 4-38 the cross sections and unit cells have the same coordinate systems as the figure. The cross sections are ordered 1-3, where the front face of the unit cell in Figure 4-38 represents cross section 1, the middle face cross section 2 and the back face is cross section 3. In Table 4.5 the black represents the Tungsten phase and the white represents the Titanium phase. Each of the points shown along the Pareto front represents an optimal solution and a design alternative. These are all non-dominant solutions and prior to other post-processing techniques are equally viable alternatives. A summary of the all the points shown in Figure 4-37 is presented in Table 4.14. Figure 4-42 is used as a reference to Table 4.14 to show which element numbers go with which material type.

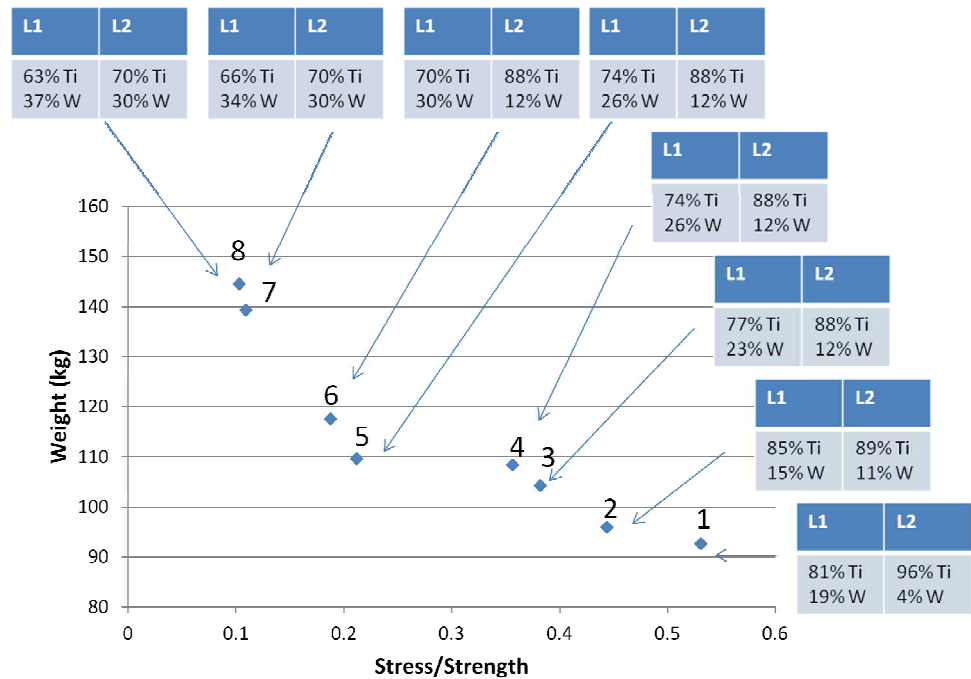


Figure 4-37 Pareto front for blast resistant 3-D composite plate optimization with 2 objective functions

As Figure 4-37 portrays the Pareto front points with lower stress to strength ratios like point 1 have the largest mass, while solutions like point 7 have the largest stress/strength ratio and smallest mass. The boundaries of the solutions space are a pure Titanium plate and a pure Tungsten plate. The Titanium plate yields the lightest structure, but experiences stresses above the elastic limit. On the other hand, a pure Tungsten plate yields the largest possible weight, but gives a very low stress/strength ratio. The case of a pure Titanium plate gives a total weight of 67 kg but has a stress/strength ratio of 2.3. The ratio of 2.3 means that the structure yielded and a pure Titanium plate would fail under the blast loading. The pure Tungsten plate would weigh 295 kg (about 5 times that of Titanium), but gives a stress/strength ratio of 0.39. When comparing these values to the solutions along the Pareto front it can be observed that the Pareto front solutions provide better designs than either of the two extreme solutions at the boundaries of the solution space. It also shows that the plate can be lightened significantly while still obtaining stress/strength ratios below 1. Pareto front point 6 gives a stress/strength ratio around 0.4 similar to a pure Tungsten case, but is almost 200 kg lighter than the pure Tungsten. Point 8 which is the heaviest optimal solution used only about 30% Tungsten per layer, which is still much lighter than a pure Tungsten case. Structures that gave stress/strength ratios above 1.0 were eliminated from the optimal results category. A stress/strength ratio above 1.0 meant that the composite structure yielded. For the purposes of this case study, yielding was considered a failure criterion. The structures with stress/strength ratios below 1.0 will have a good blast resistance to the type of blast produced in the LS-DYNA simulation. It should also be noted that when optimizing the

structures that experience stresses below the elastic limit that the strain rate effect such as the Cowper-Symonds model does not need to be included. Once yielding is included in the simulation and optimization loop then the strain rate effect should be included to give the optimal microstructure for that given scenario. Incorporating strain rate effects in the homogenization approach requires developing a new homogenization technique that is strain dependent. This part is outside the scope of this demonstration and is the study subject of other research teams [83]. The analysis here was therefore limited to solutions within the elastic limit to avoid the significance of strain rate on the behavior.

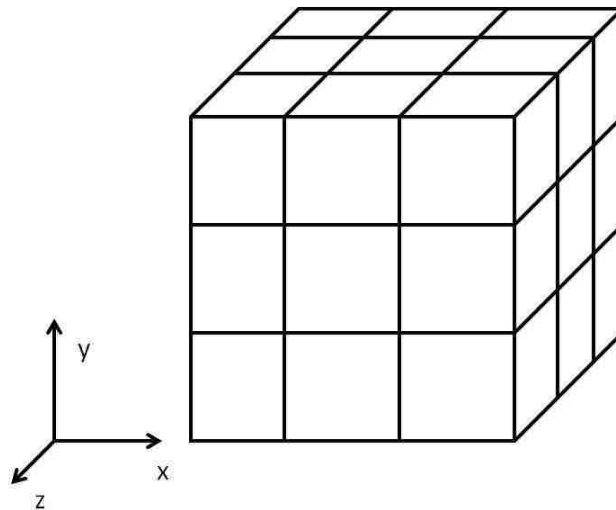


Figure 4-38 Unit cell and coordinate system reference

As was previously discussed the amount of Tungsten used in the composite plate layers is greatly reduced when moving from the high weight low stress solutions to the low weight high stress solutions. This is shown when moving along the Pareto-front from points 1-8. One can consider other constraints on the solution space such as cost in order to choose one of the non-dominant solutions from the Pareto front. In terms of today costs, commercially pure ASTM grade 1, annealed Titanium costs between 100-120 (\$US/kg),

while commercially pure Tungsten costs around 225 (\$US/kg) [84]. When examining the difference in cost between points 1 and 8 the price difference is quite significant. Figure 4-41 depicts a cost comparison analysis in \$US of the relative price difference between points 1-8. Since Tungsten is much more expensive than Titanium, it is obvious in Figure 4-41 that point 8 has the greatest Tungsten content and point 1 has the least amount of Tungsten. Solution 8 costs about \$13,500 more than solution 1. Within the scope of the blast model simulated in LS-DYNA, solution 1 gave a max stress/strength below 0.6 and solution 8 gave a stress/strength ratio slightly above 0.1, therefore based solution 1 stress/strength lowest weight and least cost may be chosen by the designer as the optimal solution. If 0.6 is considered to high of a stress/strength ratio, then points 4 or 5 may be more acceptable. By introducing cost as another objective, the end user can appropriately pick the correct design alternative that fits their application.

Figure 4-39 and Figure 4-40 show stress/strength ratio as a function of iteration number and the weight as a function of iteration number respectively. The optimal solution numbers are identified on both of the figures. It can be seen that the optimal solutions are identified and are extracted at much different iteration numbers. This is directly tied to the MOGA method. The method is not gradient based and therefore, the functional values can change drastically between iteration numbers. It is shown in the figures that all of the optimal solutions were found after about half of the functional evaluations were performed. The overall trend of Figure 4-40 is decreasing which represents a decrease in the overall weight of the structures. On the other hand, Figure 4-39 exhibits no major trend for the range of the data. This relates to the actual microstructure of the iteration number. Certain microstructural topologies cause large increases in the stress/strength

ratio. This is due to the material properties of the composite plate, which are directly tied to the microstructure. Two different iterations with similar weights and material ratios can yield much different stress/strength ratios when the microstructure is different. A microstructural difference is actually seen by the blast model as a change in the stiffness matrix. A change in the stiffness matrix results in a change in the stress distribution in the composite plate. This exemplifies a need for microstructural homogenization rather than using methods such as rule of mixtures. A rule of mixtures method would yield the same stress/strength ratio for materials of equal weight and material ratios, even when they had different microstructures.

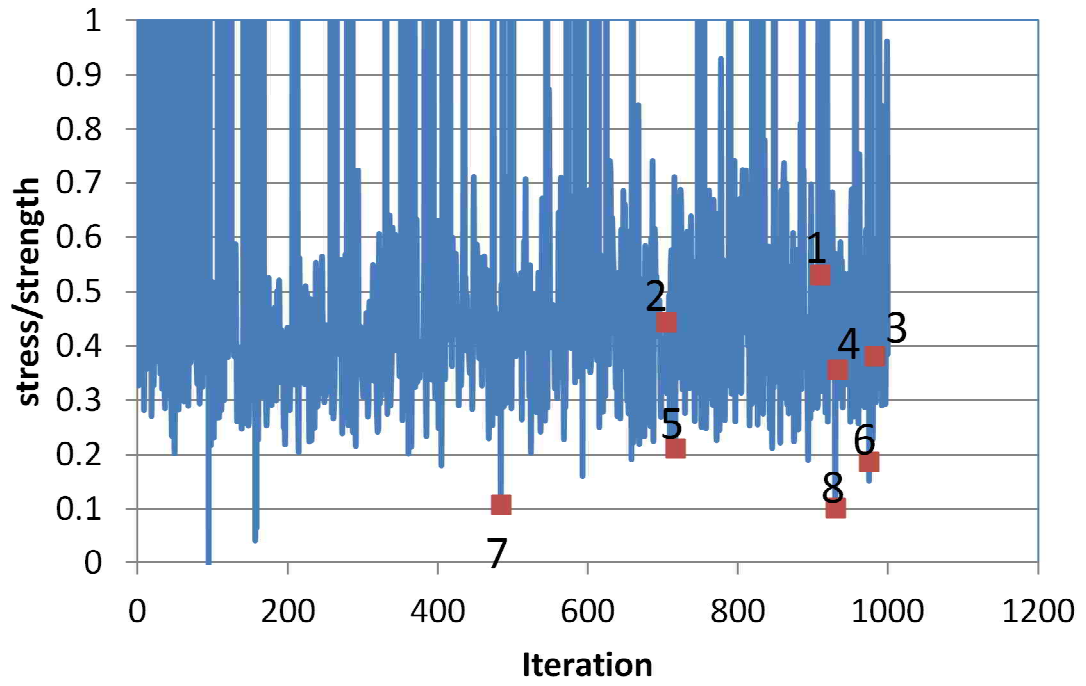


Figure 4-39 Iteration number vs. stress/strength ratio

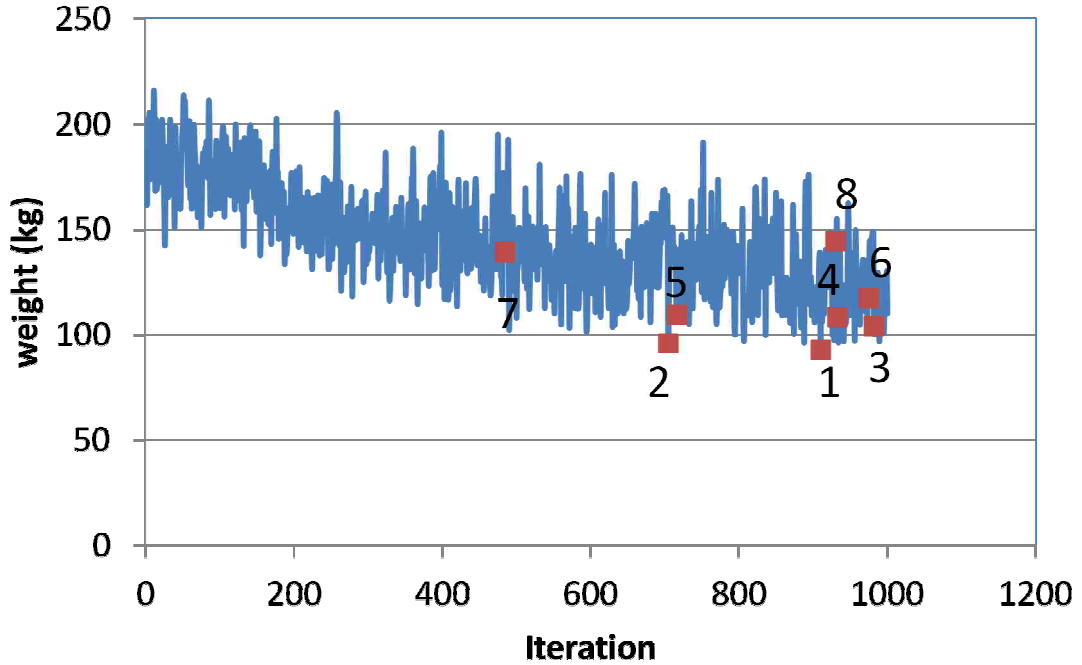


Figure 4-40 Iteration number vs. weight

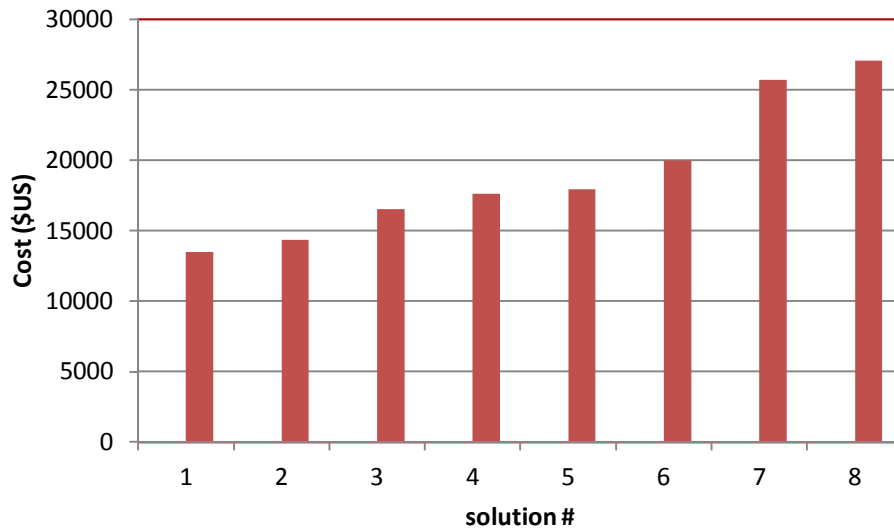
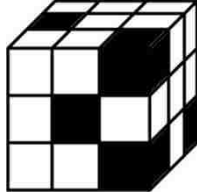
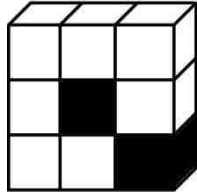
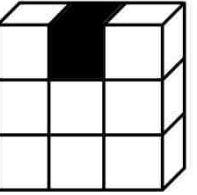
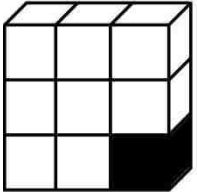
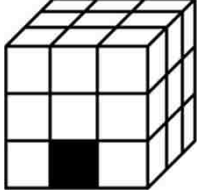
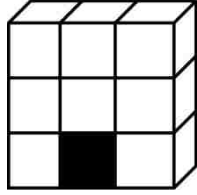
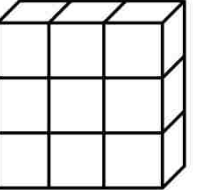
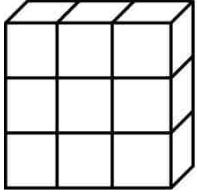
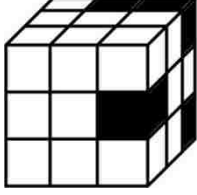
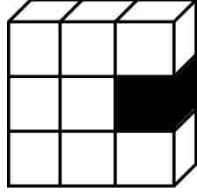
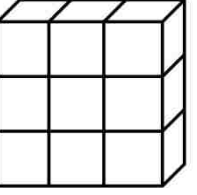
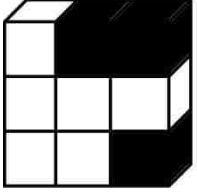
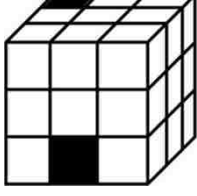
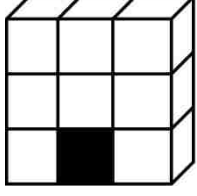
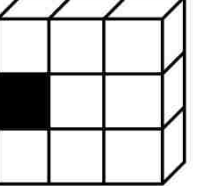
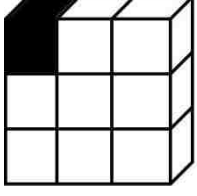
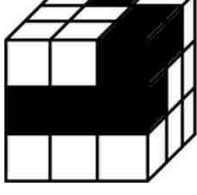
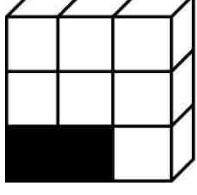
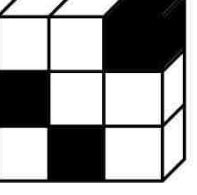
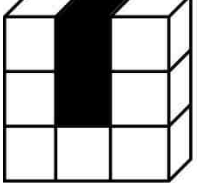
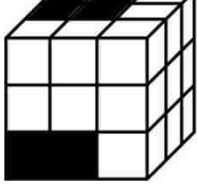
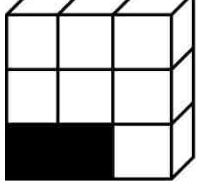
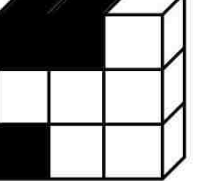
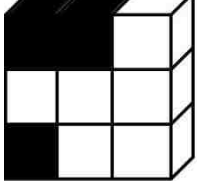
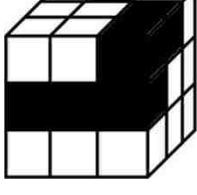
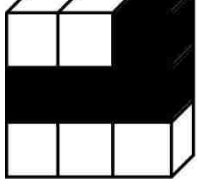
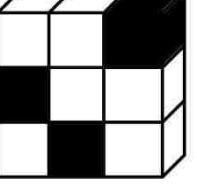
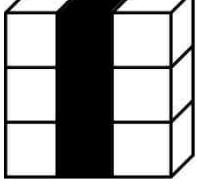


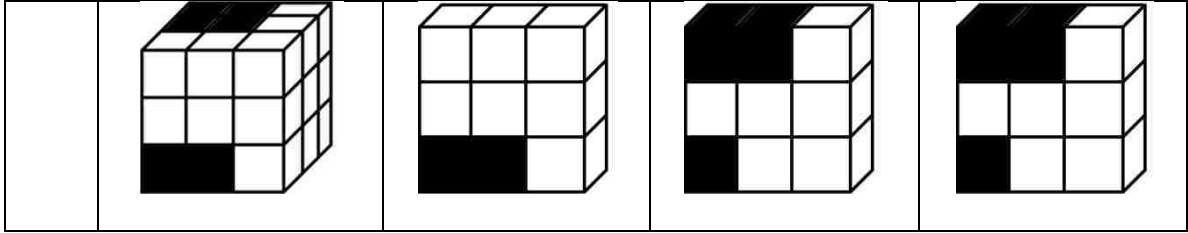
Figure 4-41 Cost comparison of design alternatives

Through optimizing the layers microstructures as well as thickness one can tailor the stress distribution in the composite plate. The optimal solution allows for lowering the stress, decreasing the overall composite weight or reducing cost.

Table 4.5 Initial start point and 4 example optimal solutions labeled on the Pareto Front (White: T, Black: W)

#	Microstructure	CS 1	CS 2	CS 3
Initial start point (50mm/120mm)				

1 (89 mm/81 mm)				
				
2 (83 mm/87 mm)				
				
7 (103 mm/67 mm)				
				
8 (103 mm/67 mm)				



The stiffness matrices and composite densities for four example solutions along the Pareto Front are presented in Table 4.6 - Table 4.13. The magnitude of the terms in the stiffness matrices decrease when moving from solution 8 to solution 1. Similarly, the densities that are directly tied to the microstructure and the percentages of Tungsten and Titanium in each layer decreases when moving from solution 8 to solution 1 along the Pareto front. It is important to note the shear-shear terms and shear extensional terms in all of the stiffness matrix terms. Using simple ROM techniques it would be impossible to determine any of these terms. This highlights one of the significant advantages of homogenization techniques when determining the properties of a composite system. These shear extensional and shear-shear terms become important under blast loading because they significantly affect the stress distribution. Certain cases greatly increase the Von Mises stress due to extra shear terms, while other cases such as those shown in Figure 4-37 reduce the shear-terms and yield a low stress/strength ratio.

Table 4.6 Stiffness matrix (GPa) Solution 8 Layer 1 $\rho = 1.38E+04 \text{ kg/m}^3$

330	139	132	-2.04	-0.319	-7.1
139	340	136	-1.5	-0.333	-7.47
136	136	338	-1.43	-7.1	-4.5
-2.04	-1.5	-1.43	96	-3.61	0.951
-0.319	-0.333	1.46	-3.61	92.3	-1.69
-7.1	-7.47	-4.5	0.951	-1.69	99.8

Table 4.7 Stiffness matrix (GPa) Solution 8 Layer 2 $\rho = 1.15E+04 \text{ kg/m}^3$

286	119	117	4.91	0.604	-5.55
119	275	124	9.83	1.27	-3.38
124	124	274	10.7	-5.55	-2.17
4.91	9.83	10.7	83.9	-2.55	0.962
0.604	1.27	1.74	-2.55	76.5	4.17
-5.55	-3.38	-2.17	0.962	4.17	77.9

Table 4.8 Stiffness matrix (GPa) Solution 7 Layer 1 $\rho = 6.56E+03 \text{ kg/m}^3$

191	91.8	90.2	0.755	-0.483	-3.35
91.8	184	89.9	0.84	-0.0198	-3.11
89.9	89.9	185	1.04	-3.35	-1.03
0.755	0.84	1.04	46	-1.26	0.136
-0.483	-0.0198	0.226	-1.26	46.8	0.656
-3.35	-3.11	-1.03	0.136	0.656	48.3

Table 4.9 Stiffness matrix (GPa) Solution 7 Layer 2 $\rho = 6.00E+03 \text{ kg/m}^3$

286	119	117	4.91	0.604	-5.55
119	275	124	9.83	1.27	-3.38
124	124	274	10.7	-5.55	-2.17
4.91	9.83	10.7	83.9	-2.55	0.962
0.604	1.27	1.74	-2.55	76.5	4.17
-5.55	-3.38	-2.17	0.962	4.17	77.9

Table 4.10 Stiffness matrix (GPa) Solution 2 Layer 1 $\rho = 9.33E+03 \text{ kg/m}^3$

229	104	105	0.23	-2.12	4.85
104	228	103	0.279	-1.1	5.08
103	103	233	0.374	4.85	2.77
0.23	0.279	0.374	60.8	2.15	-1.31
-2.12	-1.1	-2.72	2.15	62.3	0.0226
4.85	5.08	2.77	-1.31	0.0226	59.2

Table 4.11 Stiffness matrix (GPa) Solution 2 Layer 2 $\rho = 8.77E+03 \text{ kg/m}^3$

286	119	117	4.91	0.604	-5.55
119	275	124	9.83	1.27	-3.38
124	124	274	10.7	-5.55	-2.17
4.91	9.83	10.7	83.9	-2.55	0.962
0.604	1.27	1.74	-2.55	76.5	4.17
-5.55	-3.38	-2.17	0.962	4.17	77.9

Table 4.12 Stiffness matrix (GPa) Solution 1 Layer 1 $\rho = 9.88E+03 \text{ kg/m}^3$

235	106	108	-0.723	-2.11	4.87
106	242	108	-1.55	-1.15	5.15
108	108	245	-1.87	4.87	2.92
-0.723	-1.55	-1.87	66	2.5	-1.61
-2.11	-1.15	-2.62	2.5	64.5	-0.736
4.87	5.15	2.92	-1.61	-0.736	60.9

Table 4.13 Stiffness matrix (GPa) Solution 1 Layer 2 $\rho = 8.77E+03 \text{ kg/m}^3$

286	119	117	4.91	0.604	-5.55
119	275	124	9.83	1.27	-3.38
124	124	274	10.7	-5.55	-2.17
4.91	9.83	10.7	83.9	-2.55	0.962
0.604	1.27	1.74	-2.55	76.5	4.17
-5.55	-3.38	-2.17	0.962	4.17	77.9

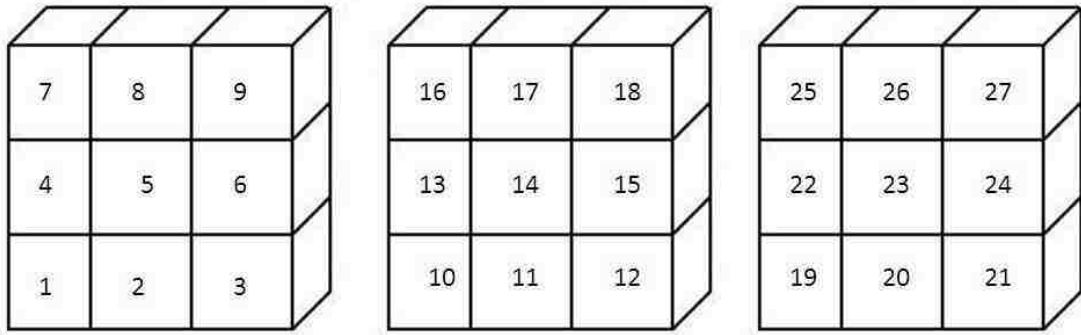


Figure 4-42 Elemental Numbering Scheme for results table

Table 4.14 Summary of all Pareto front optimal solutions

T:Titanium W:Tungsten

solution	thickness	1	2	3	4	5	6	7	8	9	10	11	12	13	14	15	16	17	18	19	20	21	22	23	24	25	26	27							
1	89 mm	T	T	W	T	W	T	T	T	W	T	T	T	T	T	T	W	T	T	T	T	W	T	T	T	T	T	T							
	81 mm	T	W	T	T	T	T	T	T	T	T	T	T	T	T	T	T	T	T	T	T	T	T	T	T	T	T	T	T						
2	83 mm	T	T	T	T	W	T	T	T	T	T	T	T	T	T	T	T	T	T	T	T	W	T	T	T	W	W	T	T						
	87 mm	T	W	T	T	T	T	T	T	T	T	T	T	T	W	T	T	T	T	T	T	T	T	T	T	T	W	T	T	T					
3	83 mm	T	T	T	T	W	T	T	T	W	T	T	T	T	T	T	T	T	W	T	T	T	T	T	T	T	T	W	W	T	W				
	87 mm	T	W	T	T	T	T	T	T	T	T	T	T	T	W	T	T	T	T	T	T	T	T	T	T	T	W	T	T	T	T				
4	83 mm	T	T	T	T	W	T	T	T	T	T	T	T	T	T	T	W	T	W	W	W	T	T	T	T	T	T	W	T	T	T				
	87 mm	T	W	T	T	T	T	T	T	T	T	T	T	T	W	T	T	T	T	T	T	T	T	T	T	T	W	T	T	T	T	T			
5	89 mm	T	T	T	T	W	T	T	T	W	T	T	T	T	T	T	T	T	T	W	T	T	T	T	W	T	T	T	T	T	T	T			
	81 mm	T	T	W	T	T	T	T	T	T	T	T	W	T	T	T	T	T	T	T	T	T	T	T	T	T	T	T	T	T	T	T	T		
6	103 mm	T	T	T	W	W	T	T	T	W	T	W	T	T	T	T	T	T	T	T	T	W	W	T	T	T	T	T	T	T	T	T	W		
	67 mm	T	T	W	T	T	T	T	T	T	T	T	W	T	T	T	T	T	T	T	T	T	T	T	T	T	T	T	T	T	T	T	T	T	
7	103 mm	T	T	T	W	W	W	T	T	W	T	W	T	T	T	T	T	T	T	T	T	T	T	T	W	T	T	T	T	T	T	T	W	T	
	67 mm	W	W	T	T	T	T	T	T	T	W	T	T	T	T	T	T	T	W	T	W	T	T	T	T	T	T	T	T	T	T	T	T	W	T
8	103 mm	T	T	T	W	W	W	T	T	W	T	W	T	T	T	T	T	T	T	T	T	T	T	T	W	T	T	T	T	T	T	T	T	W	T
	67 mm	W	W	T	T	T	T	T	T	T	W	T	T	T	T	T	T	T	T	T	T	T	T	T	T	T	T	T	T	T	T	T	T	T	W

While a direct comparison cannot be made between case studies 1,2 and 3 there are major differences and advantages between the three methods that are used in these case studies. Case study 1 utilized classical optimization methods to optimize the stacking sequence of homogeneous plates. Yet, the addition of reliability based methods was useful in determining the optimal stacking sequence and thickness when subjected to uncertain events such as blast waves due to high explosives. Moreover, the fact that no microstructural homogenization was considered allowed considering strain rate dependence of the layers. The integration of strain rate effects and reliability theory is the major contribution in case study 1. Case study 2 included the homogenization method, yet was performed using 2-D microstructures and 2-D implicit blast modeling and multi-objective genetic optimization. This technique neglected the significance of the plate stiffness on the pressure developed due to blast. This short coming occurred due to the implicit modeling, where the CFD technique was separated from the structural analysis. Nevertheless, the method proved the value of the homogenization technique to reveal optimal solutions. The final case study, case study 3, was the most general and complete method for optimizing composites for blast resistance. The method included an integrated simulation environment that included: 3-D homogenization, explicit blast modeling and an updated multi-objective genetic optimization. The third case study yielded more realistic solutions when compared with the earlier case studies. For each design alternative each layers microstructure, stiffness matrix, density and thickness were extracted. While all of the case studies were informative and gave useful information regarding design of optimal blast resistant structures, the third case study was the most advanced of the three. The final case study also showed that the integrated method may

be used to create microstructures that greatly reduce weight while limiting stress/strength ratios similar to that of very dense, heavy thick plates made of the base materials.

4.3.5 Conclusions

This section presented the case study for the design and optimization of 3-D two-layer blast resistant composite plates. The LS-DYNA explicit blast model was used for simulating the multi-physics of the structural-fluid interaction. The simulation simultaneously obtained the flow field of the blast wave as well as the resulting stress distribution in the composite plate. FEA was used to determine the three dimensional homogenized unit cell properties of each of the layers in the composite plate. The DAKOTA design optimization techniques allowed determining Pareto front optimal solutions that concurrently optimized both microstructure and thickness. A robust multi-objective optimization algorithm was developed and shown to yield a Pareto-front. A case study of a 3-D 2 layer Tungsten and Titanium composite plate subjected to blast loading using explicit blast modeling is discussed. The results of the integrated optimization simulation showed that multiple microstructures and thickness alternatives are possible. The 3-D method shows a significant advantage and is much more realistic than the 2-D case presented in case study 2. Case study 3 also introduces the anisotropic nature of 3-D microstructures that was not readily observed in the 2-D case study. The integration of the homogenization method and MOGA can produce design alternatives for blast resistant composites using two materials A and B that are not available using classical methods such as gradient based optimization and implicit blast modeling.

4.4 Conclusions

Three different blast resistant composite plate design and optimization case studies were examined and discussed in this chapter. Each of the case studies introduced innovative ways of optimizing composite structures for blast resistant applications. The methods used for each of the case studies were presented in their general theoretical forms and then presented in each study how they were specifically implemented with regard to each case. Each of the three studies resulted in optimal composite structures for the particular model parameters.

Case study 1 introduced a reliability-based approach to the design of a 2-layer blast resistant composite composed of 1 plate of Aluminum and 1 plate of Titanium. The reliability approach was utilized to take into account the uncertainty of blast events. The probabilistic nature of blast is more significant in a single degree of freedom analysis. The plates were modeled as either resisting or absorbing energy. An optimal stacking sequence and thickness per layer was presented. The results of the analysis were simulated in an advanced FE explicit blast model to verify the validity of the optimally determined solution. Although the model validated the process, it showed the need to alter reliability index values to account for yielding. The model also showed the need for strain rate dependent models for instances where yielding did occur.

Case studies 2 and 3 were very similar to one another in terms of overall scope, but utilized much different methods simulation models. Case study 2 was performed in 2-D while case study 3 was performed in 3-D. For each case a non-uniform blast was subjected to a composite plate. The mechanical properties of the composite plates were determined using the homogenization method. The homogenization method was used in

case study 2 to obtain the homogenized isotropic properties of a 2-D microstructure, where as in case study 3 it was used to obtain the 3-D 6x6 anisotropic elastic stiffness matrix of the 3-D microstructure. This is one of the major differences between case study 2 and 3.

3-D homogenization showed that the composite microstructure stiffness matrices contained shear-extensional and shear-shear coupling terms. Case study 2 simulated fluid flow and structural response separately and is therefore referred to as implicit blast modeling, on the other hand case study 3 used a multi-physics simulation in which the flow fields and the structural response are solved simultaneously. The differences between explicit and implicit modeling were discussed in the methods section. Finally, the common method used by both case study 2 and 3 was the optimization algorithm which was multi-objective genetic algorithms. This method was the only method that could be used with both continuous and discrete design variables. Gradient based methods required artificial filters that corrupted the solution space and required more computational time. Overall, both case study 2 and 3 were shown to produce multi-objective optimal design alternatives yielding both microstructure and thickness per layer. Case study 3 is the updated and improved 3-D version of case study 2.

Although the case studies presented above represent an effective means of optimizing composite microstructures and macrostructures, there are still components that may be added to increase the accuracy and validity of the design alternatives.

CHAPTER 5 CONCLUSIONS AND FUTURE WORK

5.1 Conclusions

The microstructural homogenization method was examined for design of blast resistance of composite plates. It was shown that mechanical properties are directly coupled with the microstructure of the composite plates. When integrated with blast simulation software and an optimization framework it was determined that homogenization is a capable and efficient method for extracting properties from unit cell composites. It was shown that the homogenization technique was useful in identifying optimal microstructures for composite plates that performed significantly better than the case of homogeneous plates under blast load.

- Homogenization is the process of extracting composite material properties through finite element methods by applying known strain fields to a composite unit cell. Homogenization was examined in both 2-D and 3-D. Both cases were capable of extracting material properties of unit cells. The 2-D case was more computationally efficient than the 3-D case due to the number of required strain fields. 3-D proved to be more realistic in that it was able to identify the shear-shear and shear-extensional terms in the 6x6 stiffness matrix. The 3-D homogenization revealed the anisotropy of many composite unit cells. The 3-D homogenization when coupled with the explicit blast simulation and MOGA was a necessary component for identify Pareto optimal microstructures.
- While homogenization was successfully applied to 2-D and 3-D problems it has some limitations. The homogenization method is only valid for extracting elastic stiffness values. This is the reason that all cases that resulted in stress/strength

ratios above 1.0 were excluded. This meant that plastic behavior and strain rate effects did not need to be considered in the analysis. Strain rate effects only affect the plastic properties and not the elastic properties. This is a limitation that requires further research.

- The difference between implicit and explicit blast modeling is related to the manner in which the pressure wave is transferred to the composite plate during simulation. The implicit method assumes that all composite plates experience the same pressure wave as a function of time and space. Explicit blast modeling includes the effect that displacement has upon the pressure transfer to the composite plate. Different materials with different properties displace different amounts under blast loading. This means two plates with different microstructures will experience a different amount of pressure transfer. The explicit method is a mechanically realistic method of simulating pressure transfer due to blast on a composite plate. When integrated with homogenization and optimization it is necessary to use explicit rather than implicit methods in order to truly identify the optimal solutions.
- Strain rate effects mean that the yield point and shape of the stress-strain curve are functions of the strain rate. The strain rate was shown to have a significant impact on the stress distribution in plates subjected to blast loading. For this reason, iterations that exhibited stress/strength ratios above 1.0 were eliminated. All of the optimally identified solutions had stress/strength ratios as a function of time that was below 1.0. This means that these cases never yielded and that material properties that were extracted using 3-D homogenization were completely valid.

Developing a homogenization approach considering strain rate effect is another challenge to be considered in the future.

- The connection between the homogenization and blast simulation methods was an integral step required for the simulation and analysis of blast resistant composites. The homogenization step was used to calculate properties that were used as inputs to the blast simulation. The two dimensional homogenization step was connected to the 2-D implicit blast simulation. This integrated 2-D methods were successful at extracting properties from the 2-D unit cells, but the properties were assumed to be transversely isotropic after mixing and the pressure was implicitly applied to the blast simulation. The three dimensional homogenization method extracted anisotropic properties that were forwarded to the explicit blast simulation. The integration of 3-D methods resulted in more realistic composite unit cells and changes in microstructures meant that both stiffness matrices and pressure distributions were updated at each iteration.
- Gradient based optimization methods can be used to optimize microstructures for blast resistance, but they have limitations. To use gradient methods with discrete variables artificial filters must be added to the integrated process. This increases computational time and the gradient of the objective functions is not necessarily following the gradient of the functions because the true design variables are modified from those that are output from the optimization routine. The objective functions of gradient methods is also combined using the weighted sum method, which in fact can be seen as a single objective function and not multi-objective. The results of gradient based methods are significantly affected by the initial start

point. MOGA was chosen because it solves some of the limitations of gradient methods. MOGA is multi-objective in nature and does not require combining objectives and using weights on the objective functions. MOGA was also selected because the optimization of microstructure topology of blast resistant composites requires both continuous and discrete variables. No artificial filters are needed to modify the design variables. Finally, MOGA uses methods derived from nature such as crossover and mutation to update the design variables so the start point is not nearly as significant as it is in gradient methods. A hybrid optimization is also possible and may be the most efficient method for this type of problem. A hybrid method would use both gradient and non-gradient methods to find optimum solutions. The MOGA method could be used to cover a large solution space and gradient methods could be used to search near an optimum that was generated using MOGA. The hybrid method would use the Monte Carlo method to randomly sample the solution space.

- Reliability analysis is used to analyze systems in which loading and/or material properties are uncertain and can be represented by probability distribution functions. Blast loading is a complicated process and can be modeled as an uncertain event with a probability distribution function. Reliability analysis was used to optimize plate stacking sequence and plate thickness. Reliability analysis was used to determine a limit state function which divides desirable from undesirable conditions under blast loading. A probability of failure was determined as the integration over the failure domain of the joint density function. It was shown that the probability of failure may be represented by a reliability

index and then using either the first-order-second-moment method or the Monte Carlo method, the probability of failure could be determined. The Monte Carlo method was successfully applied to the stacking sequence problem and obtained optimal solutions that were validated with the FE analysis.

- Design Analysis Kit for Optimization and Terascale Applications (DAKOTA) is a multi-level object oriented framework for design optimization, uncertainty quantification, sensitivity analysis and parameter estimation developed by Sandia National Laboratories (SNL). DAKOTA contains algorithms for optimization with both non-gradient and gradient based methods. DAKOTA controls the integrated simulation and optimization environment. It is an open source code written in C++ that is adaptable to a variety of problem types and constantly updated. DAKOTA has an extensive library of methods, strategies and optimization algorithms that may be formulated as single objective or multi-objective problems. DAKOTA proved capable of determining optimal design variables for both microstructure and thickness of blast resistant composite plates.
- Three different case studies were used to exemplify the validity of the previously described methods to the optimization problem. Case study 1's major contribution was the use of reliability analysis to aid in the design of structures subjected to uncertain events such as blast loading. Case study 1 also revealed the need and value of incorporating the strain rate effect to the design of blast resistant composite plates. The methods integrated in case study 1 could only be used for the optimization of stacking sequence of homogeneous plates. Case study 2 introduced the homogenization technique to the design of microstructures

for blast resistant composites. The blast load in case study 2 was simulated using the implicit blast method. DAKOTA was then used as the framework for optimizing design using multi-objective genetic algorithms. Case study 2 was completely formulated in 2-D. Finally, case study 3 used three dimensional homogenization and explicit blast modeling integrated with the DAKOTA framework to optimize three dimensional composite microstructures. Case study 3 identified the best methods introduced in this dissertation and identified the most realistic optimal solutions.

5.2 Future Work

- First and probably most important, is the addition of the strain rate dependent model to the integrated optimization environment of case study 3. The strain rate dependence problem was presented in section 2.5. It is clear that the yield point is a function of the rate of strain being applied to a material. Many different methods are available to simulate this effect, with the most commonly used in FE being the Cowper-Symonds model. This power law uses experimentally determined constant P and C to model the strain rate effect. This method was actually used during the verification process of case study 1. In fact it worked very well, but in terms of case study 3 in which two materials Tungsten and Titanium are arranged in a specific microstructure there is no direct means of calculating these constants. In order to obtain these values the particular microstructure of interest would have to be created and developed into a macro component that is then tested at different strain rates. As a first order

approximation the rule of mixtures method could be used to get averaged C and P values that are then included in the explicit blast simulation. This idea needs to be further examined as future work to determine how to include this effect.

- Similar to the latter issue of strain rate dependence is the calculation of the strength of the composite layers. Homogenization is used to determine the elastic properties of the microstructure, but the ROM method is used to calculate the strength of the composite. This may also suffice as a first order approximation, but more advanced testing and analysis should be performed to determine the error incurred through assuming a ROM relationship. This work is directly related to the work being done by Dr. Dan Tortorelli at the University of Illinois at Urbana-Champaign. Professor Tortorelli is investigating using homogenization methods for the determination of both the elastic and plastic properties of a composite material. The addition of this method to the currently used methods would allow the model to be tested under blast waves that yield and even fracture the composite plate models. Other methodologies for calculating strength of composites are given by Meyer et al. [85]. In case study three all design alternatives that gave stress/strength ratios above 1 were excluded, because yielding was considered a failure criterion and without the plastic homogenization method the results were going to be erroneous.
- Computational efficiency is a main challenge in the suggested design loop. Currently a quad core 64-bit work station with xenon processors running at 3.33 GHz with 48 gigs of RAM is used for the optimization process. 1000 functional evaluations takes approximately 23 hours. The addition of parallel processing

should allow decreasing the solution time, achieving a more accurate Pareto front and allow for an exponentially greater number of total functional evaluations.

Two computer clusters that may be utilized at UNM are located at the high performance computer center. These two clusters are called Pequena and Nano respectively. Pequena has 22 xenon cores that run at 2.66 GHz and has 8 GB of RAM per core. Nano has 36 xenon cores running at 3.0 GHz with 16 GB per core. Multi-threading the process would greatly increase the applicability of the integrated methods for blast resistant design optimization.

- While reliability methods were applied to the problem of stacking sequence of homogeneous isotropic plates, it should also be extended to the problem of topological microstructural optimization of blast resistant composites. LS-DYNA is very useful in determining the fluid dynamics and structural dynamics of blast loading, but there are still uncertainties in any explosive loading that should be modeled using reliability analysis. Reliability analysis should also be used to take into account the uncertainty in composite strength. The addition of reliability based methods to the integrated optimization and simulation environment as shown in case study 3 would be extremely advantageous and yield microstructures that meet reliability based design criteria. This is important because many design codes now require the design requirements to take into account uncertainty in design.

REFERENCES

1. Langdon, G.S., Nurick, G.N., Lemanski, S.L., Simmons, M.C., Cantwell, W.J., and Schleyer, G.K., *Failure Characterisation of Blast-Loaded Fibre-Metal Laminate Panels Based on Aluminium and Glass-Fibre Reinforced Polypropylene*. Composites Science and Technology, 2007. 67(7-8): p. 1385-1405.
2. Tsai, L. and Prakash, V., *Structure of Weak Shock Waves in 2-D Layered Material Systems*. International Journal of Solids and Structures, 2005. 42(2): p. 727-750.
3. Murphy, *Composites*. 2008.
4. Hyer, M.W., *Stress Analysis of Fiber-Reinforced Composite Materials*. updated ed. 2009, Lancaster: DEStech Publications.
5. Hancox, N.L., *Impact behaviour of fibre-reinforced compositematerials and structures*, ed. S.R.R.a.G. Zhou. 2000, Boca Raton Woodhead Publishing Ltd and CRC Press LLC.
6. Suiyuan, C., Jing, W., Yijie, L., Jing, L., and Changsheng, L., *Synthesis of New Cu-based Self-lubricating Composites with Great Mechanical*. Journal of Composite Materials, 2011. 45(1): p. 51-63.
7. M. Niklaus, H.R.S., *Electrical conductivity and Young's modulus of flexiblenanocomposites made by metal-ion implantationof polydimethylsiloxane: The relationship between nanostructureand macroscopic properties*. Acta Materialia, 2011. 59: p. 830-840.
8. H. Nami, H.A., M. Sharifitabar, H. Shamabadi, *Microstructure and mechanical properties of friction stir welded Al/Mg2Simetal matrix cast composite*. Materials and Design, 2011. 32: p. 976-983.
9. Conlan, T., *Scrolls of the Mongol Invasion of Japan*.
10. P.D. Smith, J.G.H., *Blast and ballistic loading of structures* 1994, Oxford ; Boston Butterworth-Heinemann.
11. Ngo, T., Mendis, P., Gupta, A., and Ramsay, J., *Blast Loading and Blast Effects on Structures – An Overview*. EJSE, 2007(Special Issue: Loading on Structures): p. 76-91.
12. Comet, M., Pichot, V., Siegert, B., Schnell, F., Ciszek, F., and Spitzer, D., *Phosphorus-based nanothermites: A new generation of energetic materials*. Journal of Physics and Chemistry of Solids, 2010. 71: p. 64-68.

13. Malik, J.S., *The yields of the Hiroshima and Nagasaki nuclear explosions*, Los Alamos National Laboratory Los Alamos.
14. Brode, H.L., *Numerical solution of spherical blastwaves*. Journal of Applied Physics, 1955.
15. Mills, C.A., *The design of concrete structure to resist explosions and weapon effects*, in *Proceedings of the 1st Int. Conference on concrete for hazard protections*. 1987: Edinburgh, UK. p. 61-73.
16. W.J. Kang, S.S.C., D. Huh, D.T. Chung, *Modified Johnson-Cook model for vehicle body crashworthiness simulation*. International Journal of Vehicle design, 1999. 21(4-5): p. 424-435.
17. Cowper, G.R. and Symonds, P.S., *Strain hardening and strain rate effects in the impact loading of cantilever beams*. 1958: Brown University, Division of Applied Mechanics.
18. A. G. Fedorenko, M.A.S., and A. G. Ivanov, *Criterion for Selecting Composite Materials for Explosion Containment Structures (Review)*. Combustion, Explosion, and Shock Waves, 2005. 41(5): p. 487-495.
19. M.R. Bambach, X.L.Z., H. Jama, *Energy absorbing characteristics of aluminium beams strengthened with CFRP subjected to transverse blast load*. International Journal of Impact Engineering, 2010. 37: p. 37-49.
20. G.S. Langdon, G.S., Chi, Y., Nurick, G.N., and Haupt, P., *Response of GLARE panels to blast loading*. Engineering Structures, 2009. 31: p. 3116-3120.
21. Bendsoe MP, K.N., *Generating optimal topologies in structural design using a homogenization method*. Computational Methods Applied Mechanics Engineering 1988. 71: p. 197-224.
22. Tortorelli, D.A., *Solid Mechanics: Analysis and Design*. 2010, Urbana, IL.
23. Pederson, P., *On the minimum mass layout of trusses*, in *Symp. Struct. Optim., AGARD Conf. Proc.* 1969: Turkey. p. 11.1-11.18.
24. Zhou M, R.G.I.N., *DCOC: an optimality criteria method for large systems, Part I: Theory*. Structural Optimization 1992. 5(1-2): p. 12-25.
25. Cheng G, O.N., *An investigation concerning optimal design of solid elastic plates*. International Journal of Solid Structures, 1981. 17(3): p. 305-323.

26. Sigmund, O., *Materials with prescribed constitutive parameters: an inverse homogenization problem*. International J of Solid Structures 1994. 31(17): p. 2313–2329.
27. Rodrigues HC, F.P., *A material based model for topology optimization of thermoelastic structures*. International J of Numerical Methods Engineering 1995. 38(12): p. 1951–1965.
28. Haslinger, J., *Finite element approximation for optimal shape design: theory and applications*. 1988, New York: Wiley.
29. Fonseca, J., *Design of microstructures of periodic composite materials*. 1997, University of Michigan: Ann Arbor.
30. Sanchez-Palencia, E., *Equations aux derivees partielles dans un type de milieux heterogenes*. Comptes Rendus de l'Academie des Sciences de Paris 1971. 272(A-B): p. A1410–A1413.
31. Keller, J.B., *Effective behavior of heterogeneous media*, in *Statistical mechanics and statistical methods in theory and application: a tribute to Elliot W. Montroll*, L. U., Editor. 1977, Plenum Press. p. 429–443.
32. Bakhvalov N, P.G., *Homogenization: averaging process in periodic media*, Nauka, Moscow.
33. De Kruijf N, Z.S., Li Q, et al., *Topological design of structures and composite materials with multiobjectives*. International Journal of Solids and Structures 2007. 44: p. 7092–7109.
34. Guedes, J.M., *Nonlinear computational models for composite materials using homogenization*. 1990, University of Michigan: Ann Arbor.
35. Osyczka, A., *Multicriterion optimization in engineering*. 1984, Chichester, W. Sussex: E. Horwood, Halsted Press.
36. Pareto, V., *Manual of political economy*. 1971, New York: Macmillan.
37. Miettinen, K., *Nonlinear multiobjective optimization*. 1999, Boston: Kluwer.
38. Rosenberg, R.S., *Simulation of genetic populations with biochemical properties*. 1967, University of Michigan: Ann Arbor.
39. Silva, G.C.d., Bahiense, L., Ochi, L.S., and Boaventura-Netto, P.O., *The dynamic space allocation problem: Applying hybrid GRASP and Tabusearch metaheuristics*. 2012, 2011. 39: p. 671-677.

40. Rao, A.R.M. and Shyjui, P.P., *A Meta-Heuristic Algorithm for Multi-Objective Optimal Design of Hybrid Laminate Composite Structures* Computer-Aided Civil and Infrastructure Engineering, 2010. 25: p. 149–170.
41. M. Abouhamze, M.S., *Multi-objective stacking sequence optimization of laminated cylindrical panels using a genetic algorithm and neural networks*. Composite Structures, 2007. 81: p. 253–263.
42. A. GILLET, P.F.a.P.S., *Single- and Multi-objective Optimization of Composite Structures: The Influence of Design Variables*. Journal of COMPOSITE MATERIALS, 2011. 44(4): p. 457-480.
43. Sigmund, O., *Design of material structures using topology optimization*. 1994, Technical University of Denmark: Lyngby.
44. Wendt, J.F., *Computational Fluids Dynamics An Introduction*. 2009, Berlin: Springer_Verlag.
45. Z., K., *Tables of Supersonic flow around cones*. 1947, Massachusetts Institute of Technology: Cambridge. p. Center of Analysis.
46. Fay, J.A. and Riddell, F.R., *Theory of Stagnation Point Heat transfer in Dissociated Air*. Journal of Aeronautical Sciences, 1958. 25(2): p. 73-85.
47. Hall, H.G., Eschenroeder, A.Q., and Marrone, P.V., *Blunt-nose Inviscid Airflows with Coupled Nonequilibrium processes*. Journal of Aerospace Sciences, 1962. 29(9): p. 1038-1051.
48. Currie, I.G., *Fundamental Mechanics of Fluids*, ed. L.L. Faulkner. 2003, Boca Raton: CRC Press.
49. D. L., L., *A First Course in the Finite Element Method*. 3 ed. 2002, Pacific Grove: Brooks/Cole.
50. Hallquist, J.O., *LS-DYNA Theory Manual*. 2006: Livermore.
51. Chopra, A.K., ed. *Dynamics of Structures: Theory and Applications to Earthquake Engineering*. 2nd ed.
52. Deb, K., *Multi-objective optimization using evolutionary algorithms*. 2001, Chichester: John Wiley.
53. Ross, T.J., *Fuzzy Logic with Engineering Applications*. 2004: John Wiley and Sons, Ltd.

54. Schaffer, J.D., *Some experiments in machine learning using vector evaluated genetic algorithms*. 1984, Vanderbilt University: Nashville.
55. Goldberg, D.E., *Genetic algorithms in search, optimization, and machine learning*. 1989, Reading: Addison-Wesley.
56. Horn J, N.N., Goldberg D.E., *A niched Pareto genetic algorithm for multiobjective optimization*, in *Proceedings of the first IEEE conference on evolutionary computation*. 1994: Orlando.
57. Srinivas, N. and Deb, K., *Multiobjective optimization using nondominated sorting in genetic algorithms*. *Evolutionary Computation* 1995. 2(3): p. 221-248.
58. Knowles J., C.D. *The Pareto archived evolution strategy: a new baseline algorithm for Pareto multiobjective optimisation*. in *Proceedings of the 1999 congress on evolutionary computation*. 1999. Washington, DC, USA.
59. Rammohan R, F.B., Su MF, et al. , *Hybrid genetic optimization for design of photonic crystal emitters*. *Engineering Optimization*, 2010. 42(9): p. 791-809.
60. Deb, K., Pratap, A., Agarwal, S., and Meyarivan, T., *A fast and elitist multiobjective genetic algorithm: NSGA-II*. *IEEE Transaction of Evolutionary Computations*, 2002. 6: p. 182–197.
61. Konak A., C.D.W.a.S.A., *Multi-objective optimization using genetic algorithms: A tutorial*. *Reliability Engineering and System Safety* 2006. 91: p. 992–1007.
62. Wang S.Y., T.K., and Wang M.Y. , *An enhanced genetic algorithm for structural topology optimization*. *International Journal for Numerical Methods in Engineering* 2006: p. 18-44.
63. Kelesoglu, O., *Fuzzy multiobjective optimization of truss-structures using genetic algorithm*. *Advances in Engineering Software* 2007. 38: p. 717–721.
64. Taboada H.A., E.J.F.a.D.W.C.D.W., *MOMS-GA: A multi-objective multi-state genetic algorithm for system reliability optimization design problems*. *IEEE Transactions on Reliability* 2008. 57(1): p. 182-191.
65. X., L., Li, Q., Yang, X., Li, W., and Zhang, W., *A two-stage multi-objective optimisation of vehicle crashworthiness under frontal impact*. *International Journal of Crashworthiness* 2008. 13(3): p. 279-288.
66. Melchers, R.E., *Structural Reliability Analysis and Prediction*. 1999, New York: John Wiley and Sons. Ltd.

67. Xia, Y., Wang, Y., Zhou, Y., and Jeelani, S., *Effect of Strain Rate on Tensile Behavior of Carbon Fiber Reinforced Aluminum Laminates*. *Materials Letters*, 2007. 61: p. 213-215.
68. Borenstein, E. and Benaroya, H., *Sensitivity Analysis of Blast Loading Parameters and Their Trends as Uncertainty Increases*. *Journal of Sound and Vibration*, 2009. 32: p. 762–785.
69. Biggs, J.M., ed. *Introduction to Structural Dynamics*. 1982, McGraw-Hill: New York, NY.
70. Nowak, A.S. and Collins, K., eds. *Reliability of Structures*. 2000, McGraw-Hill: New York, NY.
71. Beer, M. and Spanos, P.D., *A Neural Network Approach for Simulating Stationary Stochastic Processes*. *Structural Engineering and Mechanics*, 2009. 32: p. 71-94.
72. Kim, J.J., Reda Taha, M.M., and Ross, T.J., *Establishing concrete cracking strength interval using possibility theory with an application to predict the possible reinforced concrete deflection interval*. *Engineering Structures*, 2010. 32: p. 3592-3600.
73. Morka, A., Kwasniewski, L., and Wekezer, J.W., *Assessment of Passenger Security in Paratransit Buses*. *NCTR Journal of Public Transportation*, 2005. 8: p. 47-63.
74. Park, H., Lee, K., Lee, S.W., and Kim, K., *Dynamic Analysis of Nonlinear Composite Structures under Pressure Wave Loading*. *Journal of Composite Materials*, 2006. 40: p. 1361-1383.
75. Kim, H.J., Yi, N.H., Kim, B.S., Nam, J.W., Ha, J.H., and Kim, J.J., *Debonding Failure Analysis of FRP-Retrofitted Concrete Panel under Blast Loading*. *Structural Engineering and Mechanics*, 2011. 38: p. 479-501.
76. Altunc, A.B., Kim, J.J., Al-Haik, M., and Reda Taha, M.M., *Reliability-Based Design of Blast-Resistant Composite Laminates Incorporating Carbon Nanotubes*. *Composite Structures*, 2011. 93: p. 2042-2048.
77. Bodner, S.R. and Symonds, P.S., *Experimental and theoretical investigation of the plastic deformation of cantilever beams subjected to impulsive loading*. *ASME Applied Mechanics*, 1962. 29: p. 719-728.
78. Symonds, P.S. and Chon, C.T., *Approximation techniques for impulsive loading of structures of time-dependent plastic behaviour with finite deflections*, in

- Mechanical Properties at High Rates of Strain*. 1974, The Institute of Physics: London and Bristol, Oxford. p. 299.
79. Callister, W., D., Jr., *Materials Science and Engineering An Introduction*. 6 ed, ed. K. Santor. 2003, Hoboken: John Wiley and Sons.
 80. ANSYS-AUTODYN, in *Interactive non-linear dynamic analysis software*. 2007.
 81. ANSYS, *Element Reference*. 2011.
 82. Eldred, M.S., Adams, B.M., Gay, D.M., and Swiller, L.P., *DAKOTA, A Multilevel Parallel Object-Oriented Framework for Design Optimization, Parameter Estimation, Uncertainty Quantification, and Sensitivity Analysis, in Version 4.1 Reference Manual*. 2006: Livermore, Ca.
 83. B. Erzar, P.F., *Experiments and mesoscopic modelling of dynamic testing of concrete*. *Mechanics of Materials*, 2011. 43: p. 505-527.
 84. William D. Callister, D.G.R., ed. *Fundamentals of Material Science and Engineering: An Integrated Approach*. 2008, John Wiley & Sons: Hoboken, N.J.
 85. Meyers, M.A., ed. *Dynamic Behavior of Materials*. 1994, John Wiley and Sons: Hoboken, NJ.

APPENDIX

LS-DYNA EXPLICIT BLAST CODE

```

$# LS-DYNA Keyword file created by LS-PREPOST 2.4 -
10Jun2009(09:59)
$# Created on Jun-28-2011 (15:01:36)
*KEYWORD
*TITLE
$# title
LS-DYNA keyword deck by LS-Prepost
*INCLUDE
lsdynainput.k
*CONTROL_ALE
$#      dct      nadv      meth      afac      bfac      cfac
dfac      efac
2,1,2,-1.000000,0.000,0.000,0.000,0.000
$#      start      end      aafac      vfact      prit      ebc
pref      nsidebc
      0.0001.0000E+20  1.000000  1.0000E-6      0      0
0.000      0
*CONTROL_CONTACT
$#      slsfac      rwpnal      islchk      shlthk      penopt      thkchg
orien      enmass
      0.100000  0.000      1      0      0      0
1      0
$#      usrstr      usrfrc      nsbcs      interm      xpene      ssthk
ecdt      tiedprj
      0      0      0      0      0.000      0
0      0
$#      sfric      dfric      edc      vfc      th      th_sf
pen_sf
      0.000      0.000      0.000      0.000      0.000      0.000
0.000
$#      ignore      frceng      skiprwg      outseg      spotstp      spotdel
spothin
      0      0      0      0      0      0
0.000
$#      isym      nserod      rwgaps      rwgdth      rwksf      icov
swradf      ithoff
      0      0      0      0.000  1.000000      0
0.000      0
$#      shledg
      0
*CONTROL_CPU
$#      cputim
      0.000
*CONTROL_DAMPING
$#      nrcyck      drtol      drfctr      drterm      tssfdr      irelal
edttl      idrflg
```

```

0      0.000      0.000      0.000      0.000      0
0.000      0
*CONTROL_ENERGY
$#   hgen      rwen      slnten      rylen
      1      2      1      1
*CONTROL_OUTPUT
$#   npopt      neecho      nrefup      iaccop      opifs      ipnint
ikedit      iflush
      0      0      0      0      0.000      0
0      0
$#   iptrf      ierode      tet10      msgmax      ipcurv
      0      0      2      50      0
*CONTROL_SHELL
$#   wrpang      esort      irnxx      istupd      theory      bwc
miter      proj
      0.000      0      0      0      2      2
1      0
$#   rotascl      intgrd      lamsht      cstyp6      tshell      nfail1
nfail4      psnfail
      1.000000      0      0      1      0      0
0      0
$#   psstupd      irqquad
      0      0
*CONTROL_TERMINATION
$#   endtim      endcyc      dtmin      endeng      endmas
      0.001000      0      0.000      0.000      0.000
*CONTROL_TIMESTEP
$#   dtinit      tssfacc      isdo      tslimt      dt2ms      lctm
erode      mslst
      0.000      0.000      0      0.000      0.000      0
0      0
$#   dt2msf      dt2mslc      imsc1
      0.000      0      0
*DATABASE_ELOUT
$#   dt      binary      lcur      iopt
      1.0000E-6      1      0      1
*DATABASE_NODOUT
$#   dt      binary      lcur      iopt      dthf      binhf
      1.0000E-6      1      0      1      0.000      0
*DATABASE_BINARY_D3PLOT
$#   dt      lcdt      beam      npltc      psetid
      1.0000E-6      0      0      0      0
$#   iopt
      0
*DATABASE_EXTENT_BINARY
$#   neiph      neips      maxint      strflg      sigflg      epsflg
rltflg      engflg
      0      0      0      0      1      1
1      1

```

```

$# cmpflg   ieverp   beamip   dcomp   shge   stssz
n3thdt   ialemat
      0       0       0       1       1       1
2        0
$# nintsld   pkp_sen   sclp   unused   msscl   therm
iniout   iniout
      0       0  1.000000   0       0
OSTRESS   STRESS

```

```

*PART
$# title
boxsolid
$#   pid   secid   mid   eosid   hgid   grav
adpopt   tmid
      1     1     3     0     0     0
0        0
*SECTION_SOLID
$#   secid   elform   aet
      1     1     0
*MAT_ANISOTROPIC_ELASTIC
$#   mid   ro   c11   c12   c22   c13
c23   c33
3,&ro1,&c111,&c121,&c221,&c131,&c231,&c331
$#   c14   c24   c34   c44   c15   c25
c35   c45
&c141,&c241,&c341,&c441,&c151,&c251,&c351,&c451
$#   c55   c16   c26   c36   c46   c56
c66   aopt
&c551,&c161,&c261,&c361,&c461,&c561,&c661,0.000
$#   xp   yp   zp   a1   a2   a3
macf
      0.000   0.000   0.000   0.000   0.000   0.000
1
$#   v1   v2   v3   d1   d2   d3
beta   ref
      0.000   0.000   0.000   0.000   0.000   0.000
0.000   0.000

```

```

*PART
$# title
boxsolid
$#   pid   secid   mid   eosid   hgid   grav
adpopt   tmid
      2     1     4     0     0     0
0        0
*MAT_ANISOTROPIC_ELASTIC
$#   mid   ro   c11   c12   c22   c13
c23   c33
4,&ro2,&c112,&c122,&c222,&c132,&c232,&c332

```

```

$#      c14      c24      c34      c44      c15      c25
c35      c45
&c142,&c242,&c342,&c442,&c152,&c252,&c352,&c452
$#      c55      c16      c26      c36      c46      c56
c66      aopt
&c552,&c162,&c262,&c362,&c462,&c562,&c662,0.000
$#      xp      yp      zp      a1      a2      a3
macf
      0.000      0.000      0.000      0.000      0.000      0.000
1
$#      v1      v2      v3      d1      d2      d3
beta      ref
      0.000      0.000      0.000      0.000      0.000      0.000
0.000      0.000
*PART
$# title
boxsolid
$#      pid      secid      mid      eosid      hgid      grav
adpopt      tmid
      3      2      2      2      0      0
0      0
*SECTION_SOLID_ALE
$#      secid      elform      aet
      2      11      1
$#      afac      bfac      cfac      dfac      start      end
aafac
      0.000      0.000      0.000      0.000      0.000      0.000
0.000
*MAT_NULL
$#      mid      ro      pc      mu      terod      cerod
ym      pr
      2 1.290000      0.000      0.000      0.000      0.000
0.000      0.000
*EOS_LINEAR_POLYNOMIAL
$#      eosid      c0      c1      c2      c3      c4
c5      c6
      2      0.000      0.000      0.000      0.000      0.400000
0.400000      0.000
$#      e0      v0
      0.000      1.000000
*PART
$# title
boxsolid
$#      pid      secid      mid      eosid      hgid      grav
adpopt      tmid
      4      3      1      1      1      0
0      0
*SECTION_SOLID_ALE
$#      secid      elform      aet
      3      11      1

```

```

$#   afac   bfac   cfac   dfac   start   end
aafac
    0.000   0.000   0.000   0.000   0.000   0.000
0.000
*MAT_HIGH_EXPLOSIVE_BURN
$#   mid     ro     d     pcj     beta     k
g     sigy
1,1600.0000,2000.0000,2.0000E+6,0.000,0.000,0.000,0.000
*EOS_JWL
$#   eosid     a     b     r1     r2     omeg
e0     vo
1,3.045E+11,0.6500E+10,4.500000,1.400000,0.250000,0.000,0.000
*HOURLGLASS
$#   hgid     ihq     qm     ibq     q1     q2
qb/vdc     qw
    1     0     0.000     3     0.000     0.000
0.000     0.000
*INITIAL_DETONATION
$#   pid     x     y     z     lt
    0     0.000     0.000     0.210000     0.000
*SET_PART_LIST_TITLE
layer1&2
$#   sid     da1     da2     da3     da4
    1     0.000     0.000     0.000     0.000
$#   pid1     pid2     pid3     pid4     pid5     pid6
pid7     pid8
    1     2     0     0     0     0
0     0
*ALE_MULTI-MATERIAL_GROUP_PART
$#   pid
    4
*ALE_MULTI-MATERIAL_GROUP_PART
$#   pid
    3
*DAMPING_FREQUENCY_RANGE
$#   cdamp     flow     fhigh     psid
0.1,1,1.0000E+5,0

```

ANSYS HOMOGENIZATION CODE

/PREP7

/INPUT,ANSYSINPUT,IN

BLOCK,0,1/3,0,1/3,0,1/3,

BLOCK,1/3,2/3,0,1/3,0,1/3,

BLOCK,2/3,1,0,1/3,0,1/3,

BLOCK,0,1/3,0,1/3,1/3,2/3,

BLOCK,1/3,2/3,0,1/3,1/3,2/3,

BLOCK,2/3,1,0,1/3,1/3,2/3,

BLOCK,0,1/3,0,1/3,2/3,1,

BLOCK,1/3,2/3,0,1/3,2/3,1,

BLOCK,2/3,1,0,1/3,2/3,1,

BLOCK,0,1/3,1/3,2/3,0,1/3,

BLOCK,1/3,2/3,1/3,2/3,0,1/3,

BLOCK,2/3,1,1/3,2/3,0,1/3,

BLOCK,0,1/3,1/3,2/3,1/3,2/3,

BLOCK,1/3,2/3,1/3,2/3,1/3,2/3,

BLOCK,2/3,1,1/3,2/3,1/3,2/3,

BLOCK,0,1/3,1/3,2/3,2/3,1,

BLOCK,1/3,2/3,1/3,2/3,2/3,1,

BLOCK,2/3,1,1/3,2/3,2/3,1,

BLOCK,0,1/3,2/3,1,0,1/3,

BLOCK,1/3,2/3,2/3,1,0,1/3,

BLOCK,2/3,1,2/3,1,0,1/3,

BLOCK,0,1/3,2/3,1,1/3,2/3,

BLOCK,1/3,2/3,2/3,1,1/3,2/3,

BLOCK,2/3,1,2/3,1,1/3,2/3,

BLOCK,0,1/3,2/3,1,2/3,1,

BLOCK,1/3,2/3,2/3,1,2/3,1,

BLOCK,2/3,1,2/3,1,2/3,1,

ET,1,SOLID45

MPTEMP,,,,,,,,

MPTEMP,1,0

MPDATA,EX,1,,E28
MPDATA,PRXY,1,,v28
MPTEMP,,,,,,,,
MPTEMP,1,0
MPDATA,EX,2,,E29
MPDATA,PRXY,2,,v29
MPTEMP,,,,,,,,
MPTEMP,1,0
MPDATA,EX,3,,E30
MPDATA,PRXY,3,,v30
MPTEMP,,,,,,,,
MPTEMP,1,0
MPDATA,EX,4,,E31
MPDATA,PRXY,4,,v31
MPTEMP,,,,,,,,
MPTEMP,1,0
MPDATA,EX,5,,E32
MPDATA,PRXY,5,,v32
MPTEMP,,,,,,,,
MPTEMP,1,0
MPDATA,EX,6,,E33
MPDATA,PRXY,6,,v33
MPTEMP,,,,,,,,

MPTEMP,1,0
MPDATA,EX,7,,E34
MPDATA,PRXY,7,,v34
MPTEMP,,,,,,,,
MPTEMP,1,0
MPDATA,EX,8,,E35
MPDATA,PRXY,8,,v35
MPTEMP,,,,,,,,
MPTEMP,1,0
MPDATA,EX,9,,E36
MPDATA,PRXY,9,,v36

MPTEMP,,,,,,,,
MPTEMP,1,0
MPDATA,EX,10,,E37
MPDATA,PRXY,10,,v37
MPTEMP,,,,,,,,
MPTEMP,1,0
MPDATA,EX,11,,E38
MPDATA,PRXY,11,,v38
MPTEMP,,,,,,,,
MPTEMP,1,0
MPDATA,EX,12,,E39

MPDATA,PRXY,12,,v39

MPTEMP,,,,,,,,

MPTEMP,1,0

MPDATA,EX,13,,E40

MPDATA,PRXY,13,,v40

MPTEMP,,,,,,,,

MPTEMP,1,0

MPDATA,EX,14,,E41

MPDATA,PRXY,14,,v41

MPTEMP,,,,,,,,

MPTEMP,1,0

MPDATA,EX,15,,E42

MPDATA,PRXY,15,,v42

MPTEMP,,,,,,,,

MPTEMP,1,0

MPDATA,EX,16,,E43

MPDATA,PRXY,16,,v43

MPTEMP,,,,,,,,

MPTEMP,1,0

MPDATA,EX,17,,E44

MPDATA,PRXY,17,,v44

MPTEMP,,,,,,,,

MPTEMP,1,0

MPDATA,EX,18,,E45
MPDATA,PRXY,18,,v45

MPTEMP,,,,,,,,
MPTEMP,1,0
MPDATA,EX,19,,E46
MPDATA,PRXY,19,,v46

MPTEMP,,,,,,,,
MPTEMP,1,0
MPDATA,EX,20,,E47
MPDATA,PRXY,20,,v47

MPTEMP,,,,,,,,
MPTEMP,1,0
MPDATA,EX,21,,E48
MPDATA,PRXY,21,,v48

MPTEMP,,,,,,,,
MPTEMP,1,0
MPDATA,EX,22,,E49
MPDATA,PRXY,22,,v49

MPTEMP,,,,,,,,
MPTEMP,1,0
MPDATA,EX,23,,E50
MPDATA,PRXY,23,,v50

MPTEMP,,,,,,,,
MPTEMP,1,0
MPDATA,EX,24,,E51
MPDATA,PRXY,24,,v51
MPTEMP,,,,,,,,
MPTEMP,1,0
MPDATA,EX,25,,E52
MPDATA,PRXY,25,,v52
MPTEMP,,,,,,,,
MPTEMP,1,0
MPDATA,EX,26,,E53
MPDATA,PRXY,26,,v53
MPTEMP,,,,,,,,
MPTEMP,1,0
MPDATA,EX,27,,E54
MPDATA,PRXY,27,,v54

LESIZE,ALL,1/3, , , 1, , 1,

FLST,2,27,6,ORDE,2
FITEM,2,1
FITEM,2,-27
VGLUE,P51X

```
CM,_Y,VOLU
VSEL, , , 1
CM,_Y1,VOLU
CMSEL,S,_Y
!*
CMSEL,S,_Y1
VATT, 1, , 1, 0
CMSEL,S,_Y
CMDELE,_Y
CMDELE,_Y1
!*
!*
LESIZE,ALL,1/3, , , 1, , 0,
CM,_Y,VOLU
VSEL, , , 1
CM,_Y1,VOLU
CHKMSH,'VOLU'
CMSEL,S,_Y
!*
MSHAPE,0,3d
MSHKEY,1
VMESH,_Y1
```

MSHKEY,0

!*

CMDELE,_Y

CMDELE,_Y1

CMDELE,_Y2

!*

CM,_Y,VOLU

VSEL, , , 30

CM,_Y1,VOLU

CMSEL,S,_Y

*DIM,G,ARRAY,64,6

*GET,G(1,1),NODE,1,S,X

*GET,G(2,1),NODE,2,s,x

*GET,G(3,1),NODE,3,s,x

*GET,G(4,1),NODE,4,s,x

*GET,G(5,1),NODE,5,s,x

*GET,G(6,1),NODE,6,s,x

*GET,G(7,1),NODE,7,s,x

*GET,G(8,1),NODE,8,s,x

*GET,G(9,1),NODE,9,s,x

*GET,G(10,1),NODE,10,s,x
*GET,G(11,1),NODE,11,s,x
*GET,G(12,1),NODE,12,s,x
*GET,G(13,1),NODE,13,s,x
*GET,G(14,1),NODE,14,s,x
*GET,G(15,1),NODE,15,s,x
*GET,G(16,1),NODE,16,s,x
*GET,G(17,1),NODE,17,s,x
*GET,G(18,1),NODE,18,s,x
*GET,G(19,1),NODE,19,s,x
*GET,G(20,1),NODE,20,s,x
*GET,G(21,1),NODE,21,s,x
*GET,G(22,1),NODE,22,s,x
*GET,G(23,1),NODE,23,s,x
*GET,G(24,1),NODE,24,s,x
*GET,G(25,1),NODE,25,s,x
*GET,G(26,1),NODE,26,s,x
*GET,G(27,1),NODE,27,s,x
*GET,G(28,1),NODE,28,s,x
*GET,G(29,1),NODE,29,s,x
*GET,G(30,1),NODE,30,s,x
*GET,G(31,1),NODE,31,s,x
*GET,G(32,1),NODE,32,s,x

*GET,G(33,1),NODE,33,s,x
*GET,G(34,1),NODE,34,s,x
*GET,G(35,1),NODE,35,s,x
*GET,G(36,1),NODE,36,s,x
*GET,G(37,1),NODE,37,s,x
*GET,G(38,1),NODE,38,s,x
*GET,G(39,1),NODE,39,s,x
*GET,G(40,1),NODE,40,s,x
*GET,G(41,1),NODE,41,s,x
*GET,G(42,1),NODE,42,s,x
*GET,G(43,1),NODE,43,s,x
*GET,G(44,1),NODE,44,s,x
*GET,G(45,1),NODE,45,s,x
*GET,G(46,1),NODE,46,s,x
*GET,G(47,1),NODE,47,s,x
*GET,G(48,1),NODE,48,s,x
*GET,G(49,1),NODE,49,s,x
*GET,G(50,1),NODE,50,s,x
*GET,G(51,1),NODE,51,s,x
*GET,G(52,1),NODE,52,s,x
*GET,G(53,1),NODE,53,s,x
*GET,G(54,1),NODE,54,s,x
*GET,G(55,1),NODE,55,s,x

*GET,G(56,1),NODE,56,s,x
*GET,G(57,1),NODE,57,s,x
*GET,G(58,1),NODE,58,s,x
*GET,G(59,1),NODE,59,s,x
*GET,G(60,1),NODE,60,s,x
*GET,G(61,1),NODE,61,s,x
*GET,G(62,1),NODE,62,s,x
*GET,G(63,1),NODE,63,s,x
*GET,G(64,1),NODE,64,s,x

*GET,G(1,2),NODE,1,S,y
*GET,G(2,2),NODE,2,s,y
*GET,G(3,2),NODE,3,s,y
*GET,G(4,2),NODE,4,s,y
*GET,G(5,2),NODE,5,s,y
*GET,G(6,2),NODE,6,s,y
*GET,G(7,2),NODE,7,s,y
*GET,G(8,2),NODE,8,s,y
*GET,G(9,2),NODE,9,s,y
*GET,G(10,2),NODE,10,s,y
*GET,G(11,2),NODE,11,s,y
*GET,G(12,2),NODE,12,s,y
*GET,G(13,2),NODE,13,s,y

*GET,G(14,2),NODE,14,s,y
*GET,G(15,2),NODE,15,s,y
*GET,G(16,2),NODE,16,s,y
*GET,G(17,2),NODE,17,s,y
*GET,G(18,2),NODE,18,s,y
*GET,G(19,2),NODE,19,s,y
*GET,G(20,2),NODE,20,s,y
*GET,G(21,2),NODE,21,s,y
*GET,G(22,2),NODE,22,s,y
*GET,G(23,2),NODE,23,s,y
*GET,G(24,2),NODE,24,s,y
*GET,G(25,2),NODE,25,s,y
*GET,G(26,2),NODE,26,s,y
*GET,G(27,2),NODE,27,s,y
*GET,G(28,2),NODE,28,s,y
*GET,G(29,2),NODE,29,s,y
*GET,G(30,2),NODE,30,s,y
*GET,G(31,2),NODE,31,s,y
*GET,G(32,2),NODE,32,s,y
*GET,G(33,2),NODE,33,s,y
*GET,G(34,2),NODE,34,s,y
*GET,G(35,2),NODE,35,s,y
*GET,G(36,2),NODE,36,s,y

*GET,G(37,2),NODE,37,s,y
*GET,G(38,2),NODE,38,s,y
*GET,G(39,2),NODE,39,s,y
*GET,G(40,2),NODE,40,s,y
*GET,G(41,2),NODE,41,s,y
*GET,G(42,2),NODE,42,s,y
*GET,G(43,2),NODE,43,s,y
*GET,G(44,2),NODE,44,s,y
*GET,G(45,2),NODE,45,s,y
*GET,G(46,2),NODE,46,s,y
*GET,G(47,2),NODE,47,s,y
*GET,G(48,2),NODE,48,s,y
*GET,G(49,2),NODE,49,s,y
*GET,G(50,2),NODE,50,s,y
*GET,G(51,2),NODE,51,s,y
*GET,G(52,2),NODE,52,s,y
*GET,G(53,2),NODE,53,s,y
*GET,G(54,2),NODE,54,s,y
*GET,G(55,2),NODE,55,s,y
*GET,G(56,2),NODE,56,s,y
*GET,G(57,2),NODE,57,s,y
*GET,G(58,2),NODE,58,s,y
*GET,G(59,2),NODE,59,s,y

*GET,G(60,2),NODE,60,s,y
*GET,G(61,2),NODE,61,s,y
*GET,G(62,2),NODE,62,s,y
*GET,G(63,2),NODE,63,s,y
*GET,G(64,2),NODE,64,s,y

*GET,G(1,3),NODE,1,S,z
*GET,G(2,3),NODE,2,s,z
*GET,G(3,3),NODE,3,s,z
*GET,G(4,3),NODE,4,s,z
*GET,G(5,3),NODE,5,s,z
*GET,G(6,3),NODE,6,s,z
*GET,G(7,3),NODE,7,s,z
*GET,G(8,3),NODE,8,s,z
*GET,G(9,3),NODE,9,s,z
*GET,G(10,3),NODE,10,s,z
*GET,G(11,3),NODE,11,s,z
*GET,G(12,3),NODE,12,s,z
*GET,G(13,3),NODE,13,s,z
*GET,G(14,3),NODE,14,s,z
*GET,G(15,3),NODE,15,s,z
*GET,G(16,3),NODE,16,s,z
*GET,G(17,3),NODE,17,s,z

*GET,G(18,3),NODE,18,s,z
*GET,G(19,3),NODE,19,s,z
*GET,G(20,3),NODE,20,s,z
*GET,G(21,3),NODE,21,s,z
*GET,G(22,3),NODE,22,s,z
*GET,G(23,3),NODE,23,s,z
*GET,G(24,3),NODE,24,s,z
*GET,G(25,3),NODE,25,s,z
*GET,G(26,3),NODE,26,s,z
*GET,G(27,3),NODE,27,s,z
*GET,G(28,3),NODE,28,s,z
*GET,G(29,3),NODE,29,s,z
*GET,G(30,3),NODE,30,s,z
*GET,G(31,3),NODE,31,s,z
*GET,G(32,3),NODE,32,s,z
*GET,G(33,3),NODE,33,s,z
*GET,G(34,3),NODE,34,s,z
*GET,G(35,3),NODE,35,s,z
*GET,G(36,3),NODE,36,s,z
*GET,G(37,3),NODE,37,s,z
*GET,G(38,3),NODE,38,s,z
*GET,G(39,3),NODE,39,s,z
*GET,G(40,3),NODE,40,s,z

*GET,G(41,3),NODE,41,s,z
*GET,G(42,3),NODE,42,s,z
*GET,G(43,3),NODE,43,s,z
*GET,G(44,3),NODE,44,s,z
*GET,G(45,3),NODE,45,s,z
*GET,G(46,3),NODE,46,s,z
*GET,G(47,3),NODE,47,s,z
*GET,G(48,3),NODE,48,s,z
*GET,G(49,3),NODE,49,s,z
*GET,G(50,3),NODE,50,s,z
*GET,G(51,3),NODE,51,s,z
*GET,G(52,3),NODE,52,s,z
*GET,G(53,3),NODE,53,s,z
*GET,G(54,3),NODE,54,s,z
*GET,G(55,3),NODE,55,s,z
*GET,G(56,3),NODE,56,s,z
*GET,G(57,3),NODE,57,s,z
*GET,G(58,3),NODE,58,s,z
*GET,G(59,3),NODE,59,s,z
*GET,G(60,3),NODE,60,s,z
*GET,G(61,3),NODE,61,s,z
*GET,G(62,3),NODE,62,s,z
*GET,G(63,3),NODE,63,s,z

*GET,G(64,3),NODE,64,s,z

*GET,G(1,4),NODE,1,S,yz

*GET,G(2,4),NODE,2,s,yz

*GET,G(3,4),NODE,3,s,yz

*GET,G(4,4),NODE,4,s,yz

*GET,G(5,4),NODE,5,s,yz

*GET,G(6,4),NODE,6,s,yz

*GET,G(7,4),NODE,7,s,yz

*GET,G(8,4),NODE,8,s,yz

*GET,G(9,4),NODE,9,s,yz

*GET,G(10,4),NODE,10,s,yz

*GET,G(11,4),NODE,11,s,yz

*GET,G(12,4),NODE,12,s,yz

*GET,G(13,4),NODE,13,s,yz

*GET,G(14,4),NODE,14,s,yz

*GET,G(15,4),NODE,15,s,yz

*GET,G(16,4),NODE,16,s,yz

*GET,G(17,4),NODE,17,s,yz

*GET,G(18,4),NODE,18,s,yz

*GET,G(19,4),NODE,19,s,yz

*GET,G(20,4),NODE,20,s,yz

*GET,G(21,4),NODE,21,s,yz

*GET,G(22,4),NODE,22,s,yz
*GET,G(23,4),NODE,23,s,yz
*GET,G(24,4),NODE,24,s,yz
*GET,G(25,4),NODE,25,s,yz
*GET,G(26,4),NODE,26,s,yz
*GET,G(27,4),NODE,27,s,yz
*GET,G(28,4),NODE,28,s,yz
*GET,G(29,4),NODE,29,s,yz
*GET,G(30,4),NODE,30,s,yz
*GET,G(31,4),NODE,31,s,yz
*GET,G(32,4),NODE,32,s,yz
*GET,G(33,4),NODE,33,s,yz
*GET,G(34,4),NODE,34,s,yz
*GET,G(35,4),NODE,35,s,yz
*GET,G(36,4),NODE,36,s,yz
*GET,G(37,4),NODE,37,s,yz
*GET,G(38,4),NODE,38,s,yz
*GET,G(39,4),NODE,39,s,yz
*GET,G(40,4),NODE,40,s,yz
*GET,G(41,4),NODE,41,s,yz
*GET,G(42,4),NODE,42,s,yz
*GET,G(43,4),NODE,43,s,yz
*GET,G(44,4),NODE,44,s,yz

*GET,G(45,4),NODE,45,s,yz
*GET,G(46,4),NODE,46,s,yz
*GET,G(47,4),NODE,47,s,yz
*GET,G(48,4),NODE,48,s,yz
*GET,G(49,4),NODE,49,s,yz
*GET,G(50,4),NODE,50,s,yz
*GET,G(51,4),NODE,51,s,yz
*GET,G(52,4),NODE,52,s,yz
*GET,G(53,4),NODE,53,s,yz
*GET,G(54,4),NODE,54,s,yz
*GET,G(55,4),NODE,55,s,yz
*GET,G(56,4),NODE,56,s,yz
*GET,G(57,4),NODE,57,s,yz
*GET,G(58,4),NODE,58,s,yz
*GET,G(59,4),NODE,59,s,yz
*GET,G(60,4),NODE,60,s,yz
*GET,G(61,4),NODE,61,s,yz
*GET,G(62,4),NODE,62,s,yz
*GET,G(63,4),NODE,63,s,yz
*GET,G(64,4),NODE,64,s,yz

*GET,G(1,5),NODE,1,S,xz
*GET,G(2,5),NODE,2,s,xz

*GET,G(3,5),NODE,3,s,xz
*GET,G(4,5),NODE,4,s,xz
*GET,G(5,5),NODE,5,s,xz
*GET,G(6,5),NODE,6,s,xz
*GET,G(7,5),NODE,7,s,xz
*GET,G(8,5),NODE,8,s,xz
*GET,G(9,5),NODE,9,s,xz
*GET,G(10,5),NODE,10,s,xz
*GET,G(11,5),NODE,11,s,xz
*GET,G(12,5),NODE,12,s,xz
*GET,G(13,5),NODE,13,s,xz
*GET,G(14,5),NODE,14,s,xz
*GET,G(15,5),NODE,15,s,xz
*GET,G(16,5),NODE,16,s,xz
*GET,G(17,5),NODE,17,s,xz
*GET,G(18,5),NODE,18,s,xz
*GET,G(19,5),NODE,19,s,xz
*GET,G(20,5),NODE,20,s,xz
*GET,G(21,5),NODE,21,s,xz
*GET,G(22,5),NODE,22,s,xz
*GET,G(23,5),NODE,23,s,xz
*GET,G(24,5),NODE,24,s,xz
*GET,G(25,5),NODE,25,s,xz

*GET,G(26,5),NODE,26,s,xz
*GET,G(27,5),NODE,27,s,xz
*GET,G(28,5),NODE,28,s,xz
*GET,G(29,5),NODE,29,s,xz
*GET,G(30,5),NODE,30,s,xz
*GET,G(31,5),NODE,31,s,xz
*GET,G(32,5),NODE,32,s,xz
*GET,G(33,5),NODE,33,s,xz
*GET,G(34,5),NODE,34,s,xz
*GET,G(35,5),NODE,35,s,xz
*GET,G(36,5),NODE,36,s,xz
*GET,G(37,5),NODE,37,s,xz
*GET,G(38,5),NODE,38,s,xz
*GET,G(39,5),NODE,39,s,xz
*GET,G(40,5),NODE,40,s,xz
*GET,G(41,5),NODE,41,s,xz
*GET,G(42,5),NODE,42,s,xz
*GET,G(43,5),NODE,43,s,xz
*GET,G(44,5),NODE,44,s,xz
*GET,G(45,5),NODE,45,s,xz
*GET,G(46,5),NODE,46,s,xz
*GET,G(47,5),NODE,47,s,xz
*GET,G(48,5),NODE,48,s,xz

*GET,G(49,5),NODE,49,s,xz
*GET,G(50,5),NODE,50,s,xz
*GET,G(51,5),NODE,51,s,xz
*GET,G(52,5),NODE,52,s,xz
*GET,G(53,5),NODE,53,s,xz
*GET,G(54,5),NODE,54,s,xz
*GET,G(55,5),NODE,55,s,xz
*GET,G(56,5),NODE,56,s,xz
*GET,G(57,5),NODE,57,s,xz
*GET,G(58,5),NODE,58,s,xz
*GET,G(59,5),NODE,59,s,xz
*GET,G(60,5),NODE,60,s,xz
*GET,G(61,5),NODE,61,s,xz
*GET,G(62,5),NODE,62,s,xz
*GET,G(63,5),NODE,63,s,xz
*GET,G(64,5),NODE,64,s,xz

*GET,G(1,6),NODE,1,S,xy
*GET,G(2,6),NODE,2,s,xy
*GET,G(3,6),NODE,3,s,xy
*GET,G(4,6),NODE,4,s,xy
*GET,G(5,6),NODE,5,s,xy
*GET,G(6,6),NODE,6,s,xy

*GET,G(7,6),NODE,7,s,xy
*GET,G(8,6),NODE,8,s,xy
*GET,G(9,6),NODE,9,s,xy
*GET,G(10,6),NODE,10,s,xy
*GET,G(11,6),NODE,11,s,xy
*GET,G(12,6),NODE,12,s,xy
*GET,G(13,6),NODE,13,s,xy
*GET,G(14,6),NODE,14,s,xy
*GET,G(15,6),NODE,15,s,xy
*GET,G(16,6),NODE,16,s,xy
*GET,G(17,6),NODE,17,s,xy
*GET,G(18,6),NODE,18,s,xy
*GET,G(19,6),NODE,19,s,xy
*GET,G(20,6),NODE,20,s,xy
*GET,G(21,6),NODE,21,s,xy
*GET,G(22,6),NODE,22,s,xy
*GET,G(23,6),NODE,23,s,xy
*GET,G(24,6),NODE,24,s,xy
*GET,G(25,6),NODE,25,s,xy
*GET,G(26,6),NODE,26,s,xy
*GET,G(27,6),NODE,27,s,xy
*GET,G(28,6),NODE,28,s,xy
*GET,G(29,6),NODE,29,s,xy

*GET,G(30,6),NODE,30,s,xy
*GET,G(31,6),NODE,31,s,xy
*GET,G(32,6),NODE,32,s,xy
*GET,G(33,6),NODE,33,s,xy
*GET,G(34,6),NODE,34,s,xy
*GET,G(35,6),NODE,35,s,xy
*GET,G(36,6),NODE,36,s,xy
*GET,G(37,6),NODE,37,s,xy
*GET,G(38,6),NODE,38,s,xy
*GET,G(39,6),NODE,39,s,xy
*GET,G(40,6),NODE,40,s,xy
*GET,G(41,6),NODE,41,s,xy
*GET,G(42,6),NODE,42,s,xy
*GET,G(43,6),NODE,43,s,xy
*GET,G(44,6),NODE,44,s,xy
*GET,G(45,6),NODE,45,s,xy
*GET,G(46,6),NODE,46,s,xy
*GET,G(47,6),NODE,47,s,xy
*GET,G(48,6),NODE,48,s,xy
*GET,G(49,6),NODE,49,s,xy
*GET,G(50,6),NODE,50,s,xy
*GET,G(51,6),NODE,51,s,xy
*GET,G(52,6),NODE,52,s,xy

```
*GET,G(53,6),NODE,53,s,xy
*GET,G(54,6),NODE,54,s,xy
*GET,G(55,6),NODE,55,s,xy
*GET,G(56,6),NODE,56,s,xy
*GET,G(57,6),NODE,57,s,xy
*GET,G(58,6),NODE,58,s,xy
*GET,G(59,6),NODE,59,s,xy
*GET,G(60,6),NODE,60,s,xy
*GET,G(61,6),NODE,61,s,xy
*GET,G(62,6),NODE,62,s,xy
*GET,G(63,6),NODE,63,s,xy
*GET,G(64,6),NODE,64,s,xy
```

```
FINISH
```

```
/SOL
```

```
LSCLEAR,ALL
```

```
*c fopen,loadcaseL2x,txt
```

```
*vwrite, B(1,1), B(1,2), B(1,3), B(1,4), B(1,5), B(1,6)
```

```
(E10.4,' ',E10.4,' ',E10.4,' ',E10.4,' ',E10.4,' ',E10.4)
```

```
*cfclos
```

```
*c fopen,loadcaseL2y,txt
```

```
*vwrite, C(1,1), C(1,2), C(1,3), C(1,4), C(1,5), C(1,6)
(E10.4,' ',E10.4,' ',E10.4,' ',E10.4,' ',E10.4,' ',E10.4)
*cfclos
```

```
*c fopen,loadcaseL2z.txt
*vwrite, D(1,1), D(1,2), D(1,3), D(1,4), D(1,5), D(1,6)
(E10.4,' ',E10.4,' ',E10.4,' ',E10.4,' ',E10.4,' ',E10.4)
*cfclos
```

```
*c fopen,loadcaseL2yz.txt
*vwrite, E(1,1), E(1,2), E(1,3), E(1,4), E(1,5), E(1,6)
(E10.4,' ',E10.4,' ',E10.4,' ',E10.4,' ',E10.4,' ',E10.4)
*cfclos
```

```
*c fopen,loadcaseL2xz.txt
*vwrite, F(1,1), F(1,2), F(1,3), F(1,4), F(1,5), F(1,6)
(E10.4,' ',E10.4,' ',E10.4,' ',E10.4,' ',E10.4,' ',E10.4)
*cfclos
```

```
*c fopen,loadcaseL2xy.txt
*vwrite, G(1,1), G(1,2), G(1,3), G(1,4), G(1,5), G(1,6)
(E10.4,' ',E10.4,' ',E10.4,' ',E10.4,' ',E10.4,' ',E10.4)
*cfclos
```


OBJECTIVE FUNCTION CALCULATION CODE

```
// fobj.cpp : Defines the entry point for the console application.
//

#include "stdafx.h"
#include <cstdlib>
#include <iostream>
#include <fstream>
#include <vector>
#include <string>

using namespace std;

//int main(int argc, char **argv)
int main()
{
//Read weights and strengths of each layer
float w1, w2;//weights of layers 1 & 2
float s1, s2;//strength of layers 1 & 2
ifstream finws("WS.IN");
if (!finws){
    cerr << "\nError: failure opening WS" << endl;
    exit(-1);
}
finws >> w1;
finws >> w2;
finws >> s1;
finws >> s2;

finws.close();

// Find max stress for each layer
int i;
int timeL1;//number of time/data points in vonmiseses for layer1
int timeL2;//number of time/data points in vonmiseses for layer2

// timeL1=2002;
// timeL2=2002;

float Sdummy;//stresses to be read from file
float SmaxL1, SmaxL2; //max stresses from layers 1&2
// int dummy;// to get 2002
float timedummy;// to get time values

ifstream finvm("vonmises");
if (!finvm) {
    cerr << "\nError: failure opening vonmiseses" << endl;
    exit(-1);
}
finvm >> timeL1;
SmaxL1=0.001;
```

```

for(i=0; i<timeL1; i++){
    finvm >> timedummy;
    finvm >> Sdummy;
    if (Sdummy > SmaxL1){
        SmaxL1=Sdummy;
    }
}

finvm >> timeL2;
SmaxL2=0.001;
for(i=0; i<timeL2; i++){
    finvm >> timedummy;
    finvm >> Sdummy;
    if (Sdummy > SmaxL2){
        SmaxL2=Sdummy;
    }
}
finvm.close();

float SrL1, SrL2;//Stress/strength ratios for layers 1 & 2

SrL1=SmaxL1/s1;
SrL2=SmaxL2/s2;

float Wtotal;
Wtotal=w1+w2;

float Srmax;//max stress to strength ratio
Srmax=SrL1;
if (SrL2 > SrL1){
    Srmax = SrL2;
}
ofstream foutr("RESULTS.OUT");
if (!foutr) {
    cerr << "\nError: failure creating file RESULTS" << endl;
    system("PAUSE");
    exit(-1);
}

foutr << Wtotal << endl;
foutr << Srmax << endl;

foutr.close();

return 0;
}

```

ANSYS INPUT CODE

```
// generateinput.cpp : Defines the entry point for the console  
application.
```

```
//
```

```
#include "stdafx.h"
```

```
//int _tmain(int argc, _TCHAR* argv[])
```

```
//{
```

```
//    return 0;
```

```
//}
```

```
/*
```

DAKOTA: Design Analysis Kit for Optimization and Terascale
Applications

Copyright (c) 2006, Sandia National Laboratories.

This software is distributed under the GNU General Public License.

For more information, see the README file in the top Dakota
directory.

```
*/
```

```

#include <cstdlib>

#include <iostream>

#include <fstream>

#include <vector>

#include <string>

#ifdef HAVE_CONFIG_H
#include "dakota_config.h"
#endif // HAVE_CONFIG_H

#ifdef HAVE_STD
#include <cmath>
#else
#include <math.h>
#endif // HAVE_STD

using namespace std;

int main(int argc, char** argv){
    int num_vars;
    string vars_text;
    int i;
    int numnodes, numnodesL1, numnodesL2;
    numnodes=54;
    numnodesL1=27;
    numnodesL2=27;
    float t1, t2;
    t2=0;

    // Read number of nodes from the given file

```

```

// ifstream finns("numnodes.txt");
// if (!finns) {
//     cerr << "\nError: failure opening numnodes.txt" << endl;
//     exit(-1);
// }
// finns >> numnodes;
// finns.close();

struct EValues{
    float Ebinary;//Values of E's from the optimization tool
    float Ereal;//do necessary calculations on Ebinary
};

// float sumE;//sum of the ratios
EValues *E;
E= new EValues[numnodes];
float dA, dB, EA, EB, tcA, tcB, vA, vB;

//read the multipliers for E (Young modulus for Material 1 and
Material 2)
//order of Material properties in MaterialAB.txt file dA, dB, eA,
eB, t(c)A, t(c)B, vA, Vb

ifstream finab("MaterialAB.txt");
if (!finab) {
    cerr << "\nError: failure opening MaterialAB" << endl;
    exit(-1);
}
finab >> dA;

```

```

finab >> dB;

finab >> EA;

finab >> EB;

finab >> tcA;

finab >> tcB;

finab >> vA;

finab >> vB;

finab.close();

//Read the decision variables file and find sum of them
// ifstream fin(argv[1]);
ifstream fin("DESVAR.IN");
if (!fin) {
    cerr << "\nError: failure opening DESVAR" << endl;
    exit(-1);
}
fin >> num_vars >> vars_text;
// if (num_vars != numnodes) {
//     cerr << "Error: Wrong number of variables for TOPO" <<
endl;
//     system("PAUSE");
//     exit(-1);
// }
// sumE=0.0;

fin >> t1;

fin.ignore(256, '\n');

for(i=0; i<numnodes; i++){
    fin >> E[i].Ebinary;

```

```

//          sumE+=E[i].Ebinary;

          fin.ignore(256, '\n');
      }

//0: for Material A, 1 : for Material B
fin.close();

// Calculate E values to be passed to ANSYS if they are 0, replace
them with a small number (0.0001)
for (i=0;i<numnodes;i++){
    E[i].Ereal=float(E[i].Ebinary*EB+(1-E[i].Ebinary)*EA);
//          if(E[i].Ereal==0.0){
//              E[i].Ereal=0.0001;
//          }
}

// Write input file for ANSYS that contains E values of nodes
ofstream fout("ANSYSINPUT.IN");
if (!fout) {
    cerr << "\nError: failure creating INPUT" << endl;
    system("PAUSE");
    exit(-1);
}
fout.precision(2); // 16 total digits
fout.setf(ios::scientific);
fout.setf(ios::right);

for (i=0;i<numnodes;i++){

```

```

        fout << "E" << i+1 << "=" << E[i].Ereal << endl;
        if (E[i].Ebinary==0){
            fout << "v" << i+1 << "=" << vA << endl;
        }else{
            fout << "v" << i+1 << "=" << vB << endl;
        }
    }
    fout.close();

//Calculate densities of Layers 1 and 2

    float ro1, ro2;
    ro1=0.0;
    ro2=0.0;
    for (i=0;i<numnodesL1;i++){
        ro1=ro1+float(E[i].Ebinary*dB+(1-E[i].Ebinary)*dA);
    }
    ro1=ro1/(numnodesL1);
    for (i=numnodesL1;i<numnodes;i++){
        ro2=ro2+float(E[i].Ebinary*dB+(1-E[i].Ebinary)*dA);
    }
    ro2=ro2/(numnodesL2);

//write densities to a file
    ofstream foutro("RO.IN");
    if (!foutro) {
        cerr << "\n Error: failure to create RO" << endl;
        system ("PAUSE");
        exit(-1);
    }

```



```

    }

    foutro << ro1 << endl;

    foutro << ro2 << endl;

    foutro.close();

// Calculate t2
    t2=0.17-t1;

// Write the file that contains layer thickness and their sum
    ofstream foutt("T.IN");
    if (!foutt) {
        cerr << "\nError: failure creating T" << endl;
        system("PAUSE");
        exit(-1);
    }

// fout.precision(2); // 16 total digits
// fout.setf(ios::scientific);
// fout.setf(ios::right);

    foutt << t1 << endl;
    foutt << t2 << endl;
    foutt << t1+t2 << endl;

    foutt.close();

// Calculate weight and strength of Layers 1 and 2

```

```

// Weight calculation

float w1, w2;

w1=0.09*t1*ro1;

w2=0.09*t2*ro2;

// Strength calculation

float st1, st2;

st1=0.0;

st2=0.0;

for (i=0;i<numnodesL1;i++){

    st1=st1+float(E[i].Ebinary*tcB+(1-E[i].Ebinary)*tcA);

}

st1=st1/(numnodesL1);

for (i=numnodesL1;i<numnodes;i++){

    st2=st2+float(E[i].Ebinary*tcB+(1-E[i].Ebinary)*tcA);

}

st2=st2/(numnodesL2);

// write weights & strengths to a file

ofstream foutws("WS.IN");

if (!foutws) {

    cerr << "\n Error: failure to create WS" << endl;

    system ("PAUSE");

    exit(-1);

}

foutws << w1 << endl;

foutws << w2 << endl;

foutws << st1 << endl;

```

```

foutws << st2 << endl;

foutws.close();

// Write sum of the ratio of Material 1
// ofstream fouts("sumE.txt");
// if (!fouts) {
//     cerr << "\nError: failure creating INPUT" << endl;
//     system("PAUSE");
//     exit(-1);
// }
// fouts.precision(1); // 16 total digits
// fouts.setf(ios::scientific);
// fouts.setf(ios::right);

// fouts << sumE;
// fouts.close();

return 0;
}

```

LS-DYNA INPUT CODE

```
// fobj.cpp : Defines the entry point for the console application.
//

#include "stdafx.h"
#include <cstdlib>
#include <iostream>
#include <fstream>
#include <vector>
#include <string>

using namespace std;

//int main(int argc, char **argv)
int main()
{
    int i;

    //Calculate t values to be written to lsdynainput file
    float tL1, tL2; //thickness of layer 1 and 2
    float t1, t2, t3, t4, t5, t6, t7, t8 ,t9, t10; //values to be
written to lsdynainput file
    float t1dummy, t2dummy; // to keep the 1/5th of ayer thicknesses
    //read T.IN
    ifstream finT("T.IN");
    if (!finT) {
        cerr << "\nError opening file T!"<<endl;
        system ("PAUSE");
        exit (-1);
    }
    finT >> tL1;
    finT >> tL2;

    t1dummy= tL1/5;
    t1=t1dummy*1;
    t2=t1*2;
    t3=t1*3;
    t4=t1*4;
    t5=t1*5;

    t2dummy=tL2/5;
    t6=t5+t2dummy*1;
    t7=t5+t2dummy*2;
    t8=t5+t2dummy*3;
    t9=t5+t2dummy*4;
    t10=t5+t2dummy*5;

    finT.close();

    //Get densities of layers 1 and 2
    float ro1, ro2;

    ifstream finro("RO.IN");
```

```

if(!finro){
    cerr << "\nError opening file RO!"<<endl;
    system ("PAUSE");
    exit (-1);
}
finro >> ro1;
finro >> ro2;

//Calcluate c values (E averages) to be written into lsdynainput file
// int numnodes;//number of nodes
int numrows;//number of rows in the loadcase files
numrows=64;

// Read number of nodes from the given file
// ifstream finns("numnodes.txt");
// if (!finns) {
//     cerr << "\nError: failure opening numnodes.txt" << endl;
//     exit(-1);/
// }
// finns >> numnodes;
// finns >> numrows;
// finns.close();

// int j;
//Struct to hold data from ANSYS
struct LoadValues{
    float e1x1, e1x2, e1x3, e1x4, e1x5, e1x6;//values to
be derived from loadcaseL1x
    float e1xy1, e1xy2, e1xy3, e1xy4, e1xy5,
e1xy6;//values to be derived from loadcaseL1xy
    float e1xz1, e1xz2, e1xz3, e1xz4, e1xz5,
e1xz6;//values to be derived from loadcaseL1xz
    float e1y1, e1y2, e1y3, e1y4, e1y5, e1y6;//values to
be derived from loadcaseL1y
    float e1yz1, e1yz2, e1yz3, e1yz4, e1yz5,
e1yz6;//values to be derived from loadcaseL1yz
    float e1z1, e1z2, e1z3, e1z4, e1z5, e1z6;//values to
be derived from loadcaseL1z
    float e2x1, e2x2, e2x3, e2x4, e2x5, e2x6;//values to
be derived from loadcaseL2x
    float e2xy1, e2xy2, e2xy3, e2xy4, e2xy5,
e2xy6;//values to be derived from loadcaseL2xy
    float e2xz1, e2xz2, e2xz3, e2xz4, e2xz5,
e2xz6;//values to be derived from loadcaseL2xz
    float e2y1, e2y2, e2y3, e2y4, e2y5, e2y6;//values to
be derived from loadcaseL2y
    float e2yz1, e2yz2, e2yz3, e2yz4, e2yz5,
e2yz6;//values to be derived from loadcaseL2yz
    float e2z1, e2z2, e2z3, e2z4, e2z5, e2z6;//values to
be derived from loadcaseL2z
};
LoadValues *value;

```

```

value= new LoadValues[numrows];
//Targeted E values
// float Et11, Et12, Et13, Et21, Et22, Et23, Et31, Et32, Et33;// to
be read from file

//E values calculated by averaging columns

float c111;
float c121, c221;
float c131, c231, c331;
float c141, c241, c341, c441;
float c151, c251, c351, c451, c551;
float c161, c261, c361, c461, c561, c661;

float c112;
float c122, c222;
float c132, c232, c332;
float c142, c242, c342, c442;
float c152, c252, c352, c452, c552;
float c162, c262, c362, c462, c562, c662;

// float SQdiff;//squared difference of E values

//read loadcaseL1x.txt
ifstream finL1x("loadcaseL1x.txt");
if (!finL1x) {
    cerr << "\nError opening file loadcaseL1x!"<<endl;
    system ("PAUSE");
    exit (-1);
}
for (i=0; i<numrows; i++){
    finL1x >> value[i].e11x1;
    finL1x >> value[i].e11x2;
    finL1x >> value[i].e11x3;
    finL1x >> value[i].e11x4;
    finL1x >> value[i].e11x5;
    finL1x >> value[i].e11x6;
}
finL1x.close();

//read loadcaseL1xy.txt
ifstream finL1xy("loadcaseL1xy.txt");
if (!finL1xy) {
    cerr << "\nError opening file loadcaseL1xy!"<<endl;
    system ("PAUSE");
    exit (-1);
}
for (i=0; i<numrows; i++){
    finL1xy >> value[i].e11xy1;
    finL1xy >> value[i].e11xy2;
    finL1xy >> value[i].e11xy3;
    finL1xy >> value[i].e11xy4;
    finL1xy >> value[i].e11xy5;
}

```

```

        finLlxy >> value[i].ellxy6;
    }
    finLlxy.close();

    //read loadcaseLlxz.txt
    ifstream finLlxz("loadcaseLlxz.txt");
    if (!finLlxz) {
        cerr << "\nError opening file loadcaseLlxz!"<<endl;
        system ("PAUSE");
        exit (-1);
    }
    for (i=0; i<numrows; i++){
        finLlxz >> value[i].ellxz1;
        finLlxz >> value[i].ellxz2;
        finLlxz >> value[i].ellxz3;
        finLlxz >> value[i].ellxz4;
        finLlxz >> value[i].ellxz5;
        finLlxz >> value[i].ellxz6;
    }
    finLlxz.close();

    //read loadcaseLly.txt
    ifstream finLly("loadcaseLly.txt");
    if (!finLly) {
        cerr << "\nError opening file loadcaseLly!"<<endl;
        system ("PAUSE");
        exit (-1);
    }
    for (i=0; i<numrows; i++){
        finLly >> value[i].elly1;
        finLly >> value[i].elly2;
        finLly >> value[i].elly3;
        finLly >> value[i].elly4;
        finLly >> value[i].elly5;
        finLly >> value[i].elly6;
    }
    finLly.close();

    //read loadcaseLlyz.txt
    ifstream finLlyz("loadcaseLlyz.txt");
    if (!finLlyz) {
        cerr << "\nError opening file loadcaseLlyz!"<<endl;
        system ("PAUSE");
        exit (-1);
    }
    for (i=0; i<numrows; i++){
        finLlyz >> value[i].ellyz1;
        finLlyz >> value[i].ellyz2;
        finLlyz >> value[i].ellyz3;
        finLlyz >> value[i].ellyz4;
        finLlyz >> value[i].ellyz5;
        finLlyz >> value[i].ellyz6;
    }
    finLlyz.close();

```

```

//read loadcaseL1z.txt
ifstream finL1z("loadcaseL1z.txt");
if (!finL1z) {
    cerr << "\nError opening file loadcaseL1z!"<<endl;
    system ("PAUSE");
    exit (-1);
}
for (i=0; i<numrows; i++){
    finL1z >> value[i].el1z1;
    finL1z >> value[i].el1z2;
    finL1z >> value[i].el1z3;
    finL1z >> value[i].el1z4;
    finL1z >> value[i].el1z5;
    finL1z >> value[i].el1z6;
}
finL1z.close();

//read loadcaseL2x.txt
ifstream finL2x("loadcaseL2x.txt");
if (!finL2x) {
    cerr << "\nError opening file loadcaseL2x!"<<endl;
    system ("PAUSE");
    exit (-1);
}
for (i=0; i<numrows; i++){
    finL2x >> value[i].el2x1;
    finL2x >> value[i].el2x2;
    finL2x >> value[i].el2x3;
    finL2x >> value[i].el2x4;
    finL2x >> value[i].el2x5;
    finL2x >> value[i].el2x6;
}
finL2x.close();

//read loadcaseL2xy.txt
ifstream finL2xy("loadcaseL2xy.txt");
if (!finL2xy) {
    cerr << "\nError opening file loadcaseL2xy!"<<endl;
    system ("PAUSE");
    exit (-1);
}
for (i=0; i<numrows; i++){
    finL2xy >> value[i].el2xy1;
    finL2xy >> value[i].el2xy2;
    finL2xy >> value[i].el2xy3;
    finL2xy >> value[i].el2xy4;
    finL2xy >> value[i].el2xy5;
    finL2xy >> value[i].el2xy6;
}
finL2xy.close();

//read loadcaseL2xz.txt
ifstream finL2xz("loadcaseL2xz.txt");
if (!finL2xz) {

```



```

        cerr << "\nError opening file loadcaseL2xz!"<<endl;
        system ("PAUSE");
        exit (-1);
    }
    for (i=0; i<numrows; i++){
        finL2xz >> value[i].el2xz1;
        finL2xz >> value[i].el2xz2;
        finL2xz >> value[i].el2xz3;
        finL2xz >> value[i].el2xz4;
        finL2xz >> value[i].el2xz5;
        finL2xz >> value[i].el2xz6;
    }
    finL2xz.close();

    //read loadcaseL2y.txt
    ifstream finL2y("loadcaseL2y.txt");
    if (!finL2y) {
        cerr << "\nError opening file loadcaseL2y!"<<endl;
        system ("PAUSE");
        exit (-1);
    }
    for (i=0; i<numrows; i++){
        finL2y >> value[i].el2y1;
        finL2y >> value[i].el2y2;
        finL2y >> value[i].el2y3;
        finL2y >> value[i].el2y4;
        finL2y >> value[i].el2y5;
        finL2y >> value[i].el2y6;
    }
    finL2y.close();

    //read loadcaseL2yz.txt
    ifstream finL2yz("loadcaseL2yz.txt");
    if (!finL2yz) {
        cerr << "\nError opening file loadcaseL2yz!"<<endl;
        system ("PAUSE");
        exit (-1);
    }
    for (i=0; i<numrows; i++){
        finL2yz >> value[i].el2yz1;
        finL2yz >> value[i].el2yz2;
        finL2yz >> value[i].el2yz3;
        finL2yz >> value[i].el2yz4;
        finL2yz >> value[i].el2yz5;
        finL2yz >> value[i].el2yz6;
    }
    finL2yz.close();

    //read loadcaseL2z.txt
    ifstream finL2z("loadcaseL2z.txt");
    if (!finL2z) {
        cerr << "\nError opening file loadcaseL2z!"<<endl;
        system ("PAUSE");
        exit (-1);
    }
}

```

```
for (i=0; i<numrows; i++){
    finL2z >> value[i].el2z1;
    finL2z >> value[i].el2z2;
    finL2z >> value[i].el2z3;
    finL2z >> value[i].el2z4;
    finL2z >> value[i].el2z5;
    finL2z >> value[i].el2z6;
}
finL2z.close();
```

```
c111=0.0;
c121=0.0;
c221=0.0;
c131=0.0;
c231=0.0;
c331=0.0;
c141=0.0;
c241=0.0;
c341=0.0;
c441=0.0;
c151=0.0;
c251=0.0;
c351=0.0;
c451=0.0;
c551=0.0;
c161=0.0;
c261=0.0;
c361=0.0;
c461=0.0;
c561=0.0;
c661=0.0;
```

```
c112=0.0;
c122=0.0;
c222=0.0;
c132=0.0;
c232=0.0;
c332=0.0;
c142=0.0;
c242=0.0;
c342=0.0;
c442=0.0;
c152=0.0;
c252=0.0;
c352=0.0;
c452=0.0;
c552=0.0;
c162=0.0;
c262=0.0;
c362=0.0;
c462=0.0;
c562=0.0;
c662=0.0;
```

```

//sum values from the loadcase files
for (i=0; i<numrows; i++){
c111=c111+value[i].el1x1;
c121=c121+value[i].el1x2;
c221=c221+value[i].el1y2;
c131=c131+value[i].el1x3;
c231=c231+value[i].el1y3;
c331=c331+value[i].el1z3;
c141=c141+value[i].el1x4;
c241=c241+value[i].el1y4;
c341=c341+value[i].el1z4;
c441=c441+value[i].el1yz4;
c151=c151+value[i].el1x5;
c251=c251+value[i].el1y5;
c351=c351+value[i].el1z5;
c451=c451+value[i].el1yz5;
c551=c551+value[i].el1xz5;
c161=c161+value[i].el1x6;
c261=c261+value[i].el1y6;
c361=c361+value[i].el1z6;
c461=c461+value[i].el1yz6;
c561=c561+value[i].el1xz6;
c661=c661+value[i].el1xy6;

c112=c112+value[i].el2x1;
c122=c122+value[i].el2x2;
c222=c222+value[i].el2y2;
c132=c132+value[i].el2x3;
c232=c232+value[i].el2y3;
c332=c332+value[i].el2z3;
c142=c142+value[i].el2x4;
c242=c242+value[i].el2y4;
c342=c342+value[i].el2z4;
c442=c442+value[i].el2yz4;
c152=c152+value[i].el2x5;
c252=c252+value[i].el2y5;
c352=c352+value[i].el2z5;
c452=c452+value[i].el2yz5;
c552=c552+value[i].el2xz5;
c162=c162+value[i].el2x6;
c262=c262+value[i].el2y6;
c362=c362+value[i].el2z6;
c462=c462+value[i].el2yz6;
c562=c562+value[i].el2xz6;
c662=c662+value[i].el2xy6;

}
//average values from the loadcase files to find E matrix

c111=c111/numrows;
c121=c121/numrows;
c221=c221/numrows;

```

```
c131=c131/numrows;  
c231=c231/numrows;  
c331=c331/numrows;  
c141=c141/numrows;  
c241=c241/numrows;  
c341=c341/numrows;  
c441=c441/numrows;  
c151=c151/numrows;  
c251=c251/numrows;  
c351=c351/numrows;  
c451=c451/numrows;  
c551=c551/numrows;  
c161=c161/numrows;  
c261=c261/numrows;  
c361=c361/numrows;  
c461=c461/numrows;  
c561=c561/numrows;  
c661=c661/numrows;
```

```
c112=c112/numrows;  
c122=c122/numrows;  
c222=c222/numrows;  
c132=c132/numrows;  
c232=c232/numrows;  
c332=c332/numrows;  
c142=c142/numrows;  
c242=c242/numrows;  
c342=c342/numrows;  
c442=c442/numrows;  
c152=c152/numrows;  
c252=c252/numrows;  
c352=c352/numrows;  
c452=c452/numrows;  
c552=c552/numrows;  
c162=c162/numrows;  
c262=c262/numrows;  
c362=c362/numrows;  
c462=c462/numrows;  
c562=c562/numrows;  
c662=c662/numrows;
```

```
/*
```

```
if(c111<100)  
    c111=0.0;  
if(c121<100)  
    c121=0.0;  
if(c221<100)  
    c221=0.0;  
if(c131<100)  
    c131=0.0;  
if(c231<100)  
    c231=0.0;  
if(c331<100)  
    c331=0.0;  
if(c141<100)
```

```
        c141=0.0;
if(c241<100)
        c241=0.0;
if(c341<100)
        c341=0.0;
if(c441<100)
        c441=0.0;
if(c151<100)
        c151=0.0;
if(c251<100)
        c251=0.0;
if(c351<100)
        c351=0.0;
if(c451<100)
        c451=0.0;
if(c551<100)
        c551=0.0;
if(c161<100)
        c161=0.0;
if(c261<100)
        c261=0.0;
if(c361<100)
        c361=0.0;
if(c461<100)
        c461=0.0;
if(c561<100)
        c561=0.0;
if(c661<100)
        c661=0.0;
```

```
if(c112<100)
        c112=0.0;
if(c122<100)
        c122=0.0;
if(c222<100)
        c222=0.0;
if(c132<100)
        c132=0.0;
if(c232<100)
        c232=0.0;
if(c332<100)
        c332=0.0;
if(c142<100)
        c142=0.0;
if(c242<100)
        c242=0.0;
if(c342<100)
        c342=0.0;
if(c442<100)
        c442=0.0;
if(c152<100)
        c152=0.0;
if(c252<100)
```

```

        c252=0.0;
    if(c352<100)
        c352=0.0;
    if(c452<100)
        c452=0.0;
    if(c552<100)
        c552=0.0;
    if(c162<100)
        c162=0.0;
    if(c262<100)
        c262=0.0;
    if(c362<100)
        c362=0.0;
    if(c462<100)
        c462=0.0;
    if(c562<100)
        c562=0.0;
    if(c662<100)
        c662=0.0;

*/

ofstream foutin("lsdynainput.k");
if (!foutin) {
    cerr << "\nError: failure creating file lsdynainput.k" <<
endl;
    system("PAUSE");
    exit(-1);
}

foutin << "*PARAMETER" << endl;
foutin << "R " << "t1"      " << 0-t1 << endl;
foutin << "R " << "t2"      " << 0-t2 << endl;
foutin << "R " << "t3"      " << 0-t3 << endl;
foutin << "R " << "t4"      " << 0-t4 << endl;
foutin << "R " << "t5"      " << 0-t5 << endl;
foutin << "R " << "t6"      " << 0-t6 << endl;
foutin << "R " << "t7"      " << 0-t7 << endl;
foutin << "R " << "t8"      " << 0-t8 << endl;
foutin << "R " << "t9"      " << 0-t9 << endl;
foutin << "R " << "t10"     " << 0-t10 << endl;
foutin.precision(1); // 16 total digits
foutin.setf(ios::scientific);
foutin.setf(ios::right);
foutin << "R " << "r01"     " << r01 << endl;
foutin << "R " << "c111"    " << c111 << endl;
foutin << "R " << "c121"    " << c121 << endl;
foutin << "R " << "c221"    " << c221 << endl;
foutin << "R " << "c131"    " << c131 << endl;
foutin << "R " << "c231"    " << c231 << endl;
foutin << "R " << "c331"    " << c331 << endl;
foutin << "R " << "c141"    " << c141 << endl;
foutin << "R " << "c241"    " << c241 << endl;

```

```

foutin << "R " << "c341      " << c341 << endl;
foutin << "R " << "c441      " << c441 << endl;
foutin << "R " << "c151      " << c151 << endl;
foutin << "R " << "c251      " << c251 << endl;
foutin << "R " << "c351      " << c351 << endl;
foutin << "R " << "c451      " << c451 << endl;
foutin << "R " << "c551      " << c551 << endl;
foutin << "R " << "c161      " << c161 << endl;
foutin << "R " << "c261      " << c261 << endl;
foutin << "R " << "c361      " << c361 << endl;
foutin << "R " << "c461      " << c461 << endl;
foutin << "R " << "c561      " << c561 << endl;
foutin << "R " << "c661      " << c661 << endl;
foutin << "R " << "ro2       " << ro2 << endl;
foutin << "R " << "c112      " << c112 << endl;
foutin << "R " << "c122      " << c122 << endl;
foutin << "R " << "c222      " << c222 << endl;
foutin << "R " << "c132      " << c132 << endl;
foutin << "R " << "c232      " << c232 << endl;
foutin << "R " << "c332      " << c332 << endl;
foutin << "R " << "c142      " << c142 << endl;
foutin << "R " << "c242      " << c242 << endl;
foutin << "R " << "c342      " << c342 << endl;
foutin << "R " << "c442      " << c442 << endl;
foutin << "R " << "c152      " << c152 << endl;
foutin << "R " << "c252      " << c252 << endl;
foutin << "R " << "c352      " << c352 << endl;
foutin << "R " << "c452      " << c452 << endl;
foutin << "R " << "c552      " << c552 << endl;
foutin << "R " << "c162      " << c162 << endl;
foutin << "R " << "c262      " << c262 << endl;
foutin << "R " << "c362      " << c362 << endl;
foutin << "R " << "c462      " << c462 << endl;
foutin << "R " << "c562      " << c562 << endl;
foutin << "R " << "c662      " << c662 << endl;

```

```

foutin.close();

```

```

return 0;

```

```

}

```

```

/*

```

```

//Write response/results file
// ofstream foutr("RESULTS.OUT");
ofstream foutr(argv[2]);
if (!foutr) {
    cerr << "\nError: failure creating file RESULTS" << endl;
    system("PAUSE");
    exit(-1);
}
foutr.precision(15); // 16 total digits
foutr.setf(ios::scientific);

```

```

foutr.setf(ios::right);

foutr << SQdiff << endl;
foutr << sumE << endl;

foutr.close();

ofstream foute("E.txt");
if (!foute) {
    cerr << "\nError: failure creating file E" << endl;
    system("PAUSE");
    exit(-1);
}
foute.precision(15); // 16 total digits
foute.setf(ios::scientific);
foute.setf(ios::right);

foute << E11 << '\t' << E12 << '\t' << E13 << endl;
foute << E21 << '\t' << E22 << '\t' << E23 << endl;
foute << E31 << '\t' << E32 << '\t' << E33 << endl;

foute.close();

```

*/

DRIVER CODE

```
/*  
-----  
This is code written CANTILEVER PROBLEM  
with one objective on Nov 5, 2008 using  
cantilever_asis/cantilever_oneobj_asis.C  
-----*/  
#include "stdafx.h"  
  
#include <cstdlib> // Defines the macros traditionally defined in  
the Standard C library header stdlib.h  
#include <iostream> //Declares objects that control reading from  
and writing to the standard streams.  
#include <fstream> //Defines several classes that support  
iostreams operations on sequences stored in external files.  
#include <vector> //logical operators  
#include <string> //Defines the container template class basic_string  
and various supporting templatesThe string class is a container that  
enables the use of strings as normal types, such as using comparison  
and concatenation operations, iterators, and STL algorithms and copying  
and assigning with class allocator managed memory.  
#ifdef HAVE_CONFIG_H  
#include "dakota_config.h"  
#endif //HAVE_CONFIG_H  
#ifdef HAVE_STD  
#include <cmath>  
#else  
#include <math.h>  
#endif //HAVE_STD  
using namespace std;  
  
int main(int argc, char **argv){  
  
    system("ansysin.exe");  
    system("ansyscall3x3x3L1.exe");  
    system("ansyscall3x3x3L2.exe");  
    system("lsdynain.exe");  
    system("lsdynacall.exe");  
    system("fobj.exe");  
    // system("PAUSE");  
  
    return 0;  
}
```